Impact of heterogeneous soil water distribution on soil and plant water relations

DISSERTATION

zur Erlangung des akademischen Grades eines

Doktors der Naturwissenschaften (*Dr. rer. nat.*)

an der Fakultät für Biologie, Chemie und Geowissenschaften

der Universität Bayreuth

vorgelegt von

Faisal Hayat

aus *Chiniot*, Pakistan

Bayreuth, 2020

This doctoral thesis was prepared at the department of Soil Physics at the University of Bayreuth from June 2016 until June 2020 and was supervised by Prof. Dr. Andrea Carminati.

This is a full reprint of the dissertation submitted to obtain the academic degree of Doctor of Natural Sciences (Dr. rer. nat.) and approved by the Faculty of Biology, Chemistry and Geosciences of the University of Bayreuth

Date of submission: 18.06.2020

Date of defense: 14.10.2020

Acting Dean: Prof. Dr. Mathias Breuning

Doctoral committee:

Prof. Dr. Andrea Carminati (reviewer)

J. Prof. Dr. Johanna Pausch (reviewer)

Prof. Dr. Eva Lehndorff (Chairman)

Prof. Dr. Bettina Engelbrecht

Acknowledgment

First and foremost, I am thankful to Allah Almighty for endowing me with health, strength and support, and for making it possible for me to complete my PhD studies. The present work would not have been possible without the support of many people to whom I am very grateful.

I would like to express my deep and sincere gratitude to Prof. Dr. Andrea Carminati, my supervisor, for giving me outstanding opportunity to join his research group. I am very grateful for his numerous supports and encouragements throughout my study. Above of all, I would like to thank for his great understanding and friendship. I feel very lucky to have had him as my supervisor.

I offer my deepest sense of acknowledgement to my beloved wife, Dilruba, for her patience, continuous prayers and encouragements during last five years. I also thank my little wonderful daughter, Hafsa, for blessing me with her birth in the early stages of my study.

My enormous thanks go to Dr. Mohsen Zarebandkouki and Dr. Mutez Ali Ahmad for their scientific and friendly supports during my study. Their great supports and encouragements throughout the study are highly appreciated.

I appreciate very much the support of Dr. Gaochao Cai and Mohanned Abdalla Ali during my study and would like to thank all members of Soil Physics group.

I am thankful to the members of Heinz Maier-Leibnitz (FRM II), Technical University, Munich for the precious technical supports during the measurements with neutron radiography.

Summary

Soil moisture is highly variable in space and time and such variability impacts transpiration, locations of root water uptake and, ultimately, plant growth. Mechanisms by which soil drying impacts plant growth are complex and involve feedbacks between plant hydraulics, stomatal regulation and water distribution. Up to date, our understanding of how plants respond to the heterogeneous soil water contents remain controversial. The aim of this thesis was to understand the effect of soil drying on transpiration, leaf water potential, locations of root water uptake and hydraulic redistribution. The thesis is structured into four chapters where chapter 1 is a brief summary.

In chapter 2, a method combining the root pressure chamber technique, which allows measuring the average suction in the leaves of intact transpiring plants exposed to soil drying, with a hydraulic model of root water uptake was introduced. Lupines were grown in PVC pots in a sandy soil which was partitioned into two layers separated by a layer of fine gravel acting as capillary. Three scenarios of soil water contents (wet-wet, dry-wet and dry-dry) were tested.

A linear relation between transpiration rate and leaf water potential in all tested scenarios of soil water contents was observed, with a slope decreasing with decreasing water contents. Both a simplified and a complex 3D root architecture model were capable of reproducing this relation and the slopes. The soil-plant conductance in dry-wet and wet-wet scenarios decreased by a factor of 1.65 and 8.26 times compared to the conductance in the wet-wet scenario, respectively. This decrease in conductance indicated the limiting role of the soil conductivity on root water uptake. Furthermore, model simulations showed that at uniform soil water contents (wet-wet and dry-dry scenarios), the relative root water uptake depended uniquely on the root properties and its distribution along the root system did not vary with transpiration rate. In the dry-wet scenarios, root water uptake is shifted to the lower wet layer and both models predicted the occurrence of hydraulic lift in the upper dry soil layer.

In chapter 3, the effect of soil drying on the decrease in the soil-plant conductance and stomatal regulation in maize was tested. A simple soil-plant hydraulic model was coupled with measured data from a root pressure chamber and sap flow sensors. Furthermore, transpiration rates for pressurized and not-pressurized plants were measured to test to what extent leaf suction controls stomata closure in drying soils.

The results showed a linear relationship between transpiration and leaf water potential in wet soils, while non-linearity was observed at high transpiration rates in dry soil conditions. The

soil-plant hydraulic model was capable of reproducing the measured relation. The non-linearity in this relationship corresponds to a decrease in soil-plant conductance, which is interpreted as a loss of hydraulic conductivity around the roots. Transpiration measurements for not-pressurized plants showed that stomata promptly closed when the soil-plant hydraulic conductance decreased. Stomatal regulation reduced transpiration when soil-plant hydraulic conductance dropped, preventing marked non-linearity in the relationship between transpiration and leaf water potential.

Besides affecting soil-plant hydraulics and stomatal regulation, soil drying also impacts location of water uptake and hydraulic redistribution through the root system. In chapter 4, neutron radiography was used to visualize and quantify hydraulic redistribution and root growth in maize grown in soil with heterogeneous water distribution. Plants were grown in aluminum containers whose soil water contents were adjusted in both top and bottom layers to the following scenarios: i) dry-wet; and ii) wet-wet. We injected D_2O in the bottom soil layers and imaged the root system in the top soil layers overnight. A diffusion-convection model was used to estimate hydraulic redistribution in the roots.

During day, D_2O was taken up by the roots in the bottom, wet soil layer and transported to the shoot. Overnight, D_2O appeared also in nodal and lateral roots in the top compartment. There was a visible efflux of water from lateral roots into the soil (j_r=2.35×10^{-7} cm s^{-1}). The efflux from nodal roots depended on their length and growth rate and a fraction of the redistributed water flew toward the root tips to sustain their growth.

To summarize, I demonstrated the importance of soil drying on the relations between transpiration rate, leaf water potential and soil-plant hydraulic conductance. Stomatal response to soil drying prevented the drop in soil plant-hydraulic conductance by limiting the transpiration rate in drying soils. In natural conditions soils dry heterogeneously, which impact the locations and dynamics of root water uptake, including hydraulic redistribution. In a simplified approach, I have shown the importance of hydraulic redistribution to sustain root growth. These results have been obtained in simplified lab experiments that allowed me for developing the methods. Field measurements in more natural conditions are needed to investigate the ecological and agricultural implications of my findings.

Zusammenfassung

Die Bodenfeuchtigkeit unterliegt einer räumlich und zeitlich hohen Variabilität, die auf die Transpiration, die Orte der Wurzelwasseraufnahme und letztlich auf das Pflanzenwachstum Einfluss nimmt. Die Mechanismen der Bodentrocknung mit Wirkung auf das Pflanzenwachstum sind komplex und beinhalten Rückkopplungen zwischen der Pflanzenhydraulik, der stomatären Regulierung und der Wasserverteilung. Bis heute ist unser Verständnis darüber, wie Pflanzen auf den heterogenen Bodenwassergehalt reagieren, umstritten. Das Hauptziel dieser Arbeit war es, die Auswirkungen der Bodentrocknung auf die Transpiration, das Blattwasserpotenzial, die Orte der Wurzelwasseraufnahme und die hydraulische Umverteilung zu verstehen. Die Dissertation ist in vier Kapitel gegliedert, wobei Kapitel 1 eine kurze Zusammenfassung darstellt.

In Kapitel 2 wurde eine Methode vorgestellt, die die Wurzeldruckkammer-Technik mit einem hydraulischen Modell der Wasseraufnahme der Wurzeln kombiniert. Die Wurzeldruckkammer-Technik erlaubt es, die durchschnittliche Saugspannung in den Blättern intakter, transpirierender Pflanzen zu messen, die der Bodentrocknung ausgesetzt sind. Die Lupinen wurden in PVC-Töpfen befüllt mit einem zwei-geschichteten, sandigen Boden angebaut, der durch eine Schicht feinen Kieses getrennt war, der als Kapillare fungierte. Drei Szenarien des Bodenwassergehalts (nass-nass, trocken-nass und trocken-trocken) wurden getestet.

In allen getesteten Szenarien der Bodenwassergehalte wurde eine lineare Beziehung zwischen der Transpirationsrate und dem Blattwasserpotenzial beobachtet, wobei die Steigung mit sinkendem Wassergehalt abnahm. Sowohl ein vereinfachtes als auch ein komplexes 3D-Wurzelarchitekturmodell waren in der Lage, diese Beziehung und die Steigungen zu reproduzieren. Die Boden-Pflanzen-Leitfähigkeit in trocken-nassen und nass-nassen Szenarien nahm im Vergleich zur Leitfähigkeit im nass-nassen Szenario um den Faktor 1,65 bzw. 8,26 ab. Diese Abnahme der Leitfähigkeit deutete auf die limitierende Rolle der Bodenwasserleitfähigkeit für die Wasseraufnahme durch die Wurzeln hin. Darüber hinaus zeigten die Modellsimulationen, dass bei gleichmäßigen Bodenwassergehalten (nass-nass und trocken-trocken Szenarien) die relative Wurzelwasseraufnahme eindeutig von den Eigenschaften der Wurzeln abhing und ihre Verteilung entlang des Wurzelsystems nicht mit der Transpirationsrate variierte. In den trocken-nassen Szenarien wird vorhergesagt, dass sich die Wasseraufnahme der Wurzeln in die untere nasse Schicht verlagert, und beide Modelle

prognostizierten das Auftreten von hydraulischem Auftrieb in der oberen trockenen Bodenschicht voraus.

In Kapitel 3 wurde der Einfluss der Bodentrocknung auf die Abnahme der Boden-Pflanzen-Leitfähigkeit und der stomatären Regulierung bei Mais untersucht. Ein einfaches hydraulisches Boden-Pflanzen-Modell wurde mit Messdaten aus einer Wurzeldruckkammer und Saftflusssensoren gekoppelt. Darüber hinaus wurden die Transpirationsraten für unter Druck stehende und nicht unter Druck stehende Pflanzen gemessen, um zu testen, inwieweit die Blattsaugspannung das Schließen der Stomata in trocknenden Böden steuert.

Die Ergebnisse zeigten eine lineare Beziehung zwischen Transpiration und Blattwasserpotential in nassen Böden, während bei hohen Transpirationsraten in trockenen Bodenverhältnissen Nichtlinearität beobachtet wurde. Das hydraulische Boden-Pflanzen-Modell war in der Lage, die gemessene Beziehung zu reproduzieren. Die Nichtlinearität in dieser Beziehung entspricht einer Abnahme der Boden-Pflanzen-Leitfähigkeit, die als Verlust der hydraulischen Leitfähigkeit um die Wurzeln herum interpretiert wird. Transpirationsmessungen bei nicht unter Druck stehenden Pflanzen zeigten, dass sich die Stomata sofort schlossen, wenn die hydraulische Leitfähigkeit zwischen Boden und Pflanze abnahm. Die Stomata-Regulierung reduzierte die Transpiration, wenn die hydraulische Leitfähigkeit zwischen Boden und Pflanze abnahm, wodurch eine ausgeprägte Nichtlinearität in der Beziehung zwischen Transpiration und Blattwasserpotenzial verhindert wurde.

Die Austrocknung des Bodens wirkt sich nicht nur auf die Boden-Pflanzen-Hydraulik und die stomatäre Regulierung aus, sondern auch auf die Orte der Wasseraufnahme und die hydraulische Umverteilung durch das Wurzelsystem. In Kapitel 4 wurde die Neutronenradiographie zur Visualisierung und Quantifizierung der hydraulischen Umverteilung und des Wurzelwachstums bei Mais beschrieben, der in Böden mit heterogener Wasserverteilung angebaut wird. Die Pflanzen wurden in Aluminiumbehältern gezüchtet, deren Bodenwassergehalt sowohl in der oberen als auch in der unteren Schicht an die folgenden Szenarien angepasst wurde: i) trocken-nass; und ii) nass-nass. Wir injizierten D_2O in die unteren Bodenschichten und bildeten über Nacht das Wurzelsystem in den oberen Bodenschichten ab. Zur Abschätzung der hydraulischen Umverteilung in den Wurzeln wurde ein Diffusion-Konvektions-Modell verwendet.

Tagsüber wurde D_2O von den Wurzeln in der unteren, feuchten Bodenschicht aufgenommen und zum Spross transportiert. Über Nacht erschien D_2O auch in Knoten- und Seitenwurzeln im

oberen Kompartiment. Es gab einen sichtbaren Wasserausfluss von den Seitenwurzeln in den Boden (j_r=2,35×10^{-7} cm s^{-1}). Der Ausfluss aus den Knotenwurzeln hing von ihrer Länge und Wachstumsrate ab, und ein Teil des umverteilten Wassers floss in Richtung der Wurzelspitzen, um deren Wachstum zu unterstützen.

Zusammenfassend habe ich die Bedeutung der Bodentrocknung für die Beziehungen zwischen der Transpirationsrate, dem Blattwasserpotenzial und der hydraulischen Leitfähigkeit von Boden und Pflanze aufgezeigt. Die stomatäre Reaktion auf das Austrocknen des Bodens verhinderte die Verringerung der hydraulischen Leitfähigkeit von Boden und Pflanze, indem die Transpirationsrate in trockenen Böden begrenzt wurde. Unter natürlichen Bedingungen trocknen Böden heterogen aus, was sich auf die Orte und die Dynamik der Wurzelwasseraufnahme, einschließlich der hydraulischen Umverteilung, auswirkt. In einem vereinfachten Ansatz habe ich gezeigt, wie wichtig die hydraulische Umverteilung für die Aufrechterhaltung des Wurzelwachstums ist. Diese Ergebnisse wurden in vereinfachten Laborexperimenten erzielt, die es mir erlaubten, die Methoden zu entwickeln. Feldmessungen unter natürlicheren Bedingungen sind erforderlich, um die ökologischen und landwirtschaftlichen Auswirkungen meiner Ergebnisse zu untersuchen.

List of Figures

Chapter One

Chapter Two

Chapter Three

Chapter Four

Table of Contents

1   Chapter One

Extended summary

1.1   Introduction

A lack of water availability for agricultural production and its economical use is a major issue around the world. Global climate change is expected to result in greater evapotranspiration, soil drying and an increased incidence of drought in many parts of the world. These climate changes challenge our understanding of plant and ecosystem functioning. The natural resources (soil and water) are depleted through erosion, salinization, compaction and nutrient export (Montgomery, 2007; Morton, 2007; Sheldon et al., 2017; Sprague and Gronberg, 2012). We need to understand how these environmental scenarios impact plants and ecosystems. Water deficit is the major factor suppressing plant growth and productivity in most regions of the world (Boyer, 1982; Lesk et al., 2016).

Plants use different strategies to overcome drought, including facilitation of water extraction from drying soil and regulation of water loss, thereby minimize the reduction of yield (Farooq et al., 2009; Flexas et al., 2004) and crop growth under drought (Lawlor, 2013). These strategies emerge from complex feedbacks between soil water potential sensed by roots, stomatal regulation and leaf water potential. Water flows from the soil into the root, across the plant vascular system and then through the stomata to the atmosphere following a gradient in water potential. Transpiration is the driving force of this process. Transpiration generates a suction in the leaves driving water from the soil into the roots. As the soil dries, a more negative leaf water potential is needed to sustain a given transpiration rate due to an abrupt decrease in soil water potential and hydraulic conductivity.

The effect of soil drying on root water uptake has been investigated experimentally and numerically since decades (Doussan et al., 2006; Jarvis, 1989; Javaux et al., 2008; Tardieu et al., 2017). In wet soils, the soil hydraulic conductivity has little effect on water uptake, as the hydraulic resistance of the root is much greater than that of the soil (Draye et al., 2010) and the difference in water potential between soil and leaf xylem is linearly related to transpiration (Passioura, 1980). The situation changes as the soil becomes progressively dry, when its hydraulic conductivity decreases and the leaf suction that is needed to drive water from the soil into the roots increases non linearly (Fig. ES 1) (Carminati et al., 2017; Passioura, 1980). This non-linearity comes from microscopic and macroscopic gradients in water potential across the rhizosphere and along the root system.
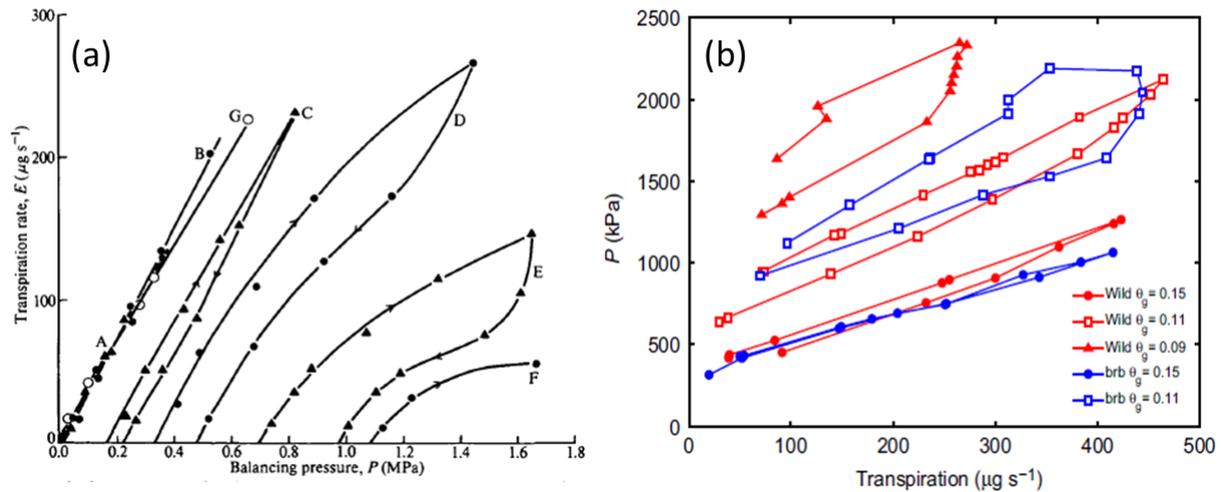
Figure ES 1. Effect of soil drying on transpiration rate and leaf xylem suction. Both figures show a linear relation in wet soils and non-linearity in drier soils. These figures are taken from Passioura, (1980) and Carminati et al. (2017).

The slope of the relation between transpiration and xylem leaf water potential is the total conductance of soil and plant system. This relation is related to the physical work required to extract water from the soil to the shoot at a given transpiration rate. This relation could be measured with high accuracy using root pressure chamber method, developed by Passioura, (1980). In this method, a pneumatic pressure is applied until a drop of water appears at a cut leaf. The pressure needed to maintain the drop of water at the cut leaf is called balancing pressure and it is equal to the suction in the xylem prior to pressurization. This method is limited to small plants grown in pots, but has the advantage to measure the leaf water potential with high precision throughout the soil drying (Matzner and Comstock, 2001; Saliendra et al., 1995). In this method, during pressurization, the leaves are kept turgor and stomata remain partially open, which allows to investigate the effect of hydraulic limits in intact plants.

A hydraulic framework is helpful to understand the physical constraints to transpiration in drying soil (Sperry and Love, 2015). The soil-plant atmospheric continuum is described as a network of elements connected in series and in parallel (Cowan, 1965; Draye et al., 2010; Mencuccini et al., 2019; Sperry et al., 1998). Each element is characterized by hydraulic conductances (which can be variable) and capacitances. The hydraulic conductivities of the xylem, of the roots and of the soil are extremely variable. Xylem vessels tend to cavitate at high tension, causing a large drop in the axial conductance of the xylem (Sperry et al., 1998). The radial conductance of the root is also variable and it is affected by anatomical changes as well as by the expression of aquaporin (Chaumont and Tyerman, 2014; Ehlert et al., 2009; Knipfer et al., 2011; Redondo et al., 2009; Simonneau et al., 2009). Finally, the soil hydraulic conductivity determines the ease of water flow through the soil. Its conductivity decreases by

several orders of magnitude as the soil dries, and it might become smaller than that of roots (Draye et al., 2010; Gardner, 1960). Eventually, when plants are exposed to severe drying, their roots shrink and lose part of their contact to the soil (Carminati et al., 2013), which further decreases the conductance between rhizosphere and root. On the other hand, plants can close this gap and attenuate the drop in conductivity by secreting mucilage (Carminati et al., 2010) or by growing root hairs (Carminati et al., 2017).

Soil drying triggers a gradual closure of stomata and a reduction in transpiration rate (Bates et al., 1981; Carter et al., 1980; Comstock, 2002; Meyer and Green, 1980; Sinclair et al., 2005). Stomatal closure depends on both hydraulic and hormonal signals, such as abscisic acid (ABA) (Brodribb and McAdam, 2017; Buckley, 2017; Tardieu and Davies, 1993). Independently from the mechanism by which stomata close, it has been proposed that stomatal regulation avoids excessive drop in leaf water potential by responding to non-linearities in the relationship between transpiration rate and leaf water potential (Sperry et al., 2016; Sperry and Love, 2015). In recent studies, it is revealed that stomata close before xylem cavitation (Martin-StPaul et al., 2017; Rodriguez-Dominguez and Brodribb, 2020; Scoffoni et al., 2017). Furthermore, Corso et al, (2020) concluded that stomatal closure, rather than by xylem collapse, cavitation or decreases in leaf conductance, is triggered by processes outside xylem. However, there is limited experimental evidence that stomatal regulation prevents and responds to drop in soil-plant hydraulic conductance. Additionally, most of the studies linking stomatal regulation to plant hydraulics focus on xylem vulnerability as the primary constraint on water flow in soil and plants (Anderegg et al., 2017), neglecting the explicit role of soil hydraulic conductivity. In the above discussions, the question appears that what are the primary constraints which regulate stomata and water flow across soil-plant continuum? An answer to this long-standing question requires methods to measure and partition the hydraulic conductance of the different elements of soil-plant continuum.

Long drought events lead to soil drying and severely shortage of available water for plants resulting in hydraulic failure and plants death (Brodribb and Cochard, 2009; Urli et al., 2013). In particular, plants possess versatile strategies such as hydraulic redistribution to cope with drought events. Hydraulic redistribution is the passive movement of water from wet to dry soil regions through the root system during night (Brooks et al., 2002; Burgess et al., 2001, 2000, 1998). The driving force for water flow is the soil-water potential gradients between dry and wet zones of soil and between roots and soil (Lee et al., 2018; Leffler et al., 2005). During the day, water moves from the wet soil to roots and then to the atmosphere via the leaves due to transpiration (Fig. ES 2a). Subsequently during night, when transpiration ceased, water

potential gradients between the soil and roots are induced and water starts to flow towards the drier soil and in the roots followed by these water potential gradients (Fig. ES 2b). Typically, the direction of water movement is towards drier and shallow regions of soil in the upwards called hydraulic lift (Sekiya et al., 2011), sap flow measurements revealed that water can be redistributed laterally or downward by roots (Sakuratani et al., 1999; Schulze et al., 1998; Smith et al., 1999) and this redistributed water could contribute to plant water balance. Hydraulic redistribution could be beneficial for plants through enhanced transpiration (Scholz et al., 2010), alleviated soil water contents in dry layers (Bleby et al., 2010), enhanced nutrients mobility and acquisition (Cardon et al., 2013; McCulley et al., 2004), prolonged growing season (Bauerle et al., 2008; Scott et al., 2008), maintained root functioning in dry layers (Domec et al., 2004) and thereby maintained plant and root growth (Dawson, 1993; Hsiao and Xu, 2000).
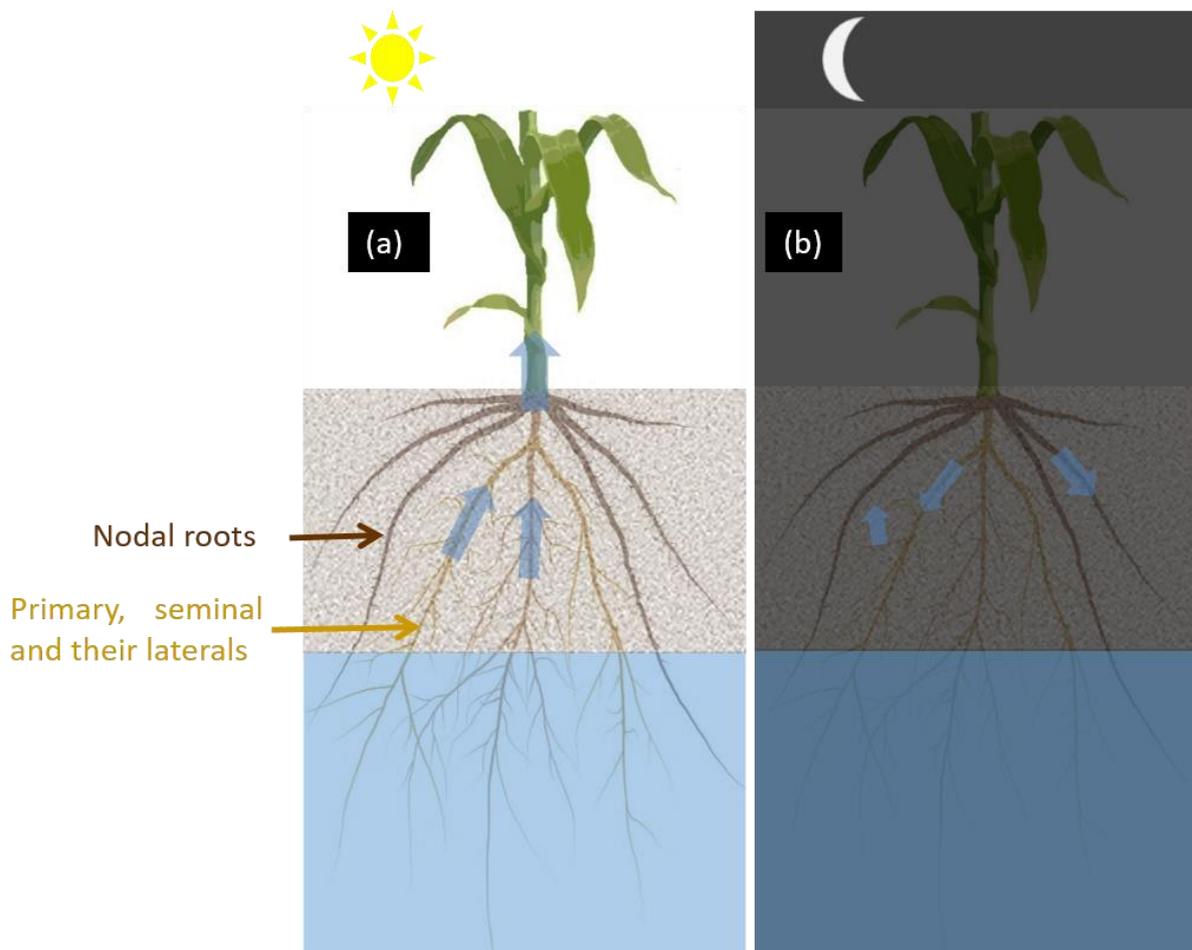
Figure ES 2. Schematic diagram of water movement in the plant during the day and night time. The blue regions are the wet soil. The left figure (a), denotes the water movement during the day time by the primary and seminal roots from the deep wet soil. The right figure (b), shows the water redistribution in the root system at night-time condition.

Although occurrence, relevance and amount of HR are well accepted and documented, resolving the spatial distribution of HR along the root system and into the soil remains challenging. Warren et al. (2013) have used neutron radiography and deuterated water (D_2O) to trace hydraulic redistribution in seedlings of *Zea mays* L. and *Panicum virgatum* L. The technique, thanks to its high sensitivity to water and thus to roots (Moradi et al., 2011; Oswald et al., 2008), has high potential to reveal the redistribution of water within the root system in a quantitative way.

Soil-plant hydraulic approaches were introduced to investigate plant response under water limiting environments (Javaux et al., 2008; Sperry et al., 2002). The relation between transpiration rate and leaf water potential – referred to as soil-plant hydraulics has both direct and indirect effects on stomatal regulation and root water uptake (Sperry and Love, 2015; Tardieu et al., 2015). The relation between transpiration and leaf water potential can be reproduced using detailed architecture models of water flow in soil and plants (Couvreur et al., 2012; Doussan et al., 2006; Javaux et al., 2008) or radial models of water flow towards a single root (Carminati et al., 2017; Deery et al., 2013; Passioura, 1980). These models are based on the cohesion-tension theory. According to this theory, water moves from soil to plants due to tension in water potential that is transmitted along the xylem down to the roots. Water loss at leaves depends on continuous supply of water in the xylem from roots to shoots (Koch et al., 2004; Walker et al., 2003). Water flow from the soil into the roots must compensate water loss from leaves. This concept of water movement is often described as analogous to Ohm's and Kirchhoff's laws. Applying these laws to plants, the water flow depends on water potential gradients and the resistance of pathways of soil-plant continuum (Fig. ES 3).

Figure ES 3. Simplified drawing of Ohm's law analogy to water flow in single plant as described in equation 1.

Assuming steady state conditions, the water flow within the system, J [cm^3 s^{-1}], can be written as:

$$J = \frac{\psi_s - \psi_l}{R_{s-l}} \qquad (1)$$

where, ψ denotes water potential [hPa] and R is the hydraulic resistance [hPa cm^{-3} s] of each element from the soil to leaf. Draye et al. (2010) showed that in wet soil conditions, the soil hydraulic conductivity is sufficient to sustain transpiration. But in drier soils, the soil is the limiting factor for water flow into the roots as its hydraulic conductivity decreases of several orders of magnitude (Draye et al., 2010; Garrigues et al., 2006; Passioura, 1988). In summary, the models to predict the relation exists, but they used detailed measurements of leaf water potential.

1.2   Objectives and Outline

The overarching aim of this dissertation was to investigate the relation between soil drying, locations of root water uptake, soil-plant conductance, stomatal regulation and leaf water potential. Reaching this objective requires the development and test of new methods. Therefore, the experiments have been conducted in simplified conditions.

The specific objectives of this dissertation were:

I.   To measure the relation between leaf xylem water potential and transpiration rates for heterogeneous soil water distributions (Chapter 2)

II.   To investigate the suitability of detailed and simplified root water uptake models to reproduce the relation between leaf water potential and transpiration rates (Chapter 2)

III. To understand the relation between soil-plant hydraulic conductance and stomatal conductance during soil drying (Chapter 3)

IV.   To develop a new technique to quantify water fluxes within root system of transpiring plant growing in soils with heterogeneous water contents (Chapter 4)

V.   To quantitatively locate hydraulic redistribution within the root system (Chapter 4).

In chapter 2, I simulated xylem leaf water potential and root water uptake under heterogeneous soil water contents in lupine. Here, I used root pressure chamber technique to measure the relation between transpiration and leaf water potential at different soil water content regimes and coupled the measured data with a simple and detailed model to predict the estimated relation and to simulate leaf water potential and root water uptake.

In chapter 3, I extended my previous concept and applied the pressure chamber method to maize during soil drying. Here, I compared transpiration of pressurized and unpressurized plants and identified when soil limits transpiration rate and triggers stomatal closure. Afterwards, I used a soil-plant hydraulic model to estimate the reduction in soil-plant conductance at different soil water contents.

In chapter 4, I visualized and quantified the spatial distribution of hydraulic redistribution overnight at minimal transpiration in different roots in young maize using neutron radiography. Here, I investigated the relative importance of the different types of maize roots (seminal, nodal and their laterals) on hydraulic redistribution

1.3   Materials and methods

1.3.1   Soil and plant preparation

I used PVC pots with 30 cm of height and 14 cm of diameter filled with quartz sand (particle size < 500 µm) for the experiments conducted with lupines (Chapter 2). The soil columns were partitioned into two soil layers separated by a one-cm thick layer of fine gravel. This layer of fine gravel was used to hydraulically disconnect the upper and lower soil layers without hindering root growth. Lupine seedlings were planted in the pots (one seedling per pot). I conducted experiments when plants were 45 days old. The following three scenarios of soil water contents were tested: i) both the top and bottom soil layers were kept at wet (wet-wet); ii) the top compartment was let dry while the bottom compartment was kept wet (dry-wet); and iii) both top and bottom compartments were let dry (dry-dry).

For the experiments conducted on maize (Chapter 3), I used PVC pots with 30 cm of height and 9 cm of diameter filled with a mixture of silt and quartz sand (1:1 ratio) with a particle size less than 1 mm in diameter. The soil hydraulic parameters (for both types of soil used in lupine and maize experiments) were measured using Hyprop (UMS, Munich, Germany). Soil water retention curve and the hydraulic conductivity curve were parameterized using the PDI model (Peters-Durner-Iden model) (Peters et al., 2015). Experiments were carried out when plants were 40 days old. In case of maize, I tested the following scenarios of soil water contents: i) wet soil; ii) mid-wet soil; iii) mid-dry soil; and iv) dry soil. Prior to the experiments, transpiration rates were measured for each scenario by Sap Flow Sensors SGA9 (Dynamax Inc,

USA). This non-intrusive, energy balance sensor measures the amount of heat carried by the sap and converts into real-time transpiration rate.

For the third experimental setup (Chapter 4), maize seedlings were grown in aluminum containers (40 cm high, 40 cm wide and 1 cm thick) filled with the same soil as used in previous experiments with maize. A layer of one cm thickness filled with fine gravel was used to divide into two layers. When plants were 40 days old neutron radiography experiment were conducted. Prior to the experiments, the soil water contents were adjusted in both top and bottom layers to the following scenarios: i) in two plants the top soil compartment was kept dry ($0.03 < SWC \leq 0.05$) and the bottom compartment was kept wet ($SWC > 0.19$) (dry-wet scenario); ii) in one plant both compartments were kept wet ($SWC > 0.19$, wet-wet scenario).

1.3.2   Root pressure chamber

The root pressure chamber was introduced by Passioura, (1980). The method allows for measuring the relation between leaf xylem water potential and transpiration rate in intact plants (Fig. ES 4). It measures the suction in the leaf xylem by applying pressure. The pressure needed to bring the water at the end of a cut leaf is numerically equal to the tension in the xylem and is referred to as balancing pressure. During pressurization, the soil-root water relation does not change because the pressure of liquid and gas phases equally changes; rather the turgor pressure of shoots increases (Passioura and Munns, 1984). Plants were imposed to different transpiration rates by changing the photosynthetic photon intensity. I conducted pressure chamber experiments on plants (lupine and maize) grown in PVC pots. The detailed description of this technique is described in Chapter 2 & 3.
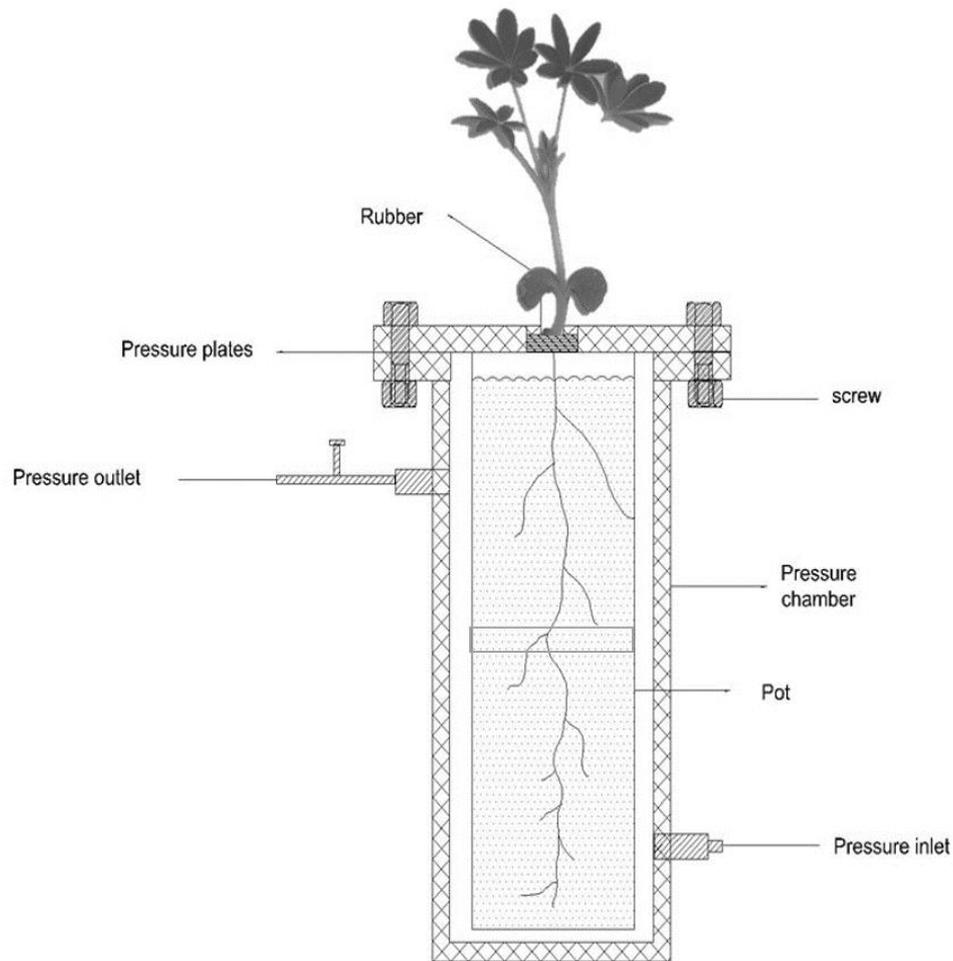
Figure ES 4. Comprehensive experimental setup of root pressure chamber. This figure is taken from Chapter 2. We also applied this technique on maize, which is described in Chapter 3.

1.3.3   Neutron radiography

Neutron radiography is a noninvasive imaging technique used to image water and root distribution in the soil (Carminati et al., 2010; Moradi et al., 2009; Oswald et al., 2008; Tumlinson et al., 2008). In this technique, the neutron beam propagates through the sample and transmitted neutrons are detected by the scintillator mounted behind the sample. The scintillator converts these neutrons into visible light, which is further converted by CCD camera into digital images. These images contain information about sample composition and thickness. The experiments were carried out at NECTAR facility (Bücherl and Söllradl, 2015) at the Heinz Maier-Leibnitz center, Technical University, Munich. We used an Andor iKon-M-BV based detection system with image resolution of 2048 x 2048 pixels.

Here, 30 ml of D_2O (purity of 99.97%) at two selected locations in the bottom wet compartment (15 ml at each location) was injected using fine syringes. The reconstructed image of one entire

sample before injection of D$_2$O is shown in Fig. ES5. The image was obtained by overlapping 4 radiographs. The grey values show the water content in the sample − i.e. the darker the image, the higher the soil water content. As roots have high water content, they appear dark. The roots in which we quantified the D$_2$O dynamics are shown in light purple and orange and [red & green] colors are categorized, in three root types, as seminal roots reaching the bottom compartment, lateral and nodal roots with their tips in the top compartment. The spatiotemporal distribution of D$_2$O in top compartment and its transport along the roots were monitored by time-series neutron radiography with a temporal resolution of one frame every 20 seconds. The detail of image analysis is described in detail in Chapter 4.
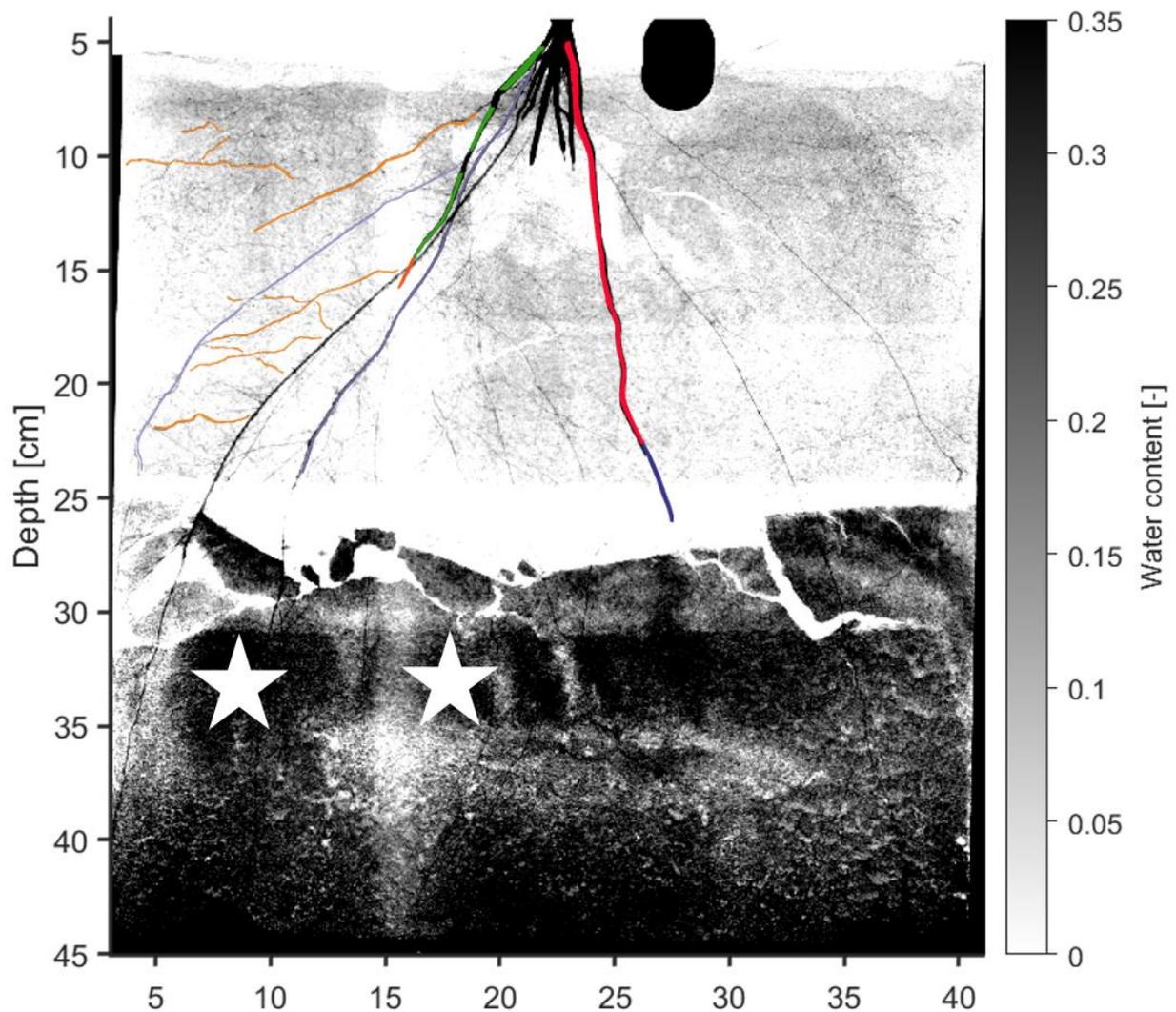
Figure ES 5. Reconstructed image of entire sample (dry-wet) before the injection of deuterated water (D$_2$O). The stars indicate the locations where D$_2$O was injected (in the bottom compartment). The image was obtained by overlapping 4 radiographs. The grey values represent water content (the darker the image, the higher the soil water content). The segmented roots in which we quantified the D$_2$O concentration are shown in light purple orange and red + green colors and are categorized as seminal roots, laterals and nodal (long + short), respectively.

1.3.4   Root water uptake models

In Chapter 2, I compared a simple and a three-dimensional detailed model of root architecture to predict the relation between leaf water potential and transpiration rates in lupine in drying soils. The simple model was represented as a series of hydraulic resistance between each element of soil-plant continuum following the Ohm's analogy.

$$Q = -K_{rs}(H_x - H_{s,eq}) \qquad \text{(Eq. 2)}$$

where Q is transpiration rate [$cm^3\,h^{-1}$], K_{rs} is the equivalent conductance [$cm^3\,hPa^{-1}\,h^{-1}$] of the root system and $H_{s,eq}$ is an equivalent soil water potential [hPa]. Here, H_x and $H_{s,eq}$ are the sum of the gravitational and hydrostatic potential (matric potential for the soil).

A detailed root architecture model was also used to simulate root water uptake radially and longitudinally. It was represented as a system of interconnected nodes in which water flows radially from the root xylem and longitudinally along the xylem vessels.

$$Q_r = -k_r\, s_r[H_s - H_x] = -K_r[H_s - H_x] \qquad \text{(Eq. 3)}$$

where Q_r is the radial flow between the soil-root interface and root xylem [$cm^3\,h^{-1}$], H_s and H_x are the water potential at root surface and in the xylem [hPa], respectively, s_r is the cross section of root segment [cm^2], k_r is the root radial conductivity [$cm\,hPa^{-1}\,h^{-1}$] and K_r is the radial conductance of the segment [$cm^3\,hPa^{-1}\,h^{-1}$].

The axial water flow within each root segment Q_x [$cm^3\,h^{-1}$] is described as:

$$Q_x = -\frac{k_x}{l}\, dH_x = -K_x[dH_x + dz] \quad \text{(Eq. 4)}$$

where H_x is water potential in xylem, k_x is axial conductivity [$cm^4\,hPa^{-1}\,h^{-1}$], h_x is xylem hydrostatic potential, z is the distance of each segment from the soil surface [cm] and K_x is axial conductivity.

In Chapter 3, I used a simple model to estimate the water flow in the soil-plant continuum. The model was represented as a series of hydraulic resistances (and one capacitance in the soil) between the bulk soil and the leaves. The flux of water in the soil was calculated using a cylindrical model as a function of radial distance to the root center. Knowing the transpiration rate and the plant hydraulic conductance, K_{plant} [$cm^3\,hPa^{-1}\,s^{-1}$], The dissipation of water potential within the plant was calculated as:

$$Q = K_{plant}(\psi_{leaf,x} - \psi_{r,s}) \qquad \text{(Eq. 5)}$$

where Q is the transpiration rate [cm^3 s^{-1}], K_{plant} is the plant hydraulic conductance in the wettest soil [cm^3 hPa^{-1} s^{-1}], $\psi_{leaf,x}$ and $\psi_{r,s}$ are the water potential in the leaf xylem and at soil-root interface [hPa], respectively.

For neutron radiography experiments (Chapter 4), we used diffusion-convection model to derive the fluxes of water from the temporal dynamics of D$_2$O concentration. The change in concentration of D$_2$O in the root can be described as:

$$\theta \frac{\partial C}{\partial t} = \frac{\partial}{r \partial r}\left(rD\left(\frac{\partial C}{\partial r}\right)\right) - \frac{\partial}{r \partial r}(rj_rC) - \frac{\partial}{\partial x}(j_xC) \qquad \text{(Eq. 6)}$$

where, $\theta(r,x)$ is the water content [cm^3 cm^{-3}], $C(r,x,t)$ is the D$_2$O concentration in the root [cm^3/cm^3], t is the time [s], r is the radial co-ordinate [cm], x is the longitudinal coordinate [cm], $j_r(r,x)$ is the radial flux of water [cm s^{-1}], $j_x(r,x)$ is the axial flux of water [cm s^{-1}] and $D(x)$ is an effective diffusion coefficient of D$_2$O [cm^2 s^{-1}]. The axial flux of water within the root xylem is estimated by mass conservation equation, assuming that the axial transport of D$_2$O occurs only in the root xylem, as

$$\pi r^2 \frac{\partial j_x(x)}{\partial x} = -2\pi r j_r \quad \text{(Eq. 10)}$$

where the axial flux j_x changes along x while j_r is assumed to be uniform along x.

The models implementation along with initial and boundary conditions are explained in each respective Chapters.

1.4 Summary of the main results

1.4.1 Reduction in soil-plant conductance and location of root water uptake (Chapter 2)

The main findings are summarized in Fig. ES 6. Here, a linear relationship between transpiration and balancing pressure in all tested scenarios of soil water contents was observed. The slope of the curves, which is interpreted as the conductance of the soil-root system, decreased by a factor of 1.65 from the uniform wet to the dry-wet scenario. In the uniform dry scenario, the conductance was severely reduced by a factor of 8.26, and the transpiration was also strongly reduced. Both, the simple and the detailed architecture models were capable of reproducing the measurements (Fig. ES 6A). The detailed model also yields the profile of the radial fluxes [m s^{-1}] into roots. In uniform wet soil (Fig. ES 6B [a]), the contribution of radial

flux was rather uniform along the root system; in dry-wet soil (Fig. ES 6B [b]) the uptake in upper-dry soil was much smaller compared to that in the lower-wet layer. In the uniform dry scenario (Fig. ES 6B [c]), the water fluxes were sharply reduced in both soil layers.
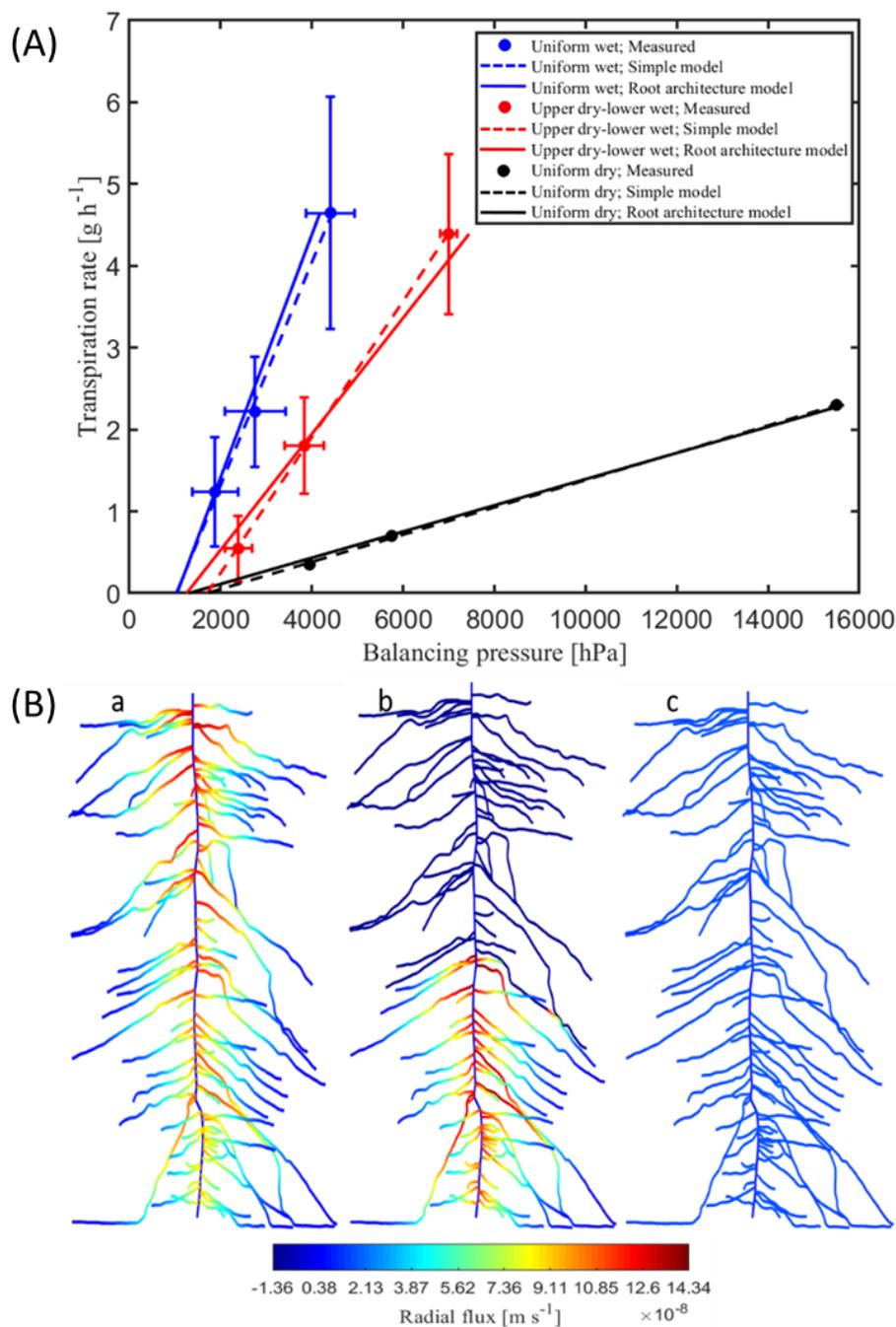
Figure ES 6. (A) Measured transpiration rate and balancing pressure for each scenario. The dotted lines are the fitting using a simple model and solid lines are the simulation results using the root architecture model. (B) Root water uptake simulated for varying soil moisture levels at medium light intensity (98.9 μmol m^{-2} s^{-1}): uniform-wet (a), top-dry bottom-wet (b) and uniform-dry (c).

A detailed root hydraulic architecture model was used to estimate the relative water uptake in the upper and lower soil layers at different transpiration rates for each scenario (Table. ES 1).

At uniform soil water contents (wet-wet & dry-dry), water uptake was slightly higher in the upper compartment than in the lower. In the dry-dry condition, the relative uptake in the upper and lower soil layers was almost the same as in the wet-wet conditions. The reason was that the difference in water potential between soil and root was larger compared to dissipation along the root. In both scenarios (wet-wet & dry-dry) we did not observe the effect of varying transpiration on the relative water uptake.

At heterogeneous soil water contents (dry-wet), the relative water uptake changed with varying transpiration rates. At high transpiration rate, water was taken up from the wet soil and it was released by the roots in the upper drier soil – the process referred to as hydraulic lift. At low transpiration rates, hydraulic lift increased significantly.

Table ES 1. Relative water uptake [%] in upper and lower layers obtained using the root architecture model. Negative values indicate water efflux and the occurrence of hydraulic lift.

Low transpiration rate	upper layer	lower layer	Medium transpiration rate	upper layer	lower layer	High transpiration rate	upper layer	lower layer
wet-wet	54.64	45.36	wet-wet	54.67	45.33	wet-wet	54.69	45.31
dry-wet	-27.57	127.57	dry-wet	-8.00	108.00	dry-wet	-2.99	102.99
dry-dry	51.27	48.72	dry-dry	51.27	48.72	dry-dry	51.27	48.72

1.4.2   Reduction in transpiration and plant conductance (Chapter 3)

I tested whether the drop in soil-plant hydraulic conductance during soil drying close stomata and this drop can be predicted based on the loss of soil hydraulic conductance. Here, I applied root pressure chamber to maize grown in silty soil at different levels of soil water contents.

The effect of pressurization and light intensity on averaged transpiration rates with and without pressurization of plants at each imposed water content are shown in Fig. ES 7. In pressurized plants, a slightly higher transpiration rate was observed. This indicates that when plants were pressurized and water in the leaf xylem was at atmospheric pressure, the stomata were more open. However, the transpiration rate increased with increasing light intensity under both, pressurized and not pressurized conditions, as long as the soil was wet or the light intensity was low. In contrast, in dry soil (WC = 9.33%) under not pressurized conditions transpiration dropped significantly at high light intensity (at 2000 µmol m^{-2} s^{-1}) (Fig. ES 7c). At the tested soil moistures, pressurization prevented stomatal closure at all soil moistures. Fig ES 7e shows

a linear response of transpiration to increasing light intensity. The increase in transpiration was even more marked in dry soil (Fig. ES 7e).
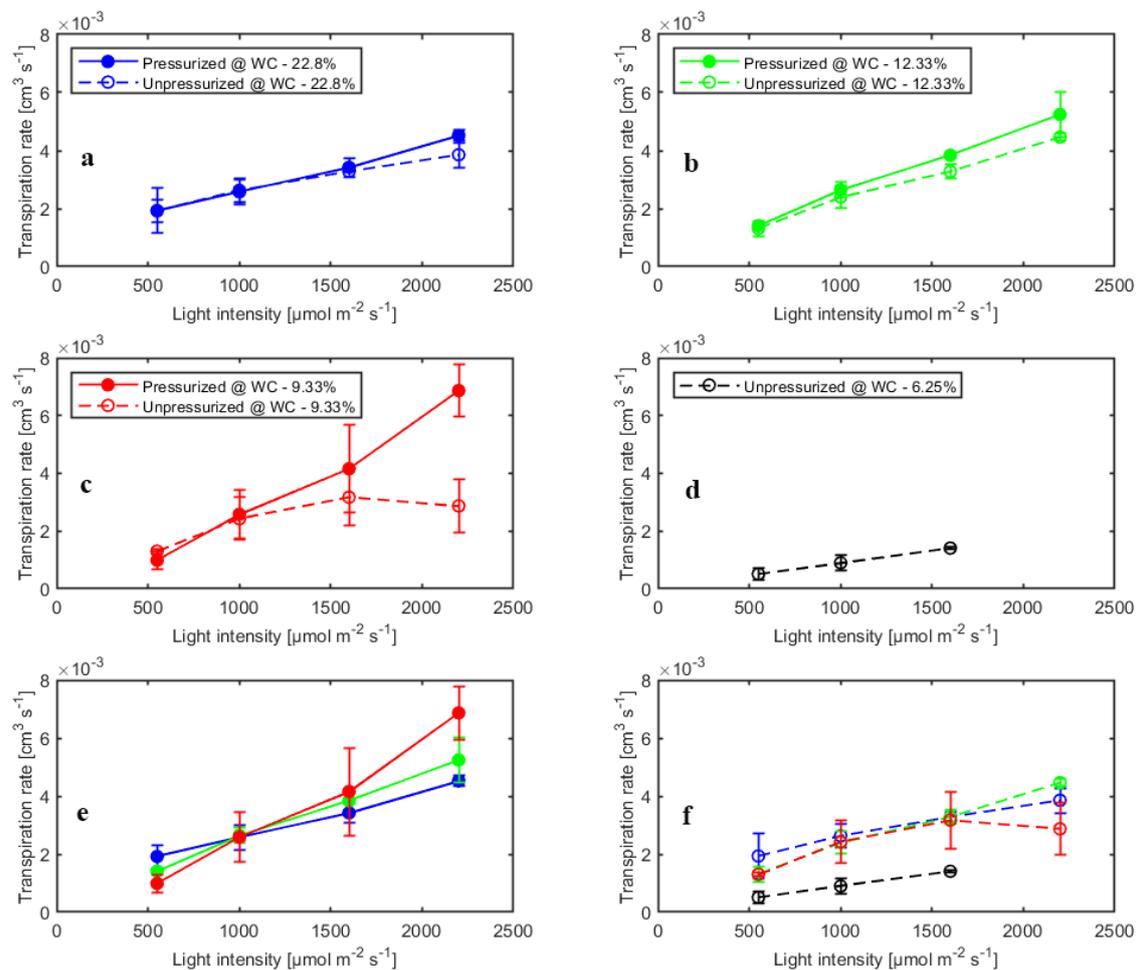
Figure ES 7. Effect of light intensity and pressurization on transpiration rates for varying soil water contents. (a-d) Effect of pressurization on transpiration. (e) Effect of light intensity and soil moisture on transpiration in pressurized and (f) unpressurized plants.

The measured transpiration rates and xylem tension along with the model fit for different water contents are shown in Fig. ES 8. In wet soil the relation was linear and non-linearity is observed in the dry soil at increasing transpiration rates. The slope of linear part of the curve in wet soil is interpreted as the plant conductance, K_{plant}. This conductance was used in the simulations. For high water content (at WC = 24.7%), the plant conductance was 1.25×10^{-6} [cm^3 hPa^{-1} s^{-1}]. The total soil-plant conductance reduced dramatically in dry soils at high transpiration rates due to the drop of soil hydraulic conductivity around the roots, which is well reproduced by the soil hydraulic model (Fig. ES 8a).

The effect of light intensity and water content on normalized soil-plant conductance $k*$ (i.e. the ratio of soil-plant conductance to the maximum conductance measured in wet soil and low light

intensity) showed that, in drier soil (at WC = 12.33% and 9.33%), $k*$ reduced with increasing light intensity. Relative soil-plant conductance, $k*$, decreased with increasing light intensity due to higher transpiration rates and with decreasing soil water contents due to the decreasing soil hydraulic conductivity. The reduction was extremely significant at WC = 9.33% where it occurred at light intensity of ca. 1500-2000 μmol m^{-2} s^{-1} (Fig. ES 8b). Note that these were the conditions when transpiration was reduced in the unpressurized plants (Fig. ES 7b and c).
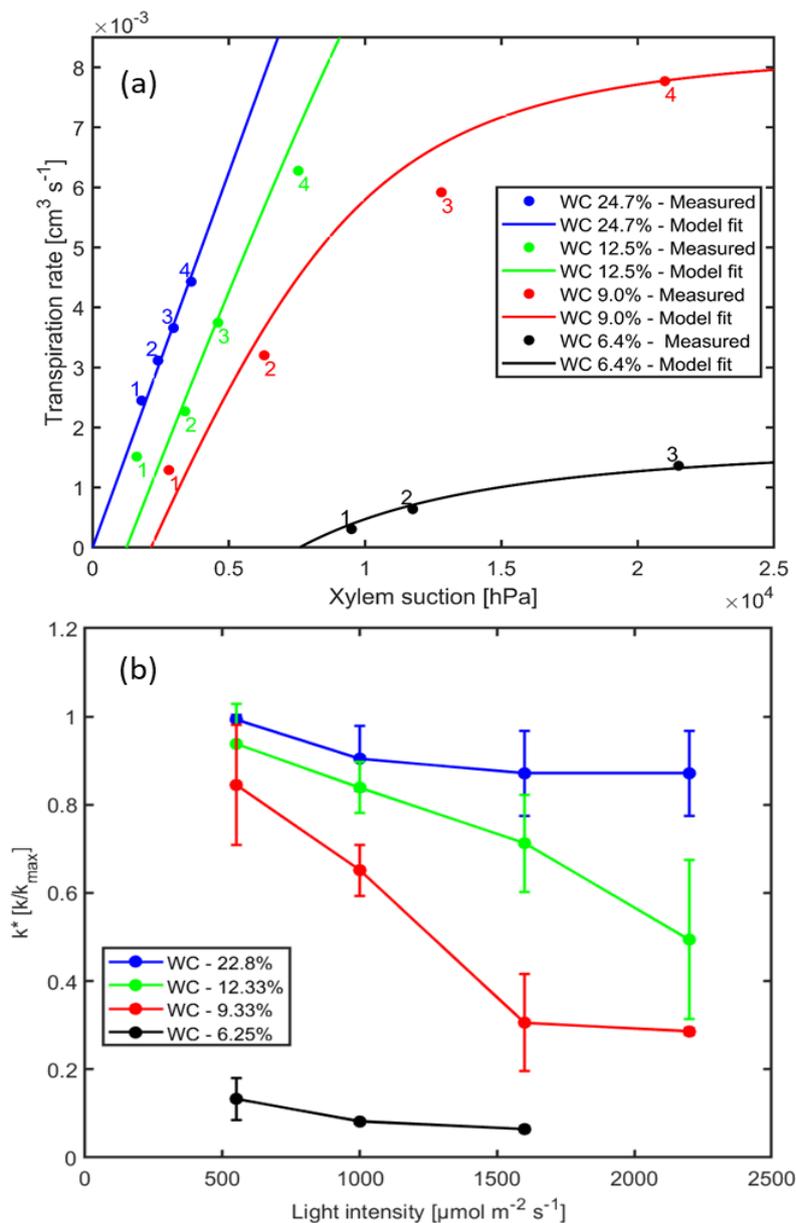
Figure ES 8. (a) Measured xylem suction and transpiration rate for decreasing water contents (WC) and increasing light intensity (1-4). The solid lines are the model fits. (b) Effect of light intensity on normalized soil-plant conductance $k*=k/k_{max}$ (where k_{max} is the soil-plant conductance in the wettest soil and lowest light intensity) at varying soil water contents (WC).

1.4.3   Hydraulic redistribution and nodal root growth (Chapter 4)

Here, I used neutron radiography technique to maize grown in aluminum containers filled with silty soil at two water distributions (dry-wet and wet-wet) to investigated the relative importance of the different types of maize roots (seminal, nodal and their laterals) in hydraulic redistribution. D_2O was injected in the bottom wet compartment and traced its transport in the roots in the top compartment using diffusion-convection model.

The measured average concentrations of D_2O in roots located in the top compartment are presented in Fig. ES 9. In seminal roots the concentration of D_2O increased shortly after D_2O injection during daytime and then it decreased and reached rather constant values during nighttime. The concentration increased again as transpiration restarted in the next morning (Fig. ES 9a). In the dry-wet scenario, D_2O concentration in lateral roots progressively increased during the nighttime. In case of lateral roots, in the wet-wet scenario a slight increase in concentration of D_2O was observed only in the first hour when the plant was still transpiring, while there was no increase overnight (Fig. ES 9b). Finally, we also plot the concentration in the nodal roots, which was similar to those of the laterals (Fig. ES 9c).

A diffusion-convection model (Eq. 6) was used to simulate the measured D_2O concentration in laterals and nodal roots in the dry-wet scenarios. By inversely fitting the measured concentrations we quantified the radial fluxes (j_r) of water during night. The best fits are shown as solid lines in Fig. ES 9 (b & c). For the nodal root whose tip was growing, the axial flux at the root tip was assumed to be equal to the root growth. The best fits for the laterals in the two dry-wet samples were obtained at radial fluxes $j_r = 2.4 \times 10^{-7}$ and $j_r = 2.3 \times 10^{-7}$ cm s^{-1}, respectively. The estimated radial flux in the nodal root was much smaller ($j_r = 1 \times 10^{-11}$ cm s^{-1}) as compared to the laterals, indicating that water was mainly redistributed to the dry soil through the laterals. For the second nodal (denoted by dark yellow color in Fig. ES 9c), the estimated radial flux was much higher ($j_r = 4.7 \times 10^{-7}$ cm s^{-1}) compared to the other nodal. This could be due to less root tip growth and overlapping with seminal roots transporting deuterated water to the shoot. However, the both nodal roots received a significant amount of water to sustain their growth ($J_x = 4.9 \times 10^{-8}$ cm^3 s^{-1} & $J_x = 2.8 \times 10^{-8}$ cm^3 s^{-1}). The estimated fluxes are summarized in Fig. ES 10.
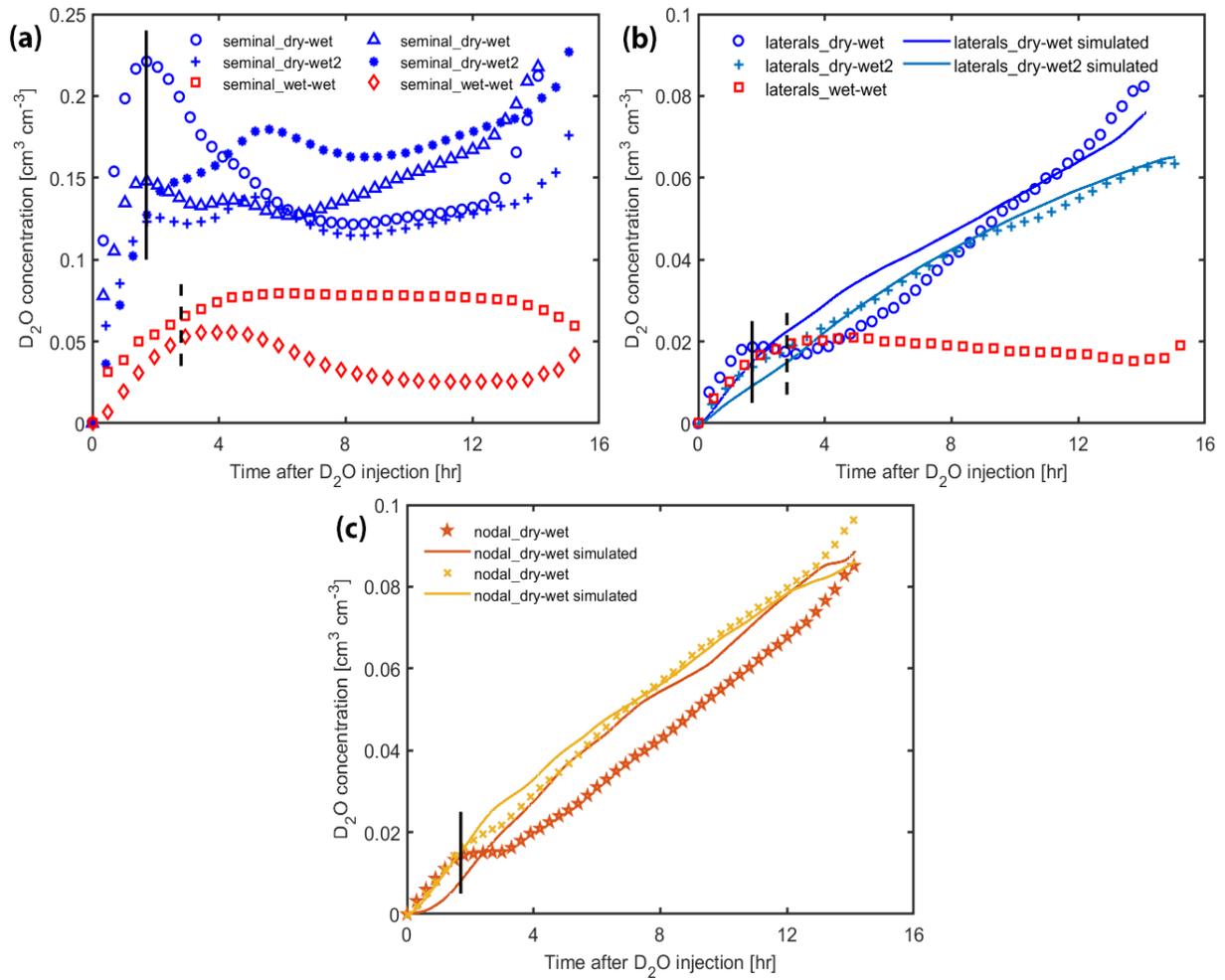
Figure ES 9. Average concentration of deuterated water (D₂O) in (a) seminal (b) lateral and (c) nodal roots in both, dry-wet and wet-wet scenarios. The best fits of the model are shown for the dry-wet scenario in (b and c). The vertical solid and dashed black lines show when the light turned off in the two dry-wet and wet-wet samples, respectively. The R^2 values for the laterals of the two dry-wet samples are .89 and .98, respectively. The R^2 values for the nodal roots are .86 and .96.

Nodal
$j_r = 4.7 \times 10^{-7}$ cm s^{-1}

Nodal
$j_r = 1.0 \times 10^{-11}$ cm s^{-1}

Nodal tip
$J_x = 2.8 \times 10^{-8}$ cm^3 s^{-1}

lateral
$j_r = 2.35 \times 10^{-7}$ cm s^{-1}

Nodal tip
$J_x = 4.9 \times 10^{-8}$ cm^3 s^{-1}
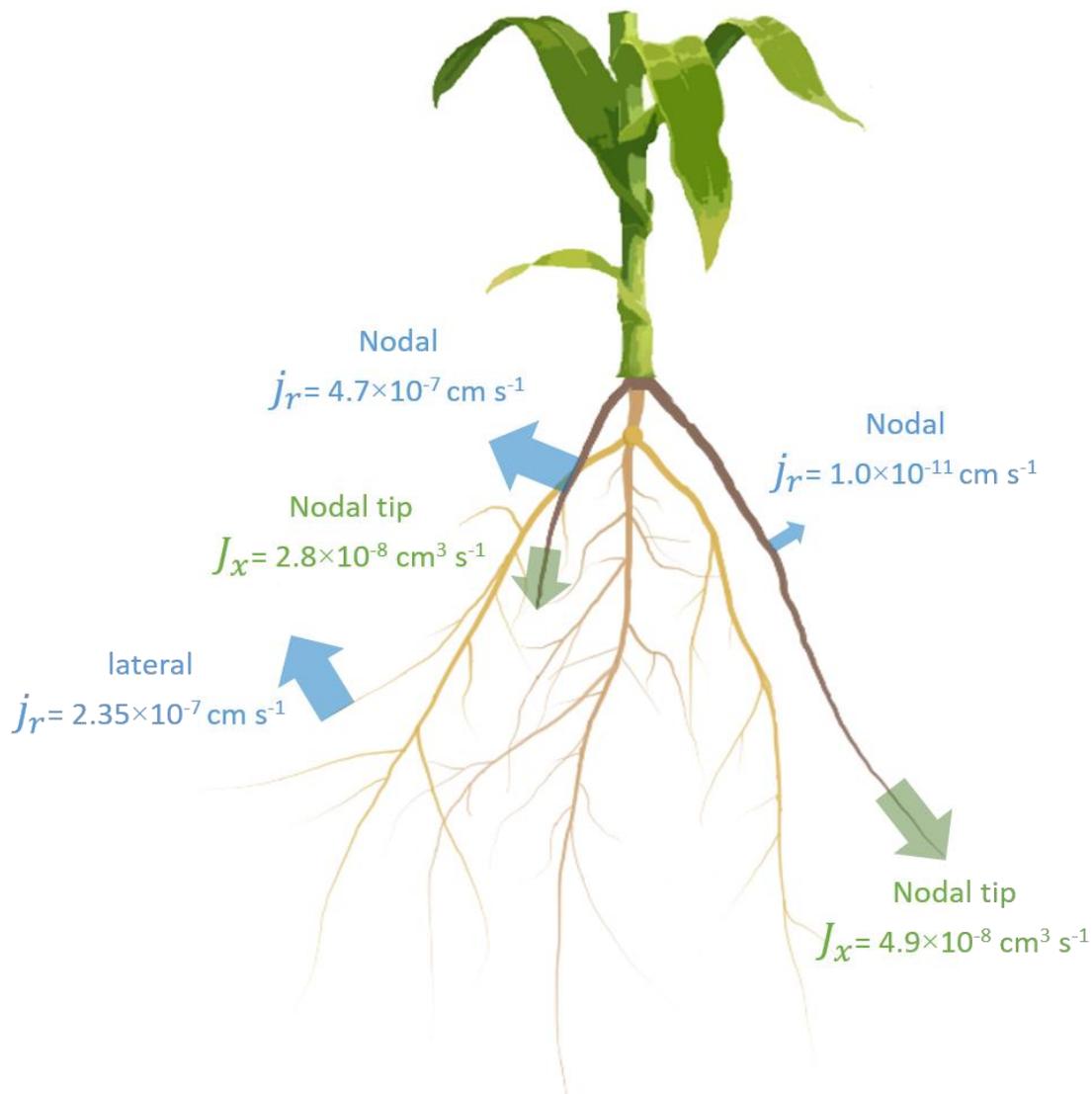
Figure ES 10. The summary of estimated fluxes for lateral and nodal roots. The fluxes of water from the root to the soil are shown in blue. The fluxes of water toward the root tip to sustain root growth are shown in green. j_r is the radial flux of water and J_x is the axial flow of water.

1.5 Conclusion and outlooks

The aim of this dissertation was to gain an understanding of soil-plant interaction at different soil water contents. More specifically, I investigated how different regimes of soil water contents impact soil-plant conductance, stomatal regulation and hydraulic redistribution.

The main conclusion of each chapter is summarized here:

1. In Chapter 2, I showed that the relation between leaf water potential and transpiration rate was linear at both uniform and heterogeneous water contents distribution and it could be well fitted with both, a simple model and a detailed root architecture model of

water uptake. The soil-root system conductance decreased by a factor of 8.26 in the dry-dry scenario as compared to the wet-wet scenario, indicating the limiting role of the soil conductivity on root water uptake. The model results showed that at uniform soil moisture distribution, either being wet-wet or dry-dry scenario, the relative root water uptake depended uniquely on the root properties and its distribution along the root system did not vary with transpiration rate. In the dry-wet scenarios, root water uptake is predicted to shift to the lower and wet layer and both models predicted the occurrence of hydraulic lift in the upper dry soil layer.

2. In Chapter 3, I have shown that reductions in transpiration (stomatal closure) occurred in correspondence to reductions in soil-plant hydraulic conductance preventing marked non-linearity in the relationship between leaf water potential and transpiration rate. Soil-plant hydraulic conductance decreased at high transpiration rates and low soil water contents. This result provides novel experimental evidence supporting the use of soil-plant hydraulic models to predict stomatal response to soil drying.

3. In Chapter 4, I proved the potential of combining neutron radiography, the injection of water isotopes and a diffusion-convection model to visualize and quantify hydraulic redistribution. Hydraulic redistribution was not uniform and varied among root types. The estimated radial fluxes of water from nodal roots were negligible (i.e. $j_r=1\times10^{-11}$ cm s^{-1}) as compared to that from the laterals (i.e. $j_r=2.35\times10^{-7}$ cm s^{-1}), indicating that hydraulic lift occurs mainly from fine roots (laterals). In nodal roots, hydraulic redistribution allowed to sustain the growth of the roots.

In summary, I showed that the soil has a key role on transpiration, leaf water potential and the spatial distribution of root water uptake. The investigated variables, leaf water potential, root water uptake, soil-plant hydraulic conductance, stomatal regulation and hydraulic redistribution, are strongly affected by soil drying. In severe dry conditions, the soil has a limiting role in the location of root water uptake, resulting in a decrease in the total soil-plant conductance and transpiration rate due to a drop in soil-plant hydraulic conductivity. If plants have access to soil water in deeper layers, root water uptake in these layers increase to sustain transpiration. Additionally, at low transpiration rates hydraulic redistribution takes place and sustains root growth. These physiological responses could help plants to sustain growth during drought periods. The techniques used in this study have high potential to solve long-standing questions about plant responses to drying soils. However, their application to larger samples and more natural conditions is challenging.

Here are some recommendations which could follow on or complement the development of these methods used in this dissertation:

In Chapter 2, dynamic processes at the root-soil interface and their impact on hydraulic lift deserve further studies and would require high spatial resolution measurements of water fluxes along the root system. Optimally, such studies would allow for a better understanding of how root-soil interactions impact water fluxes at day and night time. Experiments with different soils, and not only the quartz sand used here, are recommended.

In Chapter 3, I estimated the maize uses only 0.7-2.5% of the total root length to take up water. reality, all roots might take up water, but at variable rates. The active root length and root conductance are physically linked to each other, i.e. the longer the root the larger its interface to soil and the bigger its conductance. These two variables were treated as independently in this study but this could be further investigated using allometric relation.

In Chapter 4, my findings result from a controlled condition experiments, where we grew maize in aluminum containers of 40 cm height. These estimated hydraulic lift are specific of these conditions and not easily extendable to other, more realistic conditions.

1.6   Contribution to included publications

This dissertation is organized as a set of research papers, each of which is one main chapter of this dissertation. Each research paper is either published or accepted to peer-reviewed journals. Chapter 1 is an introductory part including literature review, objectives, materials and methods, summary of main results, conclusions and outlooks of this dissertation.

Chapter 2: Measurements and simulation of leaf xylem water potential and root water uptake in heterogeneous soil water contents by Hayat et al. (2019) published in *Advances in Water Resources*, 124:95-105, doi: https://doi.org/10.1016/j.advwatres.2018.12.009.

Author Contributions: F. H wrote the manuscript under the supervision of A.C. F.H, M.A.A and A.C developed the experimental setup. F.H conducted the experiments with the help of M.A.A. M.Z and F.H conducted the experiments to measure the soil water retention curve and soil hydraulic conductivity using Hyprop. M.Z and A.C developed root water uptake models. F.H simulated the measured data using developed models. G.C helped in improving the quality of scientific language. All authors reviewed and commented on the manuscript.

Chapter 3: Transpiration reduction in maize (*Zea mays* L) in response to soil drying by Hayat et al. (2020) published in *Frontiers in Plant Science*. 10: 1695, doi: 10.3389/fpls.2019.01695.

Author Contributions: F.H carried out the experiments and drafted the manuscript under the supervision of A.C.M. A.A and A.C participated in the design of the experimental setup and results evaluation. F.H conducted the experiments using Sap flow with the help of M.A.A. M.Z measured the soil water retention curve and soil hydraulic conductivity using Hyprop. M.Z and M.J helped in simulation of data. G.C contributed in the revision and performing statistical analysis. All authors reviewed and commented on the manuscript.

Chapter 4: Quantification of hydraulic redistribution in maize roots using neutron radiography by Hayat et al. (2020) published in *Vadose Zone Journal*. E20084, doi: http://doi.org/10.1002/vzj2.20084.

Author Contributions: F.H drafted the manuscript prepared soil-plant samples for neutron radiography under the supervision of A.C. F.H, M.A.A and A.C conducted neutron radiography experiments. T.B helped in experimental setup of neutron radiography. M.Z helped in image analysis and model simulation. All authors contributed in the revision of the manuscript.

1.7   References

Anderegg, W.R.L., Wolf, A., Arango-Velez, A., Choat, B., Chmura, D.J., Jansen, S., Kolb, T., Li, S., Meinzer, F., Pita, P., Resco de Dios, V., Sperry, J.S., Wolfe, B.T., Pacala, S., 2017. Plant water potential improves prediction of empirical stomatal models. PLoS One 12, 1–17. https://doi.org/10.1371/journal.pone.0185481

Bates, L.M., Hall, A.E., Sciences, P., 1981. Stomatal Closure with Soil Water Depletion Not Associated with Changes in Bulk Leaf Water Status. Oecologia 50, 62–65. https://doi.org/https://doi.org/10.1007/BF00378794

Bauerle, T.L., Richards, J.H., Smart, D.R., Eissenstat, D.M., 2008. Importance of internal hydraulic redistribution for prolonging the lifespan of roots in dry soil. Plant, Cell Environ. 31, 177–186. https://doi.org/10.1111/j.1365-3040.2007.01749.x

Bleby, T.M., Mcelrone, A.J., Jackson, R.B., 2010. Water uptake and hydraulic redistribution across large woody root systems to 20 m depth. Plant, Cell Environ. 33, 2132–2148. https://doi.org/10.1111/j.1365-3040.2010.02212.x

Boyer, J.S., 1982. Plant productivity and environment. Science (80). 218, 443–448. https://doi.org/10.1126/science.218.4571.443

Brodribb, T.J., Cochard, H., 2009. Hydraulic failure defines the recovery and point of death in water-stressed conifers. Plant Physiol. 149, 575–584. https://doi.org/10.1104/pp.108.129783

Brodribb, T.J., McAdam, S.A.M., 2017. Evolution of the stomatal regulation of plant water content. Plant Physiol. 174, 639–649. https://doi.org/10.1104/pp.17.00078

Brooks, J.R., Meinzer, F.C., Coulombe, R., Gregg, J., 2002. Hydraulic redistribution of soil water during summer drought in two contrasting Pacific Northwest coniferous forests. Tree Physiol. 22, 1107–1117. https://doi.org/10.1093/treephys/22.15-16.1107

Bücherl, T., Söllradl, S., 2015. NECTAR: Radiography and tomography station using fission neutrons. J. large-scale Res. Facil. JLSRF 1, 8–10. https://doi.org/10.17815/jlsrf-1-45

Buckley, T.N., 2017. Modeling stomatal conductance. Plant Physiol. 174, 572–582. https://doi.org/10.1104/pp.16.01772

Burgess, S.S.O., Adams, M.A., Turner, N.C., Ong, C.K., 1998. The redistribution of soil water

by tree root systems. Oecologia 115, 306–311. https://doi.org/10.1007/s004420050521

Burgess, S.S.O., Adams, M.A., Turner, N.C., White, D.A., Ong, C.K., 2001. Tree roots: Conduits for deep recharge of soil water. Oecologia 126, 158–165. https://doi.org/10.1007/s004420000501

Burgess, S.S.O., Pate, J.S., Adams, M.A., Dawson, T.E., 2000. Seasonal water acquisition and redistribution in the Australian woody phreatophyte, Banksia prionotes. Ann. Bot. 85, 215–224. https://doi.org/10.1006/anbo.1999.1019

Cardon, Z.G., Stark, J.M., Herron, P.M., Rasmussen, J.A., 2013. Sagebrush carrying out hydraulic lift enhances surface soil nitrogen cycling and nitrogen uptake into inflorescences. Proc. Natl. Acad. Sci. U. S. A. 110, 18988–18993. https://doi.org/10.1073/pnas.1311314110

Carminati, A., Moradi, A.B., Vetterlein, D., Vontobel, P., Lehmann, E., Weller, U., Vogel, H.J., Oswald, S.E., 2010. Dynamics of soil water content in the rhizosphere. Plant Soil 332, 163–176. https://doi.org/10.1007/s11104-010-0283-8

Carminati, A., Passioura, J.B., Zarebanadkouki, M., Ahmed, M.A., Ryan, P.R., Watt, M., Delhaize, E., 2017. Root hairs enable high transpiration rates in drying soils. New Phytol. 216, 771–781. https://doi.org/10.1111/nph.14715

Carminati, A., Vetterlein, D., Koebernick, N., Blaser, S., Weller, U., Vogel, H.J., 2013. Do roots mind the gap? Plant Soil 367, 651–661. https://doi.org/10.1007/s11104-012-1496-9

Carter, J.N., Jensen, M.E., Traveller, D.J., 1980. Effect of mid- and late-season water stress on sugarbeet growth and yield. Agron. J. 72, 806–815. https://doi.org/10.2134/agronj1980.00021962007200050028x

Chaumont, F., Tyerman, S.D., 2014. Aquaporins: Highly Regulated Channels Controlling Plant Water Relations. Plant Physiol. 164, 1600–1618. https://doi.org/10.1104/pp.113.233791

Comstock, J.P., 2002. Hydraulic and chemical signalling in the control of stomatal conductance and transpiration. J. Exp. Bot. 53, 195–200. https://doi.org/10.1093/jexbot/53.367.195

Corso, D., Delzon, S., Lamarque, L.J., Cochard, H., Torres-Ruiz, J.M., King, A., Brodribb, T., 2020. Neither xylem collapse, cavitation or changing leaf conductance drive stomatal closure in wheat. Plant. Cell Environ. https://doi.org/10.1111/pce.13722

Couvreur, V., Vanderborght, J., Javaux, M., 2012. A simple three-dimensional macroscopic root water uptake model based on the hydraulic architecture approach. Hydrol. Earth Syst. Sci. 16, 2957–2971. https://doi.org/10.5194/hess-16-2957-2012

Cowan, I.R., 1965. Transport of Water in the Soil-Plant-Atmosphere System. J. Appl. Ecol. 2, 221–239. https://doi.org/10.2307/2401706

Dawson, T.E., 1993. Hydraulic lift and water use by plants: implications for water balance, performance and plant-plant interactions. Oecologia 95, 565–574. https://doi.org/https://doi.org/10.1007/BF00317442

Deery, D.M., Passioura, J.B., Condon, J.R., Katupitiya, A., 2013. Uptake of water from a Kandosol subsoil. II. Control of water uptake by roots. Plant Soil 368, 649–667. https://doi.org/10.1007/s11104-013-1736-7

Domec, J., M, warren J., F.C, M., Brooks, J.., R, C., 2004. Native root xylem embolism and stomatal closure in stands of Douglas-fir and ponderosa pine : mitigation by hydraulic redistribution. Oecologia 141, 7–16. https://doi.org/10.1007/s00442-004-1621-4

Doussan, C., Pierret, A., Garrigues, E., Pagès, L., 2006. Water uptake by plant roots: II - Modelling of water transfer in the soil root-system with explicit account of flow within the root system - Comparison with experiments. Plant Soil 283, 99–117. https://doi.org/10.1007/s11104-004-7904-z

Draye, X., Kim, Y., Lobet, G., Javaux, M., 2010. Model-assisted integration of physiological and environmental constraints affecting the dynamic and spatial patterns of root water uptake from soils. J. Exp. Bot. 61, 2145–2155. https://doi.org/10.1093/jxb/erq077

Ehlert, C., Maurel, C., Tardieu, F., Simonneau, T., 2009. Aquaporin-Mediated Reduction in Maize Root Hydraulic Conductivity Impacts Cell Turgor and Leaf Elongation Even without Changing Transpiration. Plant Physiol. 150, 1093–1104. https://doi.org/10.1104/pp.108.131458

Farooq, M., A.Wahid, Kobayashi, N., Fujita, D., Basra, S.M.A., 2009. Plant drought stress : effects, mechanisms and management. Agron. Sustain. Dev 29, 185–212. https://doi.org/https://doi.org/10.1051/agro:2008021

Flexas, J., Bota, J., Loreto, F., Cornic, G., Sharkey, T.D., 2004. Diffusive and metabolic limitations to photosynthesis under drought and salinity in C3 plants. Plant Biol. 6, 269–

279. https://doi.org/10.1055/s-2004-820867

Gardner, W.R., 1960. Dynamic aspects of water availability to plants. Soil Sci. https://doi.org/10.1097/00010694-196002000-00001

Garrigues, E., Doussan, C., Pierret, A., 2006. Water uptake by plant roots: I - Formation and propagation of a water extraction front in mature root systems as evidenced by 2D light transmission imaging. Plant Soil 283, 83–98. https://doi.org/10.1007/s11104-004-7903-0

Hsiao, T.C., Xu, L.K., 2000. Sensitivity of with of roots versus leaves to water stress: Biophysical analysis and relation to water. J. Exp. Bot. 51, 1595–1616. https://doi.org/10.1093/jexbot/51.350.1595

Jarvis, N.J., 1989. A simple empirical model of root water uptake. J. Hydrol. 107, 57–72. https://doi.org/https://doi.org/10.1016/0022-1694(89)90050-4

Javaux, M., Schröder, T., Vanderborght, J., Vereecken, H., 2008. Use of a Three-Dimensional Detailed Modeling Approach for Predicting Root Water Uptake. Vadose Zo. J. 7, 1079–1088. https://doi.org/10.2136/vzj2007.0115

Knipfer, T., Besse, M., Verdeil, J.L., Fricke, W., 2011. Aquaporin-facilitated water uptake in barley (Hordeum vulgare L.) roots. J. Exp. Bot. 62, 4115–4126. https://doi.org/10.1093/jxb/err075

Koch, G.W., Sillett, S.C., Jennings, G.M., Davis, S.D., 2004. The limits to tree height. Nature 428, 851–854. https://doi.org/https://doi.org/10.1038/nature02417

Lawlor, david W., 2013. Genetic engineering to improve plant performance under drought: physiological evaluation of achievements, limitations, and possibilities. J. Exp. Bot. 64, 83–108. https://doi.org/10.1093/jxb/err313

Lee, E., Kumar, P., Barron-Gafford, G.A., Hendryx, S.M., Sanchez-Cañete, E.P., Minor, R.L., Colella, T., Scott, R.L., 2018. Impact of Hydraulic Redistribution on Multispecies Vegetation Water Use in a Semiarid Savanna Ecosystem: An Experimental and Modeling Synthesis. Water Resour. Res. 54, 4009–4027. https://doi.org/10.1029/2017WR021006

Leffler, A.J., Peek, M.S., Ryel, R.J., Ivans, C.Y., Caldwell, M.M., 2005. Hydraulic redistribution through the root systems of senesced plants. Ecology 86, 633–642. https://doi.org/10.1890/04-0854

Lesk, C., Rowhani, P., Ramankutty, N., 2016. Influence of extreme weather disasters on global crop production. Nature 529, 84–87. https://doi.org/10.1038/nature16467

Martin-StPaul, N., Delzon, S., Cochard, H., 2017. Plant resistance to drought depends on timely stomatal closure. Ecol. Lett. 20, 1437–1447. https://doi.org/10.1111/ele.12851

Matzner, S., Comstock, J., 2001. The temperature dependence of shoot hydraulic resistance: Implications for stomatal behaviour and hydraulic limitation. Plant, Cell Environ. 24, 1299–1307. https://doi.org/10.1046/j.0016-8025.2001.00785.x

McCulley, R.L., Jobbágy, E.G., Pockman, W.T., Jackson, R.B., 2004. Nutrient uptake as a contributing explanation for deep rooting in arid and semi-arid ecosystems. Oecologia 141, 620–628. https://doi.org/10.1007/s00442-004-1687-z

Mencuccini, M., Manzoni, S., Christoffersen, B., 2019. Modelling water fluxes in plants: from tissues to biosphere. New Phytol. 222, 1207–1222. https://doi.org/10.1111/nph.15681

Meyer, W.S., Green, G.C., 1980. Water Use by Wheat and Plant Indicators of Available Soil Water. Agron. J. 72, 253–257. https://doi.org/10.2134/agronj1980.00021962007200020002x

Montgomery, D.R., 2007. Soil erosion and agricultural sustainability. Proc. Natl. Acad. Sci. 104, 13268–13272. https://doi.org/10.1073/pnas.0611508104

Moradi, A.B., Carminati, A., Vetterlein, D., Vontobel, P., Lehmann, E., Weller, U., Hopmans, J.W., Vogel, H.-J., Oswald, S.E., 2011. Three-dimensional visualization and quantification of water content in the rhizosphere. New Phytol. 192, 653–663. https://doi.org/10.1111/j.1469-8137.2011.03826.x

Moradi, A.B., Conesa, H.M., Robinson, B., Lehmann, E., Kuehne, G., Kaestner, A., Oswald, S., Schulin, R., 2009. Neutron radiography as a tool for revealing root development in soil: Capabilities and limitations. Plant Soil 318, 243–255. https://doi.org/10.1007/s11104-008-9834-7

Morton, J.F., 2007. The impact of climate change on smallholder and subsistence agriculture. Proc. Natl. Acad. Sci. 104, 19680–19685. https://doi.org/10.1073/pnas.0701855104

Oswald, S.E., Menon, M., Carminati, A., Vontobel, P., Lehmann, E., Schulin, R., 2008. Quantitative Imaging of Infiltration, Root Growth, and Root Water Uptake via Neutron Radiography. Vadose Zo. J. 7, 1035–1047. https://doi.org/10.2136/vzj2007.0156

Passioura, J., Munns, R., 1984. Hydraulic Resistance of Plants. II. Effects of Rooting Medium, and Time of Day, in Barley and Lupin. Aust. J. Plant Physiol. 11, 341–350. https://doi.org/10.1071/pp9840341

Passioura, J.B., 1988. Water Transport in and to Roots. Annu. Rev. Plant Physiol. Plant Mol. Biol. 39, 245–265. https://doi.org/10.1146/annurev.pp.39.060188.001333

Passioura, J.B., 1980. The Transport of Water from Soil to Shoot in Wheat Seedlings. J Exp Bot. 31, 333–345. https://doi.org/10.1093/jxb/31.1.333

Peters, A., Iden, S.C., Durner, W., 2015. Revisiting the simplified evaporation method: Identification of hydraulic functions considering vapor, film and corner flow. J. Hydrol. 527, 531–542. https://doi.org/10.1016/j.jhydrol.2015.05.020

Redondo, E., Hachez, C., Parent, B., Tardieu, F., Chaumont, F., Simonneau, T., 2009. Drought and Abscisic Acid Effects on Aquaporin Content Translate into Changes in Hydraulic Conductivity and Leaf Growth Rate: A Trans-Scale Approach. Plant Physiol. 149, 2000–2012. https://doi.org/10.1104/pp.108.130682

Rodriguez-Dominguez, C.M., Brodribb, T.J., 2020. Declining root water transport drives stomatal closure in olive under moderate water stress. New Phytol. 225, 126–134. https://doi.org/10.1111/nph.16177

Sakuratani, T., Aoe, T., Higuchi, H., 1999. Reverse flow in roots of Sesbania rostrata measured using the constant power heat balance method. Plant, Cell Environ. 22, 1153–1160. https://doi.org/10.1046/j.1365-3040.1999.00464.x

Saliendra, N.Z., Sperry, J.S., Comstock, J.P., 1995. Influence of leaf water status on stomatal response to humidity, hydraulic conductance, and soil drought in Betula occidentalis. Planta 196, 357–366. https://doi.org/https://doi.org/10.1007/BF00201396

Scholz, F.G., Bucci, S.J., Hoffmann, W.A., Meinzer, F.C., Goldstein, G., 2010. Hydraulic lift in a Neotropical savanna: Experimental manipulation and model simulations. Agric. For. Meteorol. 150, 629–639. https://doi.org/10.1016/j.agrformet.2010.02.001

Schulze, E.D., Caldwell, M.M., Canadell, J., Mooney, H.A., Jackson, R.B., Parson, D., Scholes, R., Sala, O.E., Trimborn, P., 1998. Downward flux of water through roots (i.e. inverse hydraulic lift) in dry Kalahari sands. Oecologia 115, 460–462. https://doi.org/10.1007/s004420050541

Scoffoni, C., Albuquerque, C., Brodersen, C.R., Townes, S. V., John, G.P., Bartlett, M.K., Buckley, T.N., McElrone, A.J., Sack, L., 2017. Outside-xylem vulnerability, not Xylem embolism, controls leaf hydraulic decline during dehydration. Plant Physiol. 173, 1197–1210. https://doi.org/10.1104/pp.16.01643

Scott, R.L., Cable, W.L., Hultine, K.R., 2008. The ecohydrologic significance of hydraulic redistribution in a semiarid savanna. Water Resour. Res. 44, 1–12. https://doi.org/10.1029/2007WR006149

Sekiya, N., Araki, H., Yano, K., 2011. Applying hydraulic lift in an agroecosystem: Forage plants with shoots removed supply water to neighboring vegetable crops. Plant Soil 341, 39–50. https://doi.org/10.1007/s11104-010-0581-1

Sheldon, A.R., Dalal, R.C., Kirchhof, G., Kopittke, P.M., Menzies, N.W., 2017. The effect of salinity on plant-available water. Plant Soil 418, 477–491. https://doi.org/10.1007/s11104-017-3309-7

Simonneau, T., Ehlert, C., Maurel, C., Tardieu, F., 2009. Integrated control of leaf growth by cell turgor in response to combinations of evaporative demands and aquaporin-mediated reductions in root hydraulic conductivity. Comp. Biochem. Physiol. Part A Mol. Integr. Physiol. 153A, S228. https://doi.org/10.1016/j.cbpa.2009.04.572

Sinclair, T.R., Holbrook, N.M., Zwieniecki, M.A., 2005. Daily transpiration rates of woody species on drying soil. Tree Physiol. 25, 1469–1472. https://doi.org/10.1093/treephys/25.11.1469

Smith, D.M., Jackson, N.A., Roberts, J.M., Ong, C.K., 1999. Reverse flow of sap in tree roots and downward siphoning of water by Grevillea robusta. Funct. Ecol. 13, 256–264. https://doi.org/10.1046/j.1365-2435.1999.00315.x

Sperry, John S, Adler, F.R., Campbell, G.S., Comstock, J.P., 1998. Limitation of plant water use by rhizosphere and xylem conductance: Results from a model. Plant, Cell Environ. 21, 347–359. https://doi.org/10.1046/j.1365-3040.1998.00287.x

Sperry, J. S, Adler, F.R., Campbell, G.S., Comstock, J.S., 1998. Hydraulic limitation of flux and pressure in the soil–plant continuum: results from a model. Plant Cell Environ. 21, 347–359.

Sperry, J.S., Hacke, U.G., Oren, R., Comstock, J.P., 2002. Water deficits and hydraulic limits

to leaf water supply. Plant, Cell Environ. 25, 251–263. https://doi.org/10.1046/j.0016-8025.2001.00799.x

Sperry, J.S., Love, D.M., 2015. What plant hydraulics can tell us about responses to climate-change droughts. New Phytol. 207, 14–27. https://doi.org/10.1111/j.1469-8137.2010.03195.x

Sperry, J.S., Wang, Y., Wolfe, B.T., Mackay, D.S., Anderegg, W.R.L., Mcdowell, N.G., Pockman, W.T., 2016. Pragmatic hydraulic theory predicts stomatal responses to climatic water deficits. New Phytol. 212, 577–589. https://doi.org/10.1111/nph.14059

Sprague, L.A., Gronberg, J.A.M., 2012. Relating Management Practices and Nutrient Export in Agricultural Watersheds of the United States. J. Environ. Qual. 41, 1939–1950. https://doi.org/10.2134/jeq2012.0073

Tardieu, F., Davies, W.J., 1993. Integration of hydraulic and chemical signalling in the control of stomatal conductance and water status of droughted plants. Plant. Cell Environ. 16, 341–349. https://doi.org/10.1111/j.1365-3040.1993.tb00880.x

Tardieu, F., Draye, X., Javaux, M., 2017. Root Water Uptake and Ideotypes of the Root System: Whole-Plant Controls Matter. Vadose Zo. J. 16. https://doi.org/10.2136/vzj2017.05.0107

Tardieu, F., Simonneau, T., Parent, B., 2015. Modelling the coordination of the controls of stomatal aperture, transpiration, leaf growth, and abscisic acid: Update and extension of the Tardieu-Davies model. J. Exp. Bot. 66, 2227–2237. https://doi.org/10.1093/jxb/erv039

Tumlinson, L.G., Liu, H., Silk, W.K., Hopmans, J.., 2008. Thermal Neutron Computed Tomography of Soil Water and Plant Roots. Soil Sci. Soc. Am. J. 72, 1234–1242. https://doi.org/10.2136/sssaj2007.0302

Urli, M., Porté, A.J., Cochard, H., Guengant, Y., Burlett, R., Delzon, S., 2013. Xylem embolism threshold for catastrophic hydraulic failure in angiosperm trees. Tree Physiol. 33, 672–683. https://doi.org/10.1093/treephys/tpt030

Walker, T.S., Bais, H.P., Grotewold, E., Vivanco, J.M., 2003. Update on Root Exudation and Rhizosphere Biology Root Exudation and Rhizosphere Biology 1. Updat. Root Exudation Rhizosph. Biol. 132, 44–51. https://doi.org/10.1104/pp.102.019661.

Warren, J.M., Bilheux, H., Kang, M., Voisin, S., Cheng, C., Horita, J., Perfect, E., 2013. Neutron imaging reveals internal plant water dynamics. Plant Soil 366, 683–693. https://doi.org/10.2307/42952412

2   Chapter Two

Measurements and simulation of leaf xylem water potential and root water uptake in heterogeneous soil water contents

Faisal Hayat[1]*, Mutez Ali Ahmed[1,2], Mohsen Zarebanadkouki[1], Gaochao Cai[1], Andrea Carminati[1]

[1]   Chair of Soil Physics, University of Bayreuth, Bayreuth D-95447, Germany

[2]   Division of Soil Hydrology, Georg-August University of Göttingen, Büsgenweg 2,
         37077 Göttingen, Germany

*   Corresponding author: Faisal.Hayat@uni-bayreuth.de

2.1 Abstract

The relationship between leaf water potential, transpiration rate and soil water potential is complex, particularly when the soil water potential in the root zone is not uniform, which is the rule rather than the exception in soils. Our objectives were: 1) to measure the effect of heterogeneous soil water potentials on the relation between leaf water potential and transpiration rate and 2) to test whether root water uptake models could predict this relation. To this end, we combined the root pressure chamber technique, which allows measuring the suction in the leaves of transpiring plants, with two models of root water uptake, a simple one where soil and roots are presented as resistances in series and a more detailed 3D root architecture model. The experiments were carried out with lupines grown in sandy soil, for which the root architecture and root hydraulic properties had been previously estimated. The soil was partitioned in two layers separated by a coarse sand layer that allowed the roots to grow through but limited the water redistribution between the layers. Three scenarios (wet-wet, dry-wet, dry-dry) were tested. The results showed that the relation between transpiration and leaf water potential was linear in all scenarios. As the upper soil layer severely dried, the conductance of the soil-plant system decreased by ca. 1.65 times compared to the conductance of the plant-soil system in a uniform wet soil. As both layers dried, the conductivity was 8.26 times lower compared to the uniform-wet case. The combination of the experiment and modelling showed that a simple model is capable to reproduce the relation between transpiration, leaf water potential and soil water potential (despite an offset in the leaf water potential). Both simplified and the 3D root architecture models were capable of reproducing the measured changes in hydraulic conductance of the plant-soil system due to the soil drying. However, both models overestimated the measured leaf water potential by 0.1 MPa, probably because of a gradient in osmotic potential between the xylem and the soil. The simulations predicted the occurrence of hydraulic lift, even at day time conditions, although the hydraulic lift was relatively more important at low transpiration rates. The simulation suggested that a root architecture model is needed to estimate the variations of water uptake along the individual roots and this might be crucial to properly model hydraulic lift.

2.2   Introduction

Plants transpire large volume of water and understanding what processes control transpiration is important to properly predict water transfer across the soil and the atmosphere. Transpiration rates are controlled by atmospheric conditions and above ground plant properties, such as leaf area and stomata conductance (Ahmed et al., 2018). High vapour pressure deficit (VPD) induce high transpiration rates and loss of leaf water potential (Kholova et al., 2010; Will et al., 2013). Although transpiration does not depend directly on leaf water status, the dependence of stomata conductance on it results in an indirect relation between leaf water potential and transpiration (Tardieu et al., 2015). For instance, it has been hypothesized that plant closes stomata to avoid abrupt increase in xylem tension and reduce the risks of xylem cavitation (Sperry et al., 2002).

Water flows from the soil into the root, across the plant vascular system and then across the stomata to the atmosphere following a gradient in water potential. Transpiration is the driving force of this process. Transpiration generates a suction in the leaves driving water from the soil into the roots. As the soil dries, its water potential and hydraulic conductivity decrease and a more negative leaf water potential is needed for sustaining a given transpiration rate. The effect of drought on physiological traits such as stomatal conductance and leaf water potential is well documented (e.g. Mitchell et al., 2013; Thomas, 2000; Tognetti et al., 1995).

In this study, we investigated the role of soil drying on the relation between leaf water potential and transpiration. The effect of soil drying on root water uptake has been experimentally and numerically investigated since decades (Doussan et al., 2006; Jarvis, 1989; Javaux et al., 2008; Tardieu et al., 2017). In wet soils, the soil hydraulic conductivity has little effect on water uptake, as the hydraulic resistance of the root is much greater than that of the soil (Draye et al., 2010) and the difference in water potential between soil and leaf xylem is linearly related to transpiration (Passioura, 1980). The situation changes as the soil becomes progressively dry, when its hydraulic conductivity decreases and the leaf suction that is needed to drive water from the soil into the roots increases non linearly (Carminati et al., 2017; Passioura, 1980). This non-linearity comes from: 1) microscopic gradients in water potential across the rhizosphere (mm scale); and 2) macroscopic gradients in water potential along the root system (dm scale).

Macroscopic gradients in soil water potential along the root system are the consequence of non-uniform root water uptake (Doussan et al., 2006; Javaux et al., 2008). In a typical drying scenario (neglecting precipitation or irrigation events), the top soil is earlier depleted because

of higher root density and because of dissipation of water potential along the root system (Ahmed et al., 2016; Zarebanadkouki et al., 2016b, 2013). As the upper soil layers dry, water uptake shifts to deeper soil regions (Doussan et al., 2006; Jarvis, 1989).

In such conditions, roots have been reported to redistribute water from deep, wet soil layers to the upper, dry soil layers, in the process called hydraulic lift (HL) (Félicien Meunier et al., 2017; Richards and Caldwell, 1987). The magnitude of HL depends on biological and environmental variables, including atmospheric water demand, the root distribution over depth and gradients in soil water potential (Burgess et al., 2001; Meinzer et al., 2004). Domec et al. (2012) reported that large volumes of water are transported by deep roots to the top soil if the soil texture allows a large potential gradient to occur. HL occurs mainly at night time when transpiration is low and it is reduced by residual water potential gradient generated by plant water storage and nocturnal transpiration (Huang et al., 2017). Water supplied by HL can keep fine roots hydrated (Domec et al., 2004) and delay drying of top soil layers (Brooks et al., 2006), therefore sustaining water uptake during drought. Yu and D'Odorico (2015b, 2014) discussed the role of soil drying in HL and showed that HL is determinant for the coexistence of tree and grass on savannas.

Despite these advancements in our understanding of processes controlling HL and the dynamics of root water uptake in drying soils, several open questions remain: 1) models of HL typically overestimate the rates of HL (Neumann and Cardon, 2012); 2) models of root water uptake that explicitly simulate water flow in soil and roots (Doussan et al., 2006; Javaux et al., 2008) require a large number of parameters that are not easily measurable. One alternative to detailed root water uptake models (e.g. Doussan et al., 2006; Javaux et al., 2008) has been proposed by Couvreur et al. (2012), who showed that the equivalent soil water potential is the average soil water potential weighed based on the local water fluxes. In their model the transpiration rate is equal to the plant conductance multiplied by the xylem collar water potential minus the equivalent soil water potential. This simplified approach is an advantage compared to more detailed hydraulic models because it needs fewer parameters. However, although this simplified model - explicitly simulates the water potential in the xylem collar, it has not been systematically tested versus measurements of xylem collar potential for varying transpiration rates and soil moisture distribution. Finally, it is not clear whether simplified and detailed models of root water uptake differ in the prediction of HL. Our working hypothesis is that monitoring xylem water potential and transpiration for varying soil moisture distribution is a key to test models of root water uptake and HL.

Therefore, the objectives of this paper were:

I.   To measure the relation between leaf xylem water potential and transpiration rates for heterogeneous soil water distributions.

II. To test the ability of a detailed root water uptake model (Javaux et al., 2008) and of a simplified model (Couvreur et al., 2012) to reproduce the experimental relation between xylem water potential and transpiration rates.

III. To compare the HL simulated by the detailed and simplified model.

For the objective I) we applied the root pressure chamber method developed by Passioura (1980) to lupines (*Lupinus Albus* L.) growing in sandy soils with three soil water distributions: 1) the upper and lower layers were wet (homogeneous water content); 2) the upper soil layer was let dry while the lower one was maintained wet (heterogeneous water content); and 3) both soil layers were let dry (homogeneous water content). The method was used to monitor the leaf suction for varying transpiration rates and the three degrees of soil water contents (1-3).

2.3   Materials and methods

2.3.1   Soil and plant preparation

Lupines were grown in PVC columns of 30 cm height and 14 cm diameter. The pots were filled with quartz sand (particle size < 500 μm). The soil retention curve and the soil hydraulic conductivity of sand were characterized using the extended evaporation method (Peters and Durner, 2008; Schindler et al., 2010). This method was implemented in Hyprop (UMS, Munich, Germany), a commercial device that monitors evaporation rates and soil matric potentials at two depths. A soil core of 5 cm in length and 4 cm in diameter was filled with quartz sand at a bulk density of 1.52 g cm^{-3}. Soil matric potential at two depths and evaporation rate were recorded during drying at the constant temperature of 25°C. The hydraulic parameters were estimated by inversely simulating the measured matric potentials solving the Richard's equation. The Richard's equation was solved in Matlab (2016) using a fully implicit Euler time discretization and a centered finite difference space discretization scheme (Celia and Binning, 1992).

Soil water retention curve and the hydraulic conductivity curve were parameterized using the PDI model (Peters-Durner-Iden model) (Peters et al., 2015) and were inversely adjusted to best reproduce soil water content and matric potentials. The soil columns were partitioned into two

soil layers separated at a depth of 13 cm by one-cm thick layer of fine gravel (particle size of 2-3 mm). This layer of fine gravel was used to hydraulically disconnect the upper and lower soil layers without hindering root growth so that we could easily impose heterogeneous soil water contents (Fig. 1a). The pots were filled in such a way that the packed soil bulk density was 1.4 g cm^{-3}. Several holes with a diameter of 1.5 mm were placed at the bottom and sides of the pots. The holes at the bottom allowed water drainage and the holes on sides allowed to inject water using a fine needle. The soil surface of each pot was covered with fine gravels from 2 to 3.5 mm to minimize evaporation from the soil surface.
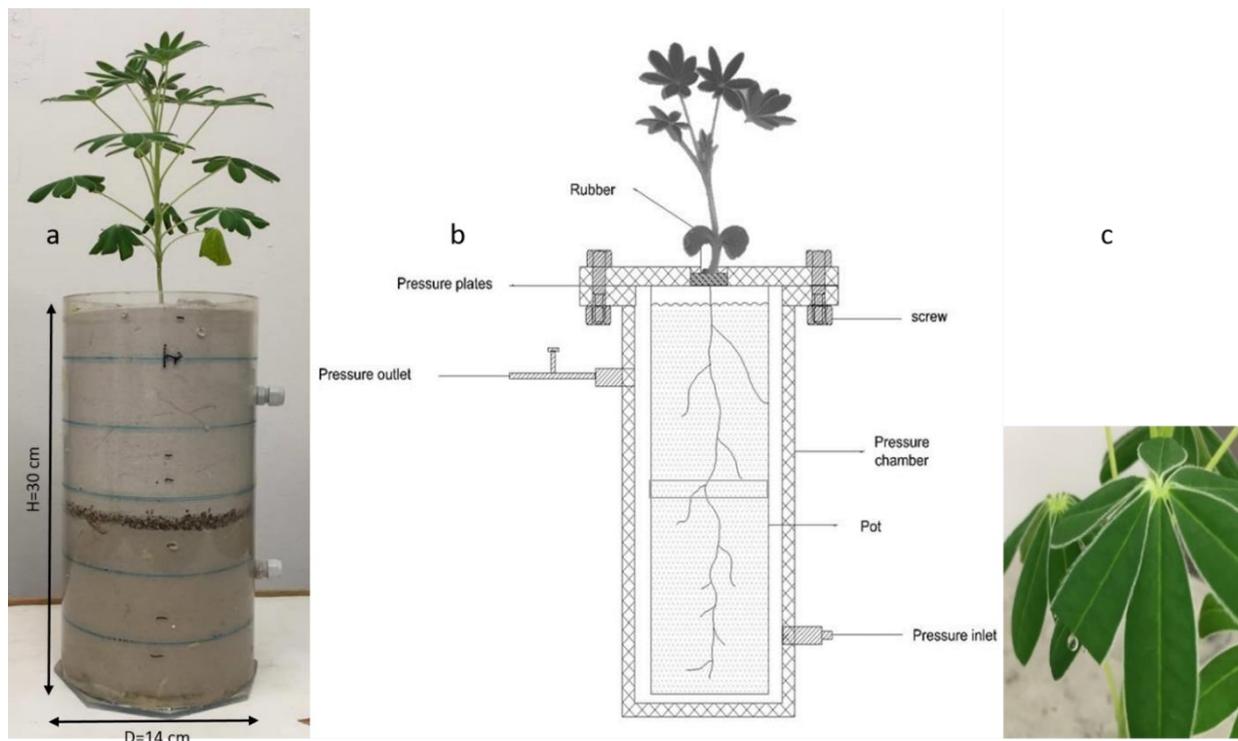
Fig. 1. Plant grown in soil with varying moisture levels; (b) comprehensive experimental setup; (c) water droplet from a cut leaf when the balancing pressure is applied.

Lupine seeds were germinated on moist filter paper for 24 hours and then planted into the pots (one seed per pot). The plants were grown in a climate room with a photoperiod of 14 hours, day/night temperature of 25°C/22°C and light intensity of 200 µmol m^{-2} s^{-1}. During the first two weeks, the samples were regularly irrigated to maintain the soil water content in both compartments at approximately 25%. After the root system grew throughout both compartments, the soil water content was adjusted to the following three scenarios: i) both the top and bottom soil layers were kept at a water content of 15-20% (wet-wet); ii) the top compartment was let dry to a water content of 2-5% while the bottom compartment was kept at a water content between 15-20% (dry-wet); and iii) both top and bottom compartments were

let dry to a water content of 2-5% (dry-dry). The soil moisture was gravimetrically determined every three days by collecting soil samples in each soil layer using a micro auger. The soil moisture content was measured at three different heights (4, 8, and 12 cm from the bottom) in the bottom compartment and at three points (18, 22 and 26 cm from the bottom) in the top compartment.

2.3.2   Root Pressure chamber

The root pressure chamber method allows measuring the relationship between transpiration rate and the pressure drop across the plant-soil continuum. The technique is described in detail in Passioura (1980). The PVC cylinders filled with soils and the intact and growing roots were enclosed in a pressure chamber with a sealing at the root-shoot junction (Fig. 1b). The plant shoot remained outside the pressure chamber and was illuminated horizontally by a LED lamp. Varying the distance between LED and shoots provided a photosynthetic photon intensity ranging from 98.9 to 1334 [μmol m^{-2} s^{-1}]. The photosynthetic photon intensity was changed to impose different transpiration rates. Transpiration was estimated gravimetrically by weighing the pots between two different time intervals. One leaf was cut and the pneumatic pressure in the chamber was increased until a drop of water at a cut leaf (Fig. 1c). Note that the chamber was pressurized with 99.999% vol. N_2. The pressure needed to maintain the drop of water at the cut leaf is called balancing-pressure ($P_{balancing}$) and it is equal to the suction in the xylem prior to pressurization (Passioura, 1980). Plants were imposed to three different transpiration rates by changing the photosynthetic photon intensity and let transpire for 30 min. Thereafter the balancing pressure and the transpiration rates were measured. The root pressure chamber experiments started when the plants were 45 days old. The experiments were performed for three scenarios of soil moisture contents (wet-wet, dry-wet, dry-dry) and three transpiration rates. Prior to the experiments, the soil moisture in each compartment was determined by collecting soil samples using micro auger through the holes in the pots. We measured soil moisture contents [%] in each compartment, recorded the transpiration rate [g h^{-1}] and the balancing pressure [hPa] at each light intensity for all replications. The time interval between each measurement was 30 minutes. We performed three replications for both uniformly-wet and top dry-bottom wet and one replication for uniformly-dry scenarios.

2.3.3 Root collection

At the end of each experiment, the soil was gently washed away from the roots. The roots grown in each compartment were collected and their total root length and radius were measured with the software WinRhizo 2008a image analysis system (reagent instruments Inc., Canada). The root segments were opened on A3 plexiglass tray of the WinRhizo flatbed scanner (Epson STD 4800) equipped with a double light source to avoid root overlapping. The images were acquired using the TWAIN interface at 800 dpi resolution. The root distribution in both compartments is shown in Table. S1 (Supplementary data).

2.3.4 Simplified model of root water uptake

Couvreur et al. (2012) showed that the relation between transpiration rate Q [cm^3 h^{-1}], collar xylem water potential H_x [hPa] and soil matric potential H_s [hPa] can be written as:

$$Q = -K_{rs}(H_x - H_{s,eq}) \qquad \text{(Eq. 1)}$$

where K_{rs} is the equivalent conductance [cm^3 hPa^{-1} h^{-1}] of the root system and $H_{s,eq}$ is an equivalent soil water potential averaged according to the Ohm analogy. Note that H_x and $H_{s,eq}$ are the sum of the gravitational and hydrostatic potential (matric potential for the soil). Eq. 1 predicts that the relation between transpiration rate and the hydraulic gradient is linear and that at no transpiration the leaf water potential is equal to that of the soil – i.e. there is an equilibrium between xylem and soil water. Eq. 1 neglects difference in osmotic potential between xylem and soil. The osmotic potential can be added in Eq. 1 as:

$$Q = -K_{rs}\left(\left(H_x - H_{s,eq}\right) + \sigma\left(H_{x,osmotic} - H_{s,osmotic}\right)\right) \quad \text{(Eq. 2)}$$

where $H_{x,osmotic}$ and $H_{s,osmotic}$ are the osmotic potential [hPa] in the xylem and soil, and σ is the reflection coefficient [-], which is 1 for selective membrane and 0 for non-selective membrane. Neglecting the osmotic potential is equivalent to assume that there is no membrane limiting the transport of solutes from the soil solution to the xylem or that the osmotic potential in the xylem and the soil are equivalent. In this study we used Eq. 1. Possible offsets between measured and simulated $H_{s,eq}$ could be explained by the osmotic pressure in Eq. 2.

To illustrate the meaning of the parameters K_{rs} and $H_{s,eq}$ we choose a simplified root system illustrated in Fig. 2 representing the experimental setup. For this set-up K_{rs} and $H_{s,eq}$ are given by:

$$K_{rs} = \left(\frac{1}{K_{x1}} + \frac{1}{\left(\frac{1}{K_{r1}}+\frac{1}{K_{s1}(h)}\right)^{-1}+\left(\frac{1}{K_{x2}}+\frac{1}{K_{r2}}+\frac{1}{K_{s2}(h)}\right)^{-1}} \right)^{-1} \quad \text{(Eq. 3)}$$

where K_{r1}, K_{r2} are the radial conductances [cm^3 hPa^{-1} h^{-1}] of the roots in the upper and lower soil layers, K_{x1} and K_{x2} are the axial conductances [cm^3 hPa^{-1} h^{-1}] of the roots in the upper and lower soil layers, and $K_{s1}(h)$, $K_{s2}(h)$ are the conductances [cm^3 hPa^{-1} h^{-1}] of the soil calculated as (Nobel and Cui, 1992):

$$K_s(h) = \frac{2\pi l}{ln\left(\frac{r_{soil}}{r_{root}}\right)} \cdot k(h) \quad \text{(Eq. 4)}$$

where r_{soil} is the radius of the soil cylinder, r_{root} is the root radius, l is the length of the root segment [cm] in each soil layer and $K_s(h)$ is the hydraulic conductivity [cm h^{-1}] of soil as a function of the soil matric potential h [cm]. This equation converts the units of k [cm h^{-1}] into units of K_s [cm^3 hPa^{-1} h^{-1}] and the soil water potential needs to be expressed as centimeter heads (1 hPa $\approx$ 1 cm). The equivalent soil water potential is given by:

$$H_{s,eq} = \left(\frac{\left(\frac{1}{K_{r1}}+\frac{1}{K_{s1}(h)}\right)^{-1}}{\left(\frac{1}{K_{r1}}+\frac{1}{K_{s1}(h)}\right)^{-1}+\left(\frac{1}{K_{x2}}+\frac{1}{K_{r2}}+\frac{1}{K_{s2}(h)}\right)^{-1}} \times H_{s1} + \frac{\left(\frac{1}{K_{x2}}+\frac{1}{K_{r2}}+\frac{1}{K_{s2}(h)}\right)^{-1}}{\left(\frac{1}{K_{r1}}+\frac{1}{K_{s1}(h)}\right)^{-1}+\left(\frac{1}{K_{x2}}+\frac{1}{K_{r2}}+\frac{1}{K_{s2}(h)}\right)^{-1}} \times H_{s2} \right) \quad \text{(Eq. 5)}$$

where H_{s1} and H_{s2} are the soil water potential in the upper and lower soil layers. Note that the sum of two terms by which the soil matric potentials H_{s1} and H_{s2} are multiplied is 1.

The measured balancing pressure, $P_{balancing}$ [hPa], is numerically equivalent to the suction in the xylem:

$$P_{balancing} = -H_x \quad \text{(Eq. 6)}$$

where the gravitational potential at the xylem collar is set to zero. If the osmotic potential of soil and xylem are equivalent or the reflection coefficient is null, $P_{balancing}$ is equivalent to minus the xylem water potential. Eq. 1 predicts that when $Q = 0$, $P_{balancing} = -H_{s,eq}$.

If the osmotic potential is included (Eq. 2), when $Q = 0$:

$$P_{balancing} = -H_{s,eq} + \sigma\left(H_{x,osmotic} - H_{s,osmotic}\right) \quad \text{(Eq. 7)}$$

We used the model without osmotic potential (Eq. 1) to fit the measured *Q(P)* relation.
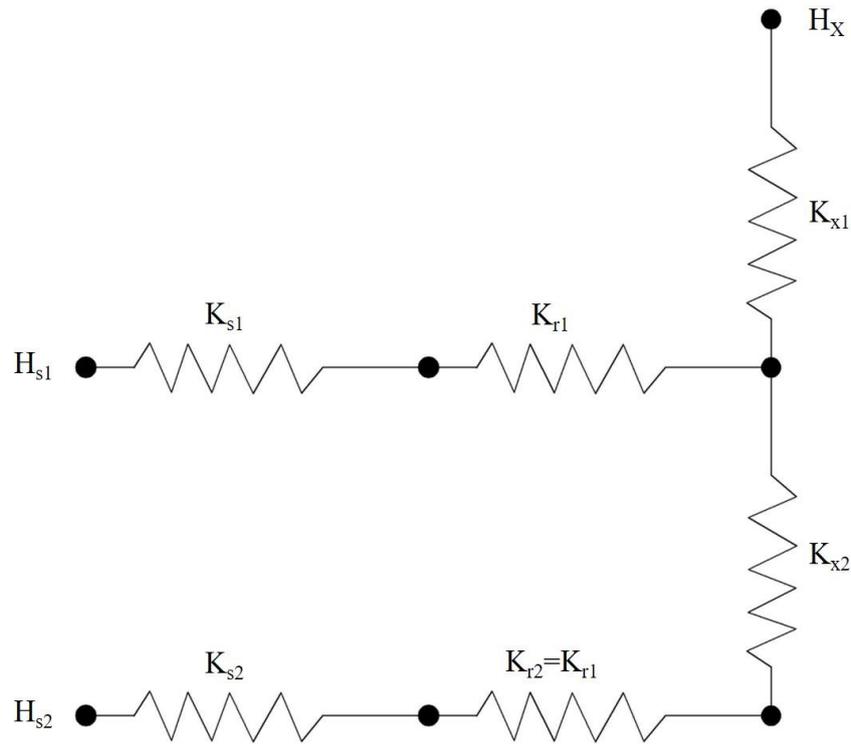
Fig. 2. Schematic of a simplified root system model used for simulation of root water uptake. Here, K_s, K_r and K_x are the conductance of the soil, the radial and the axial conductance of the root segments located in each soil layer. H_s and H_x are the soil water potential and the axial water potential at the collar of the plant, respectively. The subscripts 1 and 2 refer to the upper and lower layer, respectively.

2.3.5   Modelling of water flow into root system

The hydraulic tree model of Doussan et al. (1998) and implemented as in Javaux et al. (2008) was used to simulate root water uptake. The root architecture is represented as a system of interconnected nodes in which water flows radially from the root xylem and longitudinally along the xylem vessels. The root system is divided into small segments with uniform length of 5×10^{-2} cm. The radial flow Q_r [$cm^3 h^{-1}$] between the soil-root interface and root xylem is:

$$Q_r = -k_r \, s_r [H_s - H_x] = -K_r [H_s - H_x] \qquad \text{(Eq. 8)}$$

where H_s and H_x are the water potential at root surface and in the xylem [hPa], respectively, s_r is the cross section of root segment [cm^2], k_r is the root radial conductivity [$cm \, hPa^{-1} \, h^{-1}$] and K_r is the radial conductance of the segment [$cm^3 \, hPa^{-1} \, h^{-1}$]. In Eq. 8 Q_r is negative when the flow is towards the root – i.e. it is minus the root water uptake. The total water potential is the sum of matric potential and the gravitational potential, while the osmotic potential is not

taken into account. This equation does not take into account the dissipation of water potential in the soil. Therefore, to include the conductance of the soil, this equation was modified as:

$$Q_r = -K_{eff}(H_s - H_x) \qquad \text{(Eq. 9)}$$

where K_{eff} is an effective radial conductance of root-soil system [cm^3 hPa^{-1} h^{-1}] calculated as following:

$$K_{eff} = \frac{1}{\frac{1}{K_s(h)} + \frac{1}{K_r}} \qquad \text{(Eq. 10)}$$

where $K_s(h)$ is an effective soil hydraulic conductance given by:

$$K_s(h) = \frac{2\pi l}{ln\left(\frac{r_{soil}}{r_{root}}\right)} \cdot k(h) \qquad \text{(Eq. 11)}$$

where $k(h)$ is the soil hydraulic conductivity as a function of the matric potential h, l is the length of root segment [cm]. Here it is assumed that each root with radius r_{root} has access to a cylindrical region with an outer radius of $r_{soil} = \sqrt{V_{tot}/(\pi L_{tot})}$, where V_{tot} is the soil volume [cm^3] and L_{tot} is the total root length [cm]. Eq. 11 assumes no change in hydraulic conductivity as a function of distance to the root surface and therefore underestimates the gradient in water potential around the roots.

The axial water flow within each root segment Q_x [cm^3 h^{-1}] is described as:

$$Q_x = -\frac{k_x}{l} dH_x = -K_x[dH_x + dz] \qquad \text{(Eq. 12)}$$

where H_x is water potential in xylem, k_x is axial conductivity [cm^4 hPa^{-1} h^{-1}], h_x is xylem hydrostatic potential, z is the distance of each segment from the soil surface [cm] and K_x is axial conductivity. Applying these equations to all nodes of the root system, the radial flow of water into each root segment can be described as a system of linear equations. The details were described in Zarebanadkouki et al. (2016) and Doussan et al. (1998).

The model was used to fit the root pressure chamber experiments and to calculate the water uptake in each compartment. Note that the model can only simulate steady-state conditions and no changes in soil water content. This assumption is justified by the small time scale of the experiments and the consequent small amount of water removed from the soil samples during the measurements (less than 0.1% changes in the water contained in the sample). Additionally, the model does not include the osmotic potential.

2.3.6   Model Parameterization

The linear system of Eq. 8-12 was solved in Matlab (2016) under fixed soil water potential and transpiration rates (which was measured during pressure chamber experiments) taken as boundary conditions. The soil matric potential was obtained from the soil retention curve and the measured soil water content at three different points in each compartment. The soil water potential was assumed to be uniform within each soil layer. The soil hydraulic conductivity was estimated using HyProp (UMS, Munich, Germany) and assumed to be uniform in each compartment. The root architecture was extracted from previous experiments (Zarebanadkouki et al. 2013). The profile of axial and radial conductances was taken from the estimation of Zarebanadkouki et al. (2016). These root properties were used as initial guess to fit xylem water potential and to simulate water uptake for all the three soil moisture scenarios (wet-wet, dry-wet, dry-dry).

After implementation and parametrization of the root architecture model of Doussan et al. (1998), a forward simulation approach was used to estimate the profile of root water uptake and xylem water potential along the root system of plants growing at different soil water contents and being imposed to different transpiration rates (which was measured during pressure chamber experiment). Given the boundary condition and the transpiration rates, the estimated xylem water potential at the collar of the plant was compared with the balancing pressure obtained from the pressure chamber. As the osmotic component of water potential in the soil and the xylem was neglected during our modelling approach (not known to us), the estimated value of balancing pressure would not be comparable to the measured value. To compare the measured and estimated value of balancing pressure a constant value was added to the simulated xylem water potential at the collar of the plant. This constant is equal to the difference in osmotic potential between the soil surface (or a point outside the endodermis) and the leaf xylem (Eq. 7) and varied between different scenarios.

Note that as we did not simulate soil water distribution over time the choice of using a different architecture (from a quasi 2D container) is not critical. Instead, the distribution of radial and axial conductances as well as their absolute values is critical, and so is the total root length. Note also that the total root length in the simulation and in the experiments was similar. We started from the root parameters derived by Zarebanadkouki et al. (2016) and adapted them to match the experimental results.

2.4   Results

The fitting of the soil evaporation experiment, the water retention curve and hydraulic conductivity are shown in Fig. 3. The sandy soil was characterized by a steep decrease in water content at a matric potential between -40 and -100 hPa and a corresponding drop in hydraulic conductivity.
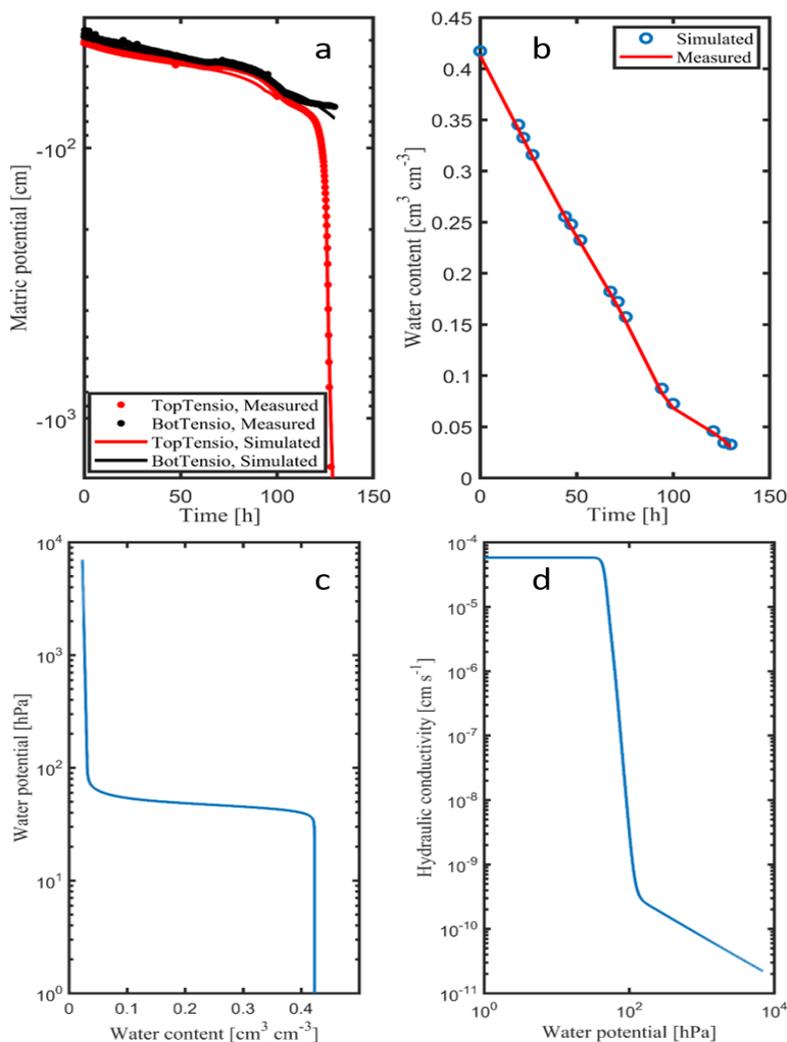
Fig. 3. Measured and fitted (a) matric potentials [cm] and (b) soil water content [cm³ cm⁻³] during the evaporation experiment. (c, d) Fitted soil hydraulic properties.

The comprehensive data set of pressure chamber experiments are shown in Fig. 4 together with the fitting of the simplified model and the root architecture model (see also supplementary data Table. S2). Fig. 4 shows the relationship between transpiration rate and balancing pressure for the three different scenarios (wet-wet, dry-wet, dry-dry). The relationship between transpiration and balancing pressure was linear in all scenarios. The slope of the curves, which is interpreted as the conductance of the soil-root system, decreased by a factor of 1.65 from the

wet-wet to the dry-wet treatment. In the dry-dry treatment, the conductance was severely reduced by a factor of 8.26, and the transpiration was also strongly reduced. The intercept (the balancing pressure at null transpiration) decreased from -1040 hPa in the wet-wet scenario to ca. -1700 hPa in the other two scenarios (dry-wet and dry-dry).
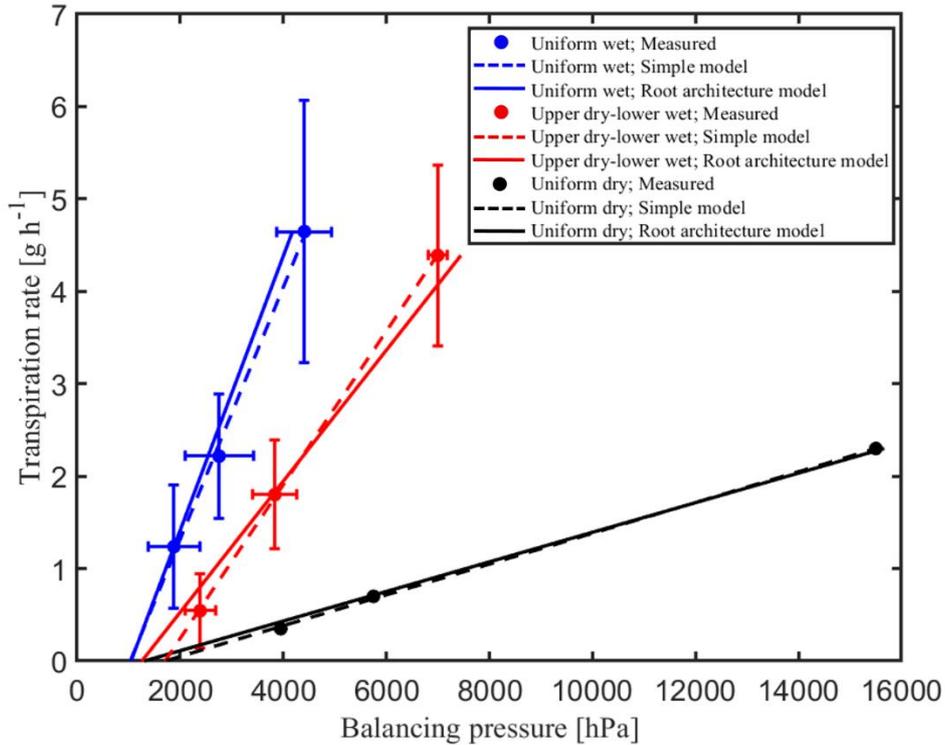
Fig. 4. Measured transpiration rate [g h^{-1}] and balancing pressure [hPa] for each scenario. The dotted lines are the fitting using simplified model and solid lines are the simulation results using the root architecture model.

The linear relation of Eq. 1 is capable of fitting the measurements. The fitting parameters are reported in Table 1.

Table 1. Fitted plant conductances (K_{rs}) and equivalent soil water potential ($H_{s,eq}$) for each soil water content scenario.

Scenario	K_{rs} [cm^3 h^{-1} hPa^{-1}]	$H_{s,eq}$ [hPa]
wet-wet	1.37×10^{-3}	-1040
dry-wet	8.28×10^{-4}	-1700
dry-dry	1.66×10^{-4}	-1730

Let us now discuss the meaning of the parameters K_{rs} and $H_{s,eq}$. We start with $H_{s,eq}$.

For the wet soil layer (θ = 15-20%) we expect a soil matric potential of -30 to -50 hPa. For the dry soil (θ = 2-5%) we expect a soil matric potential of ca. -1000 hPa, but because the shape of the water retention curve (Fig. 3) the error in the dry range is expected to be high.

For the wet-wet scenario, with both layers at a matric potential >-50 hPa, Eq. 1 would give an equivalent soil water potential of -50 hPa, which is far from the measured $H_{s,eq}$ in Table 1. It means that an additional potential of ca. -1000 hPa acts on the plant. One explanation is that this additional potential is of osmotic nature and could be caused by a difference in osmotic potential between the xylem and a point before the endodermis, being it the cortex or the root soil interface, as predicted by Eq. 7. We will discuss this and other explanations in the Discussion and Conclusions.

For the dry-dry scenario, the fitted $H_{s,eq}$ is -1700 hPa. Because the matric potential is highly variable in sand, it is possible that the offset of -1000 hPa was still acting in the dry-dry soil with the soil matric potential explaining the remaining -700 hPa or that the soil matric potential was -1700 hPa.

For the dry-wet scenario, we expect that the soil conductance reduces the importance of H_{s1} on $H_{s,eq}$. In other words, we expect that the plant would feel mainly the water potential of the lower soil layer where most of the water is taken up from. Eq. 5 would predict $H_{s,eq}$ to be close to the matric potential of the wet, lower soil layers. However, because of the uncertainties in the offset (the claimed osmotic potential) would be difficult to make a conclusive statement. Indeed, it could be that the offset becomes more negative, or that the soil matric potential in the upper layer was much more negative than -1000 hPa.

In summary, from the analysis of $H_{s,eq}$ it results that the $H_{s,eq}$ becomes more negative as the soil dries out, as expected. However, the value of $H_{s,eq}$ seems to be more negative than the one expected, particularly in wet soils. The origin of such deviation is probably of osmotic nature, originating from a difference in osmotic potential between the xylem and the root surface (the latter being at more negative osmotic potential than the xylem) as given by Eq. 7. Other explanations are discussed later in the Discussion and Conclusions.

The plant conductances K_{rs} were analyzed according to Eq. 3-4. The simplified model is capable to describe the measured K_{rs}. Taking a reasonable soil conductivity of k=10^{-5} cm s^{-1} for the wet layers and k=3x10^{-11} cm s^{-1} for the dry ones (based on Fig. 3) and inversely estimating the radial and axial conductances of the simplified root system shown in Fig. 2 gives

a good match of the measured K_{rs} without additional assumptions. The obtained conductances are shown in Table 2. In the wet soil layers, the soil conductance (36 cm^3 h^{-1} hPa^{-1}) was much higher than the radial root conductance (7.20x10^{-4}), but in dry soils the soil conductance was much lower (1.08x10^{-4}). This explains the reduction of K_{rs} in dry soil layers.

In summary, the simplified model is capable of reproducing the relation between leaf suction and transpiration for varying soil moistures, and the soil and root conductances to explain such behavior are physically sound. Note that the objective of these calculations was not to determine the conductances of the different root segments but rather to test whether Eq. 3 could be used to reproduce the relation between leaf suction and transpiration with physically sound parameters. This was the case for the conductances, but not for the equivalent soil water potential, particularly in drying soils.

Table 2. Estimated radial and axial conductances for the best fit of plant conductances (K_{rs}).

Ks wet [cm^3 h^{-1} hPa^{-1}]*	Ks dry [cm^3 h^{-1} hPa^{-1}]*	$K_{r1} = K_{r2}$ [cm^3 h^{-1} hPa^{-1}]**	K_{x1} [cm^3 h^{-1} hPa^{-1}]	K_{x2} [cm^3 h^{-1} hPa^{-1}]
36	1.08x10^{-4}	7.20x10^{-4}	0.432	2.88x10^{-2}

*estimated based on the measured retention curve and unsaturated conductivity; **The radial root conductances of the upper and lower layers were imposed to be equal.

Once these conductances are estimated, they can be used to predict the local water uptakes in each scenario (Table. 3).

Table 3. . Relative water uptake [%] in upper and lower layers obtained using the simplified model of root water uptake. Negative values indicate water efflux and occurrence of hydraulic lift.

Low transpiration rate	upper layer	lower layer	Medium transpiration rate	upper layer	lower layer	High transpiration rate	upper layer	lower layer
wet-wet	50.60	49.40	wet-wet	50.60	49.40	wet-wet	50.60	49.40
dry-wet	-2.82	102.82	dry-wet	7.65	92.35	dry-wet	10.29	89.71
dry-dry	50.08	49.92	dry-dry	50.08	49.92	dry-dry	50.08	49.92

The more complex architecture model based on the parameterization of Zarebanadkouki et al. (2016) was capable to reproduce the measurements, provided that the simulated xylem water potential at the plant collar was reduced by 1000 hPa. As for the simplified model, this value can be interpreted as the osmotic potential difference between the xylem and a point outside

the endodermis. For all curves, the relation between transpiration rate and leaf suction was linear. The intercept of the line with x-axis indicates the equivalent soil water potential experienced by the plant. Note that the root distribution in each compartment was equal (i.e. 50%).

The root architecture model provides the water potential in the root system. Fig. 5 shows the distribution at medium light intensity.
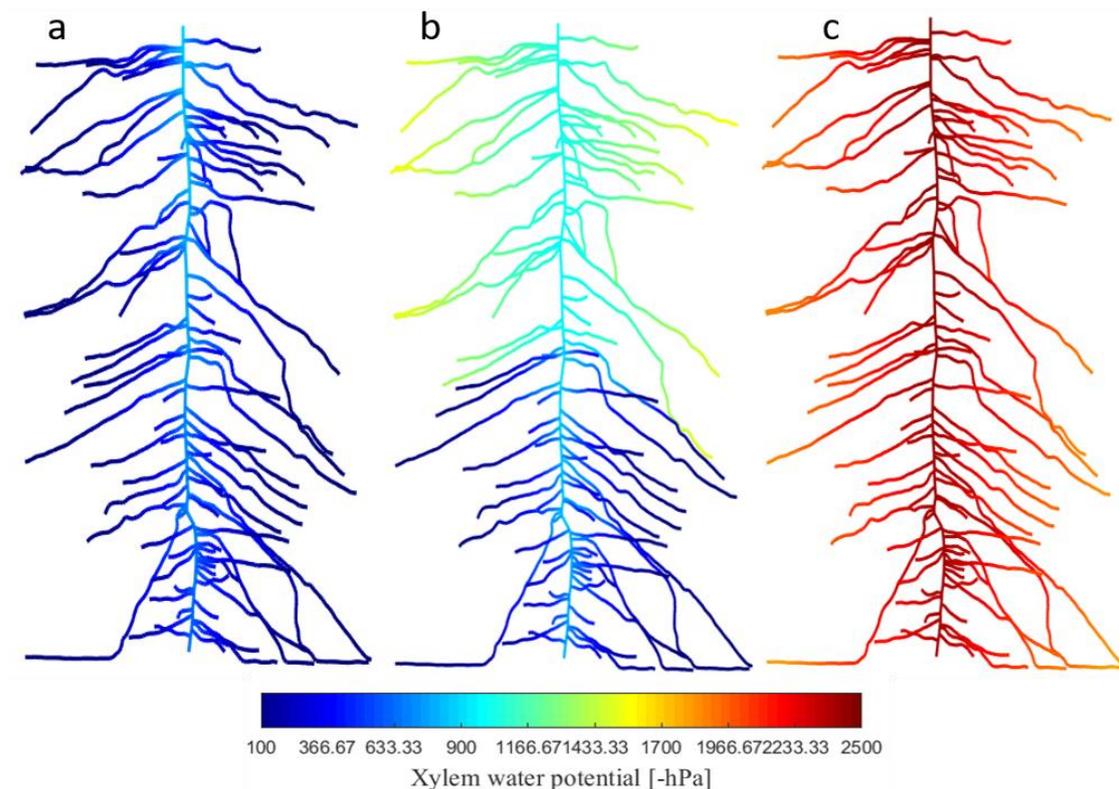
Fig. 5. Root water potential simulated at varying soil moisture levels at medium light intensity (98.9 µmol m^{-2} s^{-1}): uniform-wet (a), top-dry bottom-wet (b) and uniform-dry (c).

When the soil was uniformly wet, the root system felt almost the same water potential in both compartments and there was a little dissipation of water potential along the root system, particularly along the tap root. In the dry-wet scenario (Fig. 5b) the roots in the upper-dry compartment were at much more negative water potential than the roots in the lower-wet compartment. Interestingly, the tips of the roots in the upper-dry compartment were at a more negative potential than the corresponding more proximal segments, indicating water efflux from the root tips. In the dry-dry soils, the root system was at a more negative but rather uniform water potential, with similar gradients from the tips of the lateral roots to the tap root.

The model also yields the profile of the radial fluxes [m s^{-1}] into the roots (Fig. 6). In wet-wet soil (Fig. 6a), the contribution of radial flux was rather uniform along the root system, indicating a moderate dissipation of water potential along the depth; in dry-wet soil (Fig. 6b) the uptake in upper-dry soil was much smaller compared to that in the lower-wet layer. In the dry-dry scenario, the water fluxes were strongly reduced in both soil layers.
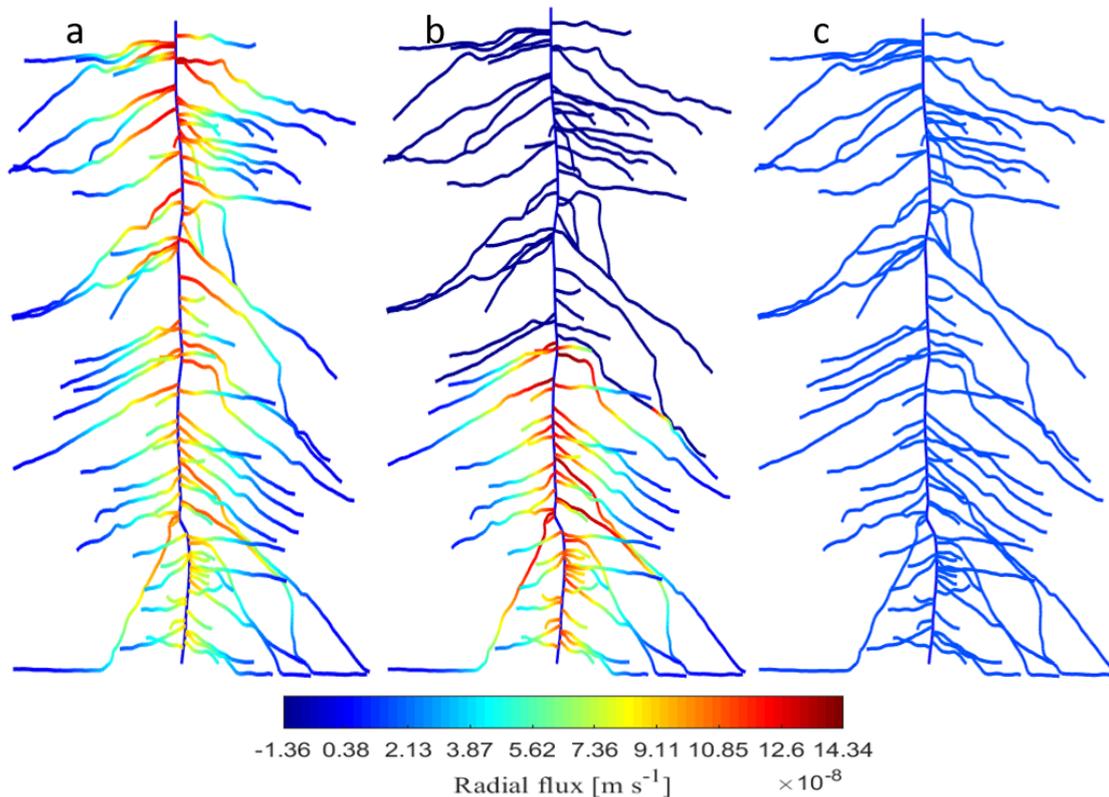
Fig. 6. Roots water uptake simulated for varying soil moisture levels at medium light intensity (98.9 μmol m^{-2} s^{-1}): uniform-wet (a), top-dry bottom-wet (b) and uniform-dry (c).

This detailed root hydraulic architecture gives the relative water uptake in the upper and lower soil layers for each scenario. In homogeneous soil water content scenarios (wet-wet & dry-dry), water uptake was slightly higher in the upper compartment than in the lower, despite the root length being imposed to be 50-50% (Table. 4). This was caused by the dissipation of water potential along the roots. In the dry-dry condition, the relative uptake in the upper and lower soil layers was almost the same as in the wet-wet conditions. The reason was that the difference in water potential between soil and root was larger compared to dissipation along the root. In both conditions (wet-wet & dry-dry) there was no effect of varying transpiration on the relative water uptake.

When the soil water content was not uniform (dry-wet), the relative water uptake changed with varying transpiration rates. At high transpiration rates water was taken up from the wet soil and

it was released by the roots in the upper compartment – the process referred to as hydraulic lift. At decreasing transpiration rates, hydraulic lift increased significantly.

The main difference between the two models is in the hydraulic lift, which is higher in the root architecture model.

Table 4. Relative water uptake [%] in upper and lower layers obtained using the root architecture model. Negative values indicate water efflux and occurrence of hydraulic lift.

Low transpiration rate	upper layer	lower layer	Medium transpiration rate	upper layer	lower layer	High transpiration rate	upper layer	lower layer
wet-wet	54.64	45.36	wet-wet	54.67	45.33	wet-wet	54.69	45.31
dry-wet	-27.57	127.57	dry-wet	-8.00	108.00	dry-wet	-2.99	102.99
dry-dry	51.27	48.72	dry-dry	51.27	48.72	dry-dry	51.27	48.72

2.5   Discussion and Conclusions

We showed that the relation between leaf water potential and transpiration rate was linear at both uniform and heterogeneous water contents distribution and it could be well fitted with both, a simple model (Couvreur et al., 2012) and a detailed root architecture model of water uptake. At uniform soil moisture distribution, either being wet-wet or dry-dry scenario, the relative root water uptake depended uniquely on the root properties and its distribution along the root system did not vary with transpiration rate. In the dry-wet scenarios, root water uptake is predicted to shift to the lower and wet layer and both models predicted the occurrence of hydraulic lift in the upper dry soil layer.

The slope of the transpiration rate versus balancing pressure, which is interpreted as the soil-plant conductance, decreased by a factor of 8.26 in the dry-dry scenario as compared to the wet-wet scenario, indicating the limiting role of the soil conductivity on root water uptake. In contrast to the measurements by Passioura (1980) and Carminati et al. (2017) we found a linear relation between transpiration and balancing pressure also in dry soil. However, it is likely that in the present study we did not reach transpiration rates high enough to observe the deviations from the linear relationship and the consequent hysteric behaviour reported in the studies above. Similarly, to Carminati et al. (2017), we found an offset in the balancing pressure, which we interpreted as the effect of the difference in osmotic potential between the xylem and the soil (Eq. 2 and 7). Osmotic potential of ca. 0.1 MPa are reported in the classic work by Fiscus

(1977) and are consistent with our interpretations. Another explanation of the offset is that at low flow rates (i.e. $Q \approx 0$) the relation between transpiration and leaf xylem water potential is not linear. This could be caused by capacitance effects, with the plant tissues being slowly rehydrated. The models employed here did not include plant capacitance and, although we could argue that for young lupines plant capacitance should not play a big role, we cannot conclude that the model simplification introduced some error at low flow rates. Another explanation is that roots extracted water from a small soil volume which could have become significantly drier than the bulk soil. However, such moisture gradients are not expected in wet soils (as in the wet-wet scenario) and should have quickly disappeared.

When the upper soil layer was dry, the soil-plant conductance decreased by a factor of 1.65 compared to wet-wet scenario. Both the simplified and the architecture models were capable to reproduce the results. The parameterization based on the data from Zarebanadkouki et al. (2016) well fitted the data without any need to adjust the parameters. This might be a coincidence, as the plants in this study were 2 weeks older. Possibly, the fact that here the conductance of the shoot (from the collar to the cut leaf) is not included can explain the quality of the fit. It could be that the actual root conductance of this study was slightly higher than that in Zarebanadkouki et al. (2016) and neglecting the shoot conductance resulted in this good fit.

The simulations predicted that the location of water uptake shifted to the lower soil region while a significant amount of water taken up by the roots in the wet region was released from the root tips into the upper-dry soil layer, in the process referred to as hydraulic lift (Caldwell et al., 1998; Richards and Caldwell, 1987). HL is known to increase at low transpiration rates. At low transpiration rates, the root architecture model predicted a hydraulic lift corresponding to ca. 28% of the transpiration (0.49 mm water day^{-1}), which is within the range in the literature (Neumann and Cardon, 2012; Scott et al., 2008; Kailiang Yu and D'Odorico, 2014). Interestingly, the architecture model predicts hydraulic lift also at high transpiration rates and not just when transpiration is low.

The impacts of hydraulic lift on ecohydrological and soil processes are manifold: it supports shallow-rooted competitors (Dawson, 1993; Hawkins et al., 2009; Moreira et al., 2003; Yu and D'Odorico, 2015), it maintains root in contact with drying soil (Bauerle et al., 2008; Domec et al., 2004) and it stimulates microbial activity (Lehto and Zwiazek, 2011; Wang et al., 2009). Hydraulic lift also alters the profiles of soil moisture and impacts carbon assimilation, canopy transpiration and the water use efficiency during dry season (Amenu and Kumar, 2008). Manoli

et al., (2017) also showed that hydraulic redistribution produced by deep-rooted trees enhances ecosystem resilience to drought and maintains photosynthesis in shallow-rooted trees.

In summary, this study shows the potential of combining the root pressure chamber method, which allows for monitoring the average leaf suction in intact transpiring plants exposed to soil drying, with hydraulics model of water uptake. Both root water uptake models were capable to reproduce the measured relationship between transpiration and leaf water potential. However, the models differ in the prediction of hydraulic lift. The detailed architecture model allows for assigning variable hydraulic conductivities to different root segments. According to parametrization by Zarebanadkouki et al. (2016), the root tips were the most (radially) conductive regions and these are the locations where hydraulic lift takes place. The simplified model summarizes all the different root conductivities in effective terms and predicts less hydraulic lift. From this comparison between the models, we conclude that a simplified model is sufficient to describe the relationship between leaf water potential and transpiration, but a more detailed model is needed to understand the mechanisms impacting hydraulic lift.

Concerning hydraulic lift, we cannot conclude on which model is better, because we have not measured hydraulic lift. However, the more detailed model is more adequate to calculate water potential gradients and fluxes along the root system. Such a model should be used to test open questions, such as the potential mechanisms plants employ to control hydraulic lift. For instance, root exudation of mucilage induces water repellency in the rhizosphere and it is likely to reduce water fluxes (Zarebanadkouki et al., 2016a). Similarly, root shrinkage and the consequent loss of contacts between soil and roots (Carminati et al., 2013) will reduce the leakage of water from the roots. Since it is known that current models overestimate HL (Neumann and Cardon, 2012), including such dynamic processes at the root-soil interface into existing models would be interesting. In this case, the water flow into and from the root should account for soil capacitance and its hysteresis, which was not done in the present study where radial flow to the roots was solved assuming steady state conditions. In analogy with what has been done for plant tissues, it could be found that rhizosphere capacitances decrease modelled HL (Huang et al., 2017). Dynamic processes at the root-soil interface and their impact on hydraulic lift deserve further studies and would require high spatial resolution measurements of water fluxes along the root system. Optimally, such studies would allow for a better understanding of how root-soil interactions impact water fluxes at day and night.

Acknowledgment

2.6   References

Ahmed, M.A., Passioura, J., Carminati, A., 2018. Hydraulic processes in roots and the rhizosphere pertinent to increasing yield of water-limited grain crops : a critical review. J. Exp. Bot. 69, 3255–3265. https://doi.org/10.1093/jxb/ery183

Ahmed, M.A., Zarebanadkouki, M., Kaestner, A., Carminati, A., 2016. Measurements of water uptake of maize roots: the key function of lateral roots. Plant Soil 398, 59–77. https://doi.org/10.1007/s11104-015-2639-6

Amenu, G.G., Kumar, P., 2008. A model for hydraulic redistribution incorporating coupled soil-root moisture transport. Hydrol. Earth Syst. Sci. 12, 55–74. https://doi.org/10.5194/hess-12-55-2008

Bauerle, T.L., Richards, J.H., Smart, D.R., Eissenstat, D.M., 2008. Importance of internal hydraulic redistribution for prolonging the lifespan of roots in dry soil. Plant, Cell Environ. 31, 177–186. https://doi.org/10.1111/j.1365-3040.2007.01749.x

Brooks, J.R., Meinzer, F.C., Warren, J.M., Domec, J.C., Coulombe, R., 2006. Hydraulic redistribution in a Douglas-fir forest: Lessons from system manipulations. Plant, Cell Environ. 29, 138–150. https://doi.org/10.1111/j.1365-3040.2005.01409.x

Burgess, S.S.O., Adams, M.A., Turner, N.C., White, D.A., Ong, C.K., 2001. Tree roots: Conduits for deep recharge of soil water. Oecologia 126, 158–165. https://doi.org/10.1007/s004420000501

Caldwell, M.M., Dawson, T.E., Richards, J.H., 1998. Hydraulic lift: Consequences of water efflux from the roots of plants. Oecologia 113, 151–161. https://doi.org/10.1007/s004420050363

Carminati, A., Passioura, J.B., Zarebanadkouki, M., Ahmed, M.A., Ryan, P.R., Watt, M., Delhaize, E., 2017. Root hairs enable high transpiration rates in drying soils. New Phytol.

771–781. https://doi.org/10.1111/nph.14715

Carminati, A., Vetterlein, D., Koebernick, N., Blaser, S., Weller, U., Vogel, H.J., 2013. Do roots mind the gap? Plant Soil 367, 651–661. https://doi.org/10.1007/s11104-012-1496-9

Celia, M.A., Binning, P., 1992. A mass conservative numerical solution for two-phase flow in porous media with application to unsaturated flow. Water Resour. Res. 28, 2819–2828. https://doi.org/10.1029/92WR01488

Couvreur, V., Vanderborght, J., Javaux, M., 2012. A simple three-dimensional macroscopic root water uptake model based on the hydraulic architecture approach. Hydrol. Earth Syst. Sci. 16, 2957–2971. https://doi.org/10.5194/hess-16-2957-2012

Dawson, T.E., 1993. Hydraulic lift and water use by plants: implications for water balance, performance and plant-plant interactions. Oecologia 565–574.

Domec, J., M, warren J., F.C, M., Brooks, J.., R, C., 2004. Native root xylem embolism and stomatal closure in stands of Douglas-fir and ponderosa pine : mitigation by hydraulic redistribution. Oecologia 141, 7–16. https://doi.org/10.1007/s00442-004-1621-4

Domec, J., Ogée, J., Noormets, A., Jouangy, J., Gavazzi, M., Treasure, E., Sun, G., Mcnulty, S.G., King, J.S., 2012. Interactive effects of nocturnal transpiration and climate change on the root hydraulic redistribution and carbon and water budgets of southern United States pine plantations. Tree Physiol. 32, 707–723. https://doi.org/10.1093/treephys/tps018

Doussan, C., Pierret, A., Garrigues, E., Pagès, L., 2006. Water uptake by plant roots: II - Modelling of water transfer in the soil root-system with explicit account of flow within the root system - Comparison with experiments. Plant Soil 283, 99–117. https://doi.org/10.1007/s11104-004-7904-z

Doussan, C., Vercambr, G., Page, L., 1998. Modelling of the Hydraulic Architecture of Root Systems: An Integrated Approach to Water Absorption—Distribution of Axial and Radial Conductances in Maize. Ann. Bot. 81, 225–232. https://doi.org/10.1006/anbo.1997.0541

Draye, X., Kim, Y., Lobet, G., Javaux, M., 2010. Model-assisted integration of physiological and environmental constraints affecting the dynamic and spatial patterns of root water uptake from soils. J. Exp. Bot. 61, 2145–2155. https://doi.org/10.1093/jxb/erq077

Fiscus, E.L., 1977. Determination of hydraulic and osmotic properties of soybean root systems. Plant Physiol. 59, 1013–1020. https://doi.org/10.1104/pp.59.6.1013

Hawkins, H., Hettasch, H., Adam G. West, Cramer, M.D., 2009. Hydraulic redistribution by Protea ' Sylvia ' (Proteaceae) facilitates soil water replenishment and water acquisition by an understorey grass and shrub. Funct. Plant Biol. 752–760.

Huang, C.-W., Domec, J.-C., Ward, E.J., Duman, T., Manoli, G., Parolari, A.J., Katul, G.G., 2017. The effect of plant water storage on water fluxes within the coupled soil-plant system. New Phytol. 213, 1093–1106. https://doi.org/10.1111/nph.14273

Jarvis, N.J., 1989. A simple empirical model of root water uptake. J. Hydrol. 107, 57–72.

Javaux, M., Schröder, T., Vanderborght, J., Vereecken, H., 2008. Use of a Three-Dimensional Detailed Modeling Approach for Predicting Root Water Uptake. Vadose Zo. J. 7, 1079–1088. https://doi.org/10.2136/vzj2007.0115

Kholova, J., Hash, C.T., Kumar, P.L., Yadav, R.S., Koc, M., Vadez, V., 2010. Terminal drought-tolerant pearl millet [Pennisetum glaucum (L .) R . Br .] have high leaf ABA and limit transpiration at high vapour pressure deficit. J. Exp. Bot. 61, 1431–1440. https://doi.org/10.1093/jxb/erq013

Lehto, T., Zwiazek, J.J., 2011. Ectomycorrhizas and water relations of trees : a review. Mycorrhiza 21, 71–90. https://doi.org/10.1007/s00572-010-0348-9

Manoli, G., Manoli, G., Huang, C., Bonetti, S., Domec, J., 2017. Competition for Light and Water in a Coupled Soil-Plant System Advances in Water Resources Competition for light and water in a coupled soil-plant system. Adv. Water Resour. 108, 216–230. https://doi.org/10.1016/j.advwatres.2017.08.004

Meinzer, F.C., Brooks, J.R., Bucci, S., Goldstein, G., Scholz, F.G., Warrent, J.M., 2004. Converging pattern of hydraulic redistribution of soil water in contrasting woody vegetation types. Tree Physiol. 24, 919–928.

Meunier, F., Rothfuss, Y., Bariac, T., Biron, P., Richard, P., Durand, J.-L., Couvreur, V., Vanderborght, J., Javaux, M., 2017. Measuring and Modeling Hydraulic Lift of Using Stable Water Isotopes. Vadose Zo. J. 17, 1–15. https://doi.org/10.2136/vzj2016.12.0134

Mitchell, P.J., Grady, A.P.O., Tissue, D.T., White, D.A., Ottenschlaeger, M.L., Pinkard, E.A., Mitchell, P.J., 2013. Drought response strategies define the relative contributions of hydraulic dysfunction and carbohydrate depletion during tree mortality. New Phytol. 197, 862–872.

Moreira, M.Z., Scholz, F.G., Goldstein, G., Franco, A.C., 2003. Hydraulic lift in a neotropical savanna. Funct. Ecol. 17, 573–581.

Neumann, R.B., Cardon, Z.G., 2012. The magnitude of hydraulic redistribution by plant roots : a review and synthesis of empirical and modeling studies. New Phytol. 194, 337–352.

Nobel, P.S., Cui, M., 1992. Hydraulic conductances of the soil, the root-soil air gap, and the root: Changes for desert succulents in drying soil. J. Exp. Bot. 43, 319–326. https://doi.org/10.1093/jxb/43.3.319

Passioura, J.B., 1980. The Transport of Water from Soil to Shoot in Wheat Seedlings. J Exp Bot. 31, 333–345.

Peters, A., Durner, W., 2008. Simplified evaporation method for determining soil hydraulic properties. J. Hydrol. 356, 147–162. https://doi.org/10.1016/j.jhydrol.2008.04.016

Peters, A., Iden, S.C., Durner, W., 2015. Revisiting the simplified evaporation method: Identification of hydraulic functions considering vapor, film and corner flow. J. Hydrol. 527, 531–542. https://doi.org/10.1016/j.jhydrol.2015.05.020

Richards, J.H., Caldwell, M.M., 1987. Hydraulic lift: Substantial nocturnal water transport between soil layers by Artemisia tridentata roots. Oecologia 73, 486–489. https://doi.org/10.1007/BF00379405

Schindler, U., Durner, W., Unold, G. Von, Mueller, L., Wieland, R., 2010. The evaporation method : Extending the measurement range of soil hydraulic properties using the air-entry pressure of the ceramic cup. J. Plant Nutr. Soil Sci. 173, 563–572. https://doi.org/10.1002/jpln.200900201

Scott, R.L., Cable, W.L., Hultine, K.R., 2008. The ecohydrologic significance of hydraulic redistribution in a semiarid savanna. Water Resour. Res. 44, 1–12. https://doi.org/10.1029/2007WR006149

Sperry, J.S., Hacke, U.G., Oren, R., Comstock, J.P., 2002. Water deficits and hydraulic limits to leaf water supply. Plant, Cell Environ. 25, 251–263. https://doi.org/10.1046/j.0016-8025.2001.00799.x

Tardieu, F., Draye, X., Javaux, M., 2017. Root Water Uptake and Ideotypes of the Root System: Whole-Plant Controls Matter. Vadose Zo. J. 16, 0. https://doi.org/10.2136/vzj2017.05.0107

Tardieu, F., Simonneau, T., Parent, B., 2015. Modelling the coordination of the controls of stomatal aperture, transpiration, leaf growth, and abscisic acid: Update and extension of the Tardieu-Davies model. J. Exp. Bot. 66, 2227–2237. https://doi.org/10.1093/jxb/erv039

Thomas, F.M., 2000. Growth and water relations of four deciduous tree species (Fagus sylvatica L ., Quercus petraea [MATT .] LIEBL ., Q . pubescens WILLD ., Sorbus aria [L .] CR .) occurring at Central-European tree-line sites on shallow calcareous soils : physiological r. Flora - Morphol. Distrib. Funct. Ecol. Plants 195, 104–115. https://doi.org/10.1016/S0367-2530(17)30958-1

Tognetti, R., Johnson, J.D., Michelozzi, M., 1995. The response of European beech (Fagus sylvatica L .) seedlings from two Italian populations to drought and recovery. Trees 9, 348–354.

Wang, X., Tang, C., Guppy, C.N., Sale, P.W.G., 2009. The role of hydraulic lift and subsoil P placement in P uptake of cotton (Gossypium hirsutum L .). Plant Soil 325, 263–275. https://doi.org/10.1007/s11104-009-9977-1

Will, R.E., Wilson, S.M., Zou, C.B., Hennessey, T.C., 2013. Increased vapor pressure deficit due to higher temperature leads to greater transpiration and faster mortality during drought for tree seedlings common to the forest – grassland ecotone. New Phytol. 200, 366–274.

Yu, K., D'Odorico, P., 2015. Hydraulic lift as a determinant of tree – grass coexistence on savannas. New Phytol. 207, 1038–1051.

Yu, K., D'Odorico, P., 2014. Advances in Water Resources Climate , vegetation , and soil controls on hydraulic redistribution in shallow tree roots. Adv. Water Resour. 66, 70–80. https://doi.org/10.1016/j.advwatres.2014.02.003

Zarebanadkouki, M., Ahmed, M.A., Carminati, A., 2016a. Hydraulic conductivity of the root-soil interface of lupin in sandy soil after drying and rewetting. Plant Soil 398, 267–280. https://doi.org/10.1007/s11104-015-2668-1

Zarebanadkouki, M., Kim, Y.X., Carminati, A., 2013. Where do roots take up water? Neutron radiography of water flow into the roots of transpiring plants growing in soil. New Phytol. 199, 1034–1044. https://doi.org/10.1111/nph.12330

Zarebanadkouki, M., Meunier, F., Couvreur, V., Cesar, J., Javaux, M., Carminati, A., 2016b.

Estimation of the hydraulic conductivities of lupine roots by inverse modelling of high-resolution measurements of root water uptake. Ann. Bot. 118, 853–864. https://doi.org/10.1093/aob/mcw154

2.7 Supplementary data

Table S1. The root distribution in each compartment for all replications.

Scenario	Replication	upper layer [cm]	bottom layer [cm]	total length [cm]	upper layer [%]	bottom layer [%]
wet-wet & dry-wet	R1	316	317	633	49.9	50.1
	R2	232	245	477	48.6	51.4
	R3	432.3	325.5	757.8	57	43
				Averaged	51.83	48.17
dry-dry	R4	Without layer	----	526	----	----

Table S2. Comprehensive data set of pressure chamber experiments.

Scenario	pressure [hPa]	transpiration [g/hr]	standard deviation		moisture content	
			pressure	transpiration	upper layer [%]	bottom layer [%]
wet-wet	1876	1.24	0.50	0.67	15-20	15-20
	2754	2.22	0.66	0.67		
	4411	4.65	0.53	1.42		
dry-wet	2383	0.54	0.30	0.40	2-5	15-20
	3833	1.80	0.44	0.59		
	7000	4.39	0.19	0.98		
dry-dry (only one replication)	3950	0.35	----	----	2.42 - 5	without layer
	5750	0.70	----	----		
	1550	2.30	----	----		

Table S3. Hydraulic properties of soil used in this experiment. These parameters are obtained from fitting of PDI model to the data of an evaporation experiment using a HyProp technique.

θ_s [cm^3 cm^{-3}]	omega	alpha_1 [cm^{-1}]	n_1 [-]	k_sat [cms^{-1}]	Lambda [-]
0.416704	1.09E-05	0.023445	7.82537	0.013207	0.851693
θ_r [cm^3 cm^{-3}]	a	alpha_2 [cm^{-1}]	n_2 [-]	Pf_dry [cm]	w2 [-]
0.009722	-3.70691	1.92E-05	14.9907	8.57308	0.062562

3   Chapter Three

Transpiration reduction in maize (*Zea mays* L) in response to soil drying

Faisal Hayat[1*], Mutez Ali Ahmed[1,2], Mohsen Zarebanadkouki[1], Mathieu Javaux[3,4], Gaochao Cai[1], Andrea Carminati[1]

[1]   Chair of Soil Physics, University of Bayreuth, Bayreuth D-95447, Germany

[2]   Division of Soil Hydrology, University of Göttingen, Göttingen D-37077, Germany

[3]   Earth and Life Institute-Environmental Sciences, Universite Catholique de Louvain, Louvain la Neuve, B-1348, Belgium

[4]   Agrosphere (IBG-3), Forschungszentrum Juelich GmbH, Juelich D-52425, Germany

[*]   Corresponding author: Faisal.Hayat@uni-bayreuth.de

3.1   Abstract

The relationship between leaf water potential, soil water potential and transpiration depends on soil and plant hydraulics and stomata regulation. Recent concepts of stomatal response to soil drying relate stomatal regulation to plant hydraulics, neglecting the loss of soil hydraulic conductance around the roots. Our objective was to measure the effect of soil drying on the soil-plant hydraulic conductance of maize and to test whether stomatal regulation avoids a loss of soil-plant hydraulic conductance in drying soils. We combined a root pressure chamber, in which the soil-root system is pressurized to maintain the leaf xylem at atmospheric pressure, with sap flow sensors to measure transpiration rate. The method provides accurate and high temporal resolution measurements of the relationship between transpiration rate and xylem leaf water potential. A simple soil-plant hydraulic model describing the flow of water across the soil, root and xylem was used to simulate the relationship between leaf water potential and transpiration rate. The experiments were carried out with 5-week-old maize grown in cylinders of 9 cm diameter and 30 cm height filled with silty soil. The measurements were performed at four different soil water contents (WC). The results showed that the relationship between transpiration and leaf water potential was linear in wet soils, but as the soil dried, the xylem tension increased, and non-linearities were observed at high transpiration rates. Nonlinearity in the relationship between transpiration and leaf water potential indicated a decrease in the soil-plant hydraulic conductance, which was explained by the loss of hydraulic conductivity around the roots. The hydraulic model well reproduced the observed leaf water potential. Parallel experiments performed with plants not being pressurized showed that plants closed stomata when the soil-plant hydraulic conductance decreased, maintaining the linearity between leaf water potential and transpiration rate. We conclude that stomata closure during soil drying is caused by the loss of soil hydraulic conductivity in a predictable way.

Keywords

Maize (*Zea mays* L), Pressure chamber, Soil drying, Stomatal closure, Transpiration rates.

3.2   Introduction

Drought is a primary constraint to plant growth and crop production worldwide. Mechanisms by which drought impacts plant growth are complex and involve feedbacks between stomata regulation, plant hydraulics and soil drying. A hydraulic framework is helpful to understand the physical constraints to transpiration (Sperry and Love, 2015). The soil-plant atmospheric continuum is described as a network of elements connected in series and in parallel (Cowan, 1965; Draye et al., 2010; Mencuccini et al., 2019; Sperry et al., 1998). Each element is characterized by hydraulic conductances (which can be variable) and capacitances. Water flows from soil to the roots, and then along the xylem till the leaf tissues and stomata, where it evaporates into the atmosphere following the cohesion-tension theory (Pickard, 1981; Sperry et al., 1998). The driving force for transpiration is the water tension generated in the leaves because of the evaporating water. The tension propagates down along the xylem to the roots and to the soil. The hydraulic conductivities of the xylem, of the roots and of the soil are extremely variable. Xylem vessels tend to cavitate at high tension, causing a large drop in the axial conductance of the xylem (Sperry et al., 1998). The radial conductance of the root is also variable and it is affected by anatomical changes as well as by the expression of aquaporin (Chaumont and Tyerman, 2014; Ehlert et al., 2009; Knipfer et al., 2011; Redondo et al., 2009; Simonneau et al., 2009). Finally, the soil hydraulic conductivity determines the ease of water flow through the soil. Its conductivity decreases by several orders of magnitude as the soil dries, and it might become smaller than that of roots (Draye et al., 2010; Gardner, 1960). Eventually, when plants are exposed to severe drying, their roots shrink and lose part of their contact to the soil (Carminati et al., 2013), which further decreases the conductance between rhizosphere and root. On the other hand, plants can close this gap and attenuate the drop in conductivity by secreting mucilage (Carminati et al., 2010) or by growing root hairs (Carminati et al., 2017).

Soil drying triggers a gradual closure of stomata and a reduction in transpiration rate (Bates et al., 1981; Carter et al., 1980; Comstock, 2002; Meyer and Green, 1980; Sinclair et al., 2005). Stomatal closure depends on both hydraulic and hormonal signals, such as abscisic acid (ABA) (Brodribb and McAdam, 2017; Buckley, 2017; Tardieu and Davies, 1993). Independently from the mechanism by which stomata close, it has been proposed that stomatal regulation avoids excessive drop in leaf water potential by responding to non-linearities in the relationship between transpiration rate and leaf water potential (Sperry et al., 2016; Sperry and Love, 2015). However, there is limited experimental evidence that stomatal regulation prevents and responds

to drop in soil-plant hydraulic conductance. Additionally, most of the studies linking stomatal regulation to plant hydraulics focus on xylem vulnerability as the primary constraint on water flow in soil and plants (Anderegg et al., 2017), neglecting the explicit role of soil hydraulic conductivity.

Our objective was to test whether stomata close when the soil-plant hydraulic conductance drops during soil drying. Here we use a soil-plant hydraulic model that solves the radial flow of water around a representative single root (Gardner, 1960; Van Lier et al., 2008) and water flow in the plant (Sperry et al., 1998) to test whether the drop in hydraulic conductance can be predicted based on the loss of soil hydraulic conductance.

Experimentally, we applied the pressure chamber method (Passioura, 1980) to maize (*Zea mays* L) growing in silty soil. The root-soil system of intact transpiring plants is pressurized to maintain the leaf xylem at atmospheric pressure. The applied pressure is then equivalent to the tension of water in the leaf xylem (Passioura, 1980). The method allows accurate measurements at high temporal resolution of leaf water potential for varying transpiration rates and soil water potential. Furthermore, we measured transpiration rates for pressurized (in the pressure chamber) and not-pressurized (outside the pressure chamber) plants to test to what extent leaf tension controls stomata closure in drying soils.

3.3   Materials and Methods

3.3.1   Soil and plant preparation

Three replicates of maize (*Zea mays* L.) were grown in PVC pots with 30 cm of height and 9 cm of diameter. The pots were filled with a mixture of silt and quartz sand (1:1 ratio) – which were sieved to a particle diameter < 1 mm. The soil was poured into each pot to achieve a bulk density of 1.4 g cm^{-3}. The soil surface of each pot was covered with fine gravels (2 - 3.5 mm) to minimize evaporation from the soil surface. Several holes with a diameter of 1.5 mm were drilled at the bottom and sides of the pots to allow, respectively, water drainage and lateral injection of water using a fine needle. Five holes were placed with diameter of 5 mm and with a distance of 5 cm from each other at the sides of the pots to measure soil water content using a TDR (time domain reflectometer, FOM/mts, E-Test (IA PAS), Lublin, Poland). The soil hydraulic properties were estimated using extended evaporation method (Peters and Durner, 2008; Schindler et al., 2010). The implementation of this method using Hyprop (Meters,

Munich, Germany) and the parameterization of retention curve and soil hydraulic conductivity has been described in Hayat et al, (2018).

Maize seeds were germinated on moist filter paper for 48 hours and the seedlings were planted in the containers. The plants were grown for 40 days in a climate room with a photoperiod of 14 hours, day/night temperature of 25 °C/22°C, relative humidity of 60% and light intensity 200 μmol m^{-2} s^{-1}. During the first three weeks, the plants were irrigated every third day by immersing the pots in a nutrient solution to achieve an average soil water content of 25%. Afterward, the soil water contents were adjusted to the following scenarios: i) water content of 21-25% (wet soil); ii) water content of 12-13% (mid-wet soil); iii) water content of 9-10% (mid-dry soil); iv) and water content of 6-6.5% (dry soil). The soil water contents were measured every third day using TDR. The soil moisture content was measured at five different heights (5, 10, 15, 20, 25 and 30 cm).

3.3.2   Transpiration measurements

Prior to the experiment, we measured soil water contents at five different heights as described above. Afterwards, transpiration rates for each scenario were recorded by Sap Flow Sensors SGA9 (Dynamax Inc, USA). This non-intrusive, energy balance sensor measures the amount of heat carried by the sap and converts into real-time transpiration rate.

Transpiration rates were also measured by weighing the plants before and after the recordings, and the decrease in weight was compared to the cumulative flow measured with the sap flow sensors (Fig. S1a). A LED lamp (GC 9, photo flux density (15 cm), 2450 μmol m^{-2} s^{-1}, Greenception GmbH, Hamburg) was installed at a distance of 16 cm above the shoots (Fig. S1b). Transpiration was increased in four steps (from low to high transpiration) by increasing photosynthetic photon intensity. Transpiration was measured for a period of one and a half hour for each step. At the end of transpiration measurements, water was injected in the pot through the holes to bring the soil to the initial soil water content.

3.3.3   Pressure chamber

Xylem water potential of transpiring plants was measured using the pressure chamber method, based on Passioura, (1980). We started the experiment when plants were 40 days old. Briefly, the soil core and the roots were put inside the pressure chamber in such a way that the shoot

remained outside and it was carefully sealed to avoid air leakage (Fig. S1b). One leaf was cut and the pressure in the chamber was increased (using 99.9% vol. N_2) until a water droplet appeared on a cut leaf (Fig. S1c). The pressure needed to keep a drop of water at the cut end of the leaves is numerically equal to the tension in the xylem (Passioura, 1980). Transpiration was increased stepwise by imposing leaves to four increasing photosynthetic photon intensities. In each step, we let the plant to transpire for 1.5 hours. During this time, transpiration was measured using a sap flow sensor that was installed on the stem of the plant. The measurements were performed for four scenarios of moisture levels and four transpiration rates. To reveal the effect of soil and plant pressurizing on the transpiration rate (stomata closure), each measurement was performed with and without pressurizing the soil.

3.3.4 Soil-plant hydraulic model

We used a simple model to estimate the water flow in the soil-plant continuum. The model was represented as a series of hydraulic resistances (and one capacitance in the soil) between the bulk soil and the leaves. The flux of water in the soil q [cm s^{-1}] is calculated using a cylindrical model as a function of radial distance r to the root center:

$$q(r) = -k_{soil}(\psi)\frac{\partial \psi}{\partial r} \qquad \text{(Eq. 1)}$$

where k_{soil} is the soil conductivity [cm s^{-1}] (when the matric potential is expressed as hydraulic head – i.e. 1 hPa ≈ 1 cm), which is function of matric potential ψ [hPa], and $\frac{\partial \psi}{\partial r}$ is the gradient in matric potential. As boundary condition at the root-soil interface, we set $q(r_0) = -\frac{T}{2\pi r_0 L}$, where T is the transpiration rate [cm^3 s^{-1}], r_0 is the root radius [cm] and L is the active root length [cm]. We imposed no flow at the outer root radius r_b [cm], i.e. $q(r_b) = 0$, where $r_b = \sqrt{\frac{V}{\pi L}}$ where V is the soil volume [cm^3] and $\psi = \psi_b$.

The soil hydraulic conductivity k_{soil} [cm s^{-1}] is parameterized using Brooks and Corey model (Brooks and Corey, 1964):

$$k_{soil}(\psi) = k_{sat}\left(\frac{\psi}{\psi_o}\right)^{\tau} \qquad \text{(Eq. 2)}$$

where k_{sat} is the soil saturated hydraulic conductivity [cm s^{-1}], τ is a fitting parameters [-], ψ_o is the soil air entry value [hPa^{-1}].

Equation (1) is linearized following (Schröder et al., 2007; van Lier et al., 2006), who assumed a steady-rate behavior and used the matric flux potential [$cm^2 s^{-1}$]:

$$\Phi(\psi) = \int_{-\infty}^{\psi} k(x) dx \qquad \text{(Eq. 3)}$$

Following this approach, we obtain:

$$\Phi_{r,s} = -\frac{T}{2\pi r_0 L}\left(\frac{r_0}{2} - r_0 r_b^2 \frac{ln(r_b/r_0)}{r_b^2 - r_0^2}\right) + \Phi_b \quad \text{(Eq. 4)}$$

where Φ_b is obtained from inserting ψ_b in Eq. (2-3). Inverting Eq. 3 and using the parameterization of Eq. 2, from $\Phi_{r,s}$ (Eq. 4) we obtain $\psi_{r,s}$.

Knowing the transpiration rate and the plant hydraulic conductance, K_{plant} [$cm^3 hPa^{-1} s^{-1}$], the dissipation of water potential within the plant is calculated as:

$$T = K_{plant}(\psi_{leaf,x} - \psi_{r,s}) \quad \text{(Eq. 5)}$$

where $\psi_{leaf,x}$ is the water potential in the leaf xylem [hPa].

In this model, we assumed that: 1) the total length of the roots taking up water is L; 2) all the roots take up water at similar rate; 3) the soil water potential is at at distance r_b from the root center is equal for all roots; 4) there is no cavitation in the xylem. The last assumption is justified by the fact that during the measurements the plant was maintained pressurized and water in the leaf xylem was at atmospheric pressure. The illustration of these parameters is shown in Fig. S2.

The model allows to calculate the leaf water potential ψ_{leaf} for varying soil water potential ψ_b and transpiration rates T. The model requires the parameters K_{plant}, L, r_b, r_0 and the function $k_{soil}(\psi)$ (Eq. 2). $k_{soil}(\psi)$ was measured and parameterized independently (Fig. S3). The root radius r_0 was set to 0.05 cm. r_b is calculated as $r_b = \sqrt{\frac{V}{\pi L}}$. The independent parameters were K_{plant} and L and were adjusted to best reproduce the measured balancing pressure P [hPa] for the different transpiration rates and soil water potentials.

The root pressure chamber is numerically equal to minus of the leaf water potential:

$$P = -\psi_{leaf,x} \qquad \text{(Eq. 6)}$$

assuming that gradients in osmotic potential are negligible. Additionally, the root length was independently measured using WinRhizo and then compared to the fitted L.

3.3.5   Statistical analysis

The effects of soil water content, light intensity, pressurization, and the interactions between them on transpiration were analysed using N-way analysis of variance (ANOVA) followed by Tukey-Kramer multiple comparison tests. In all cases, $p < 0.05$ was taken as the lowest level of significance. Matlab (**9.5.0**) and the corresponding statistic packages were used to perform all the statistical analysis.

3.4   Results

The soil water retention and unsaturated conductivity curves obtained by fitting the evaporation method are shown in Fig. S3a. The fitting parameters of the water retention curve were further used to estimate the soil hydraulic conductivity using Brooks and Corey parameterization (Brooks and Corey, 1964) (Fig. S3b).

The soil water content profiles were measured by the TDR in all replications are shown in Fig. 1. The measurements showed that the distribution of water content was relatively homogeneous throughout the soil profile.

We calibrated the sap flow sensors using the gravimetric measurements (Fig. S4). The transpiration rate measured by sap flow was linearly related to the gravimetric measurements. We repeated the calibration for each measurement (e.g. for each water content and for each sample).

The effect of pressurization and light intensity on averaged transpiration rates (measured with sap flow sensors) with and without pressurization at each water content are shown in Fig. 2. In general, we observed a slightly higher transpiration rate when the plants were pressurized. This indicates that when plants were pressurized and water in the leaf xylem was at atmospheric pressure, the stomata were more open. However, as long as the soil was wet or the light intensity was low, transpiration rate increased with increasing light intensity under both, pressurized and not pressurized conditions. In contrast, in dry soil (WC = 9.33%) under not pressurized conditions transpiration dropped significantly ($p < 0.05$, Tukey-Kramer test) at

high photosynthetic photon intensity (at 2000 µmol m^{-2} s^{-1}) (Fig. 2c). At the tested soil moistures, pressurization prevented stomatal closure at all soil moistures. Figure 2e shows a linear response of transpiration to increasing light intensity and the increase in transpiration was even more marked in dry soil (Fig. 2e).
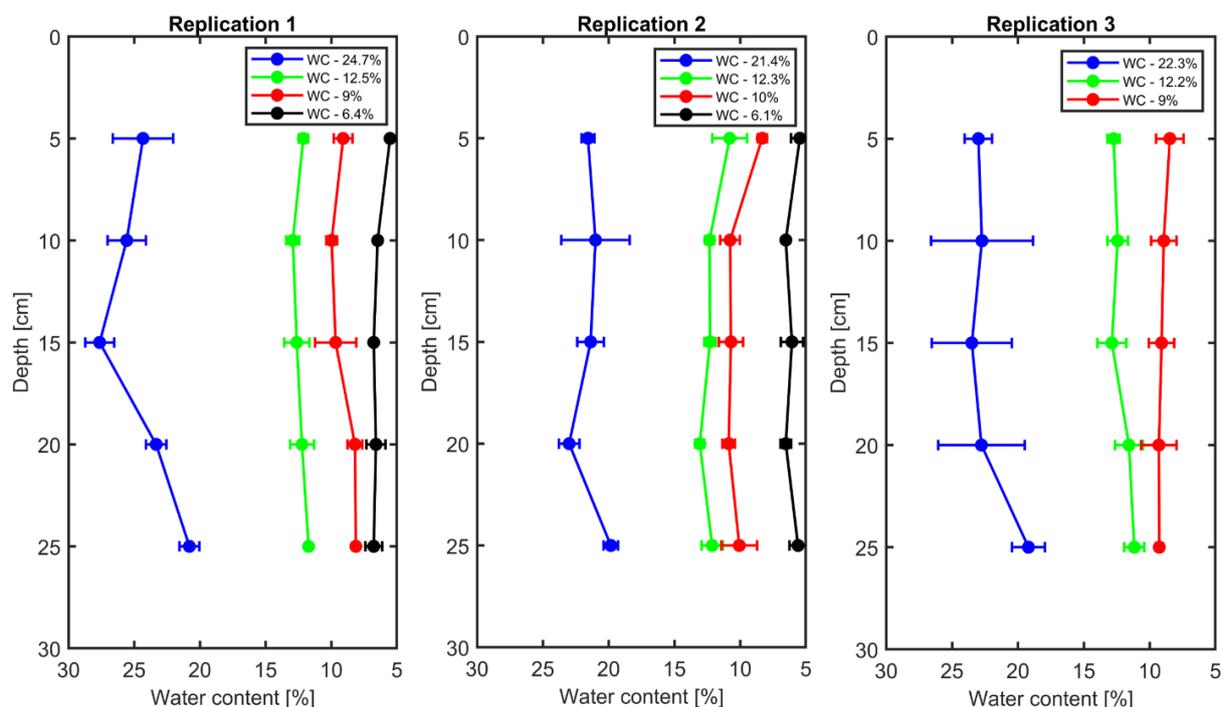
Figure 1. Vertical profiles of volumetric soil water content in each replication.

We tested the statistical significance of the effect of different factors (i.e., pressurization, soil water content and light intensity) and the interaction on transpiration rate by ANOVA (see supplementary material Table S1). Transpiration rate was significantly influenced by light intensity and pressurization. The effect of pressurization interacted with that of light intensity on transpiration rate. This implies that for different light intensities the impact of pressurization was different. Soil water content and its interaction with other two factors did not show significant impact, which was possibly because of limited measurements at low soil moistures.

The comprehensive data sets of transpiration rates, measured xylem tension and the model fitting for different water contents for replication 1 are shown in Fig. 3. Dots are transpiration rates and leaf water potential measured when plants were pressurized for four imposed photosynthetic photon intensities (550, 1000, 1600 and 2200 µmol m^{-2} s^{-1} marked as 1-4). The solid lines are the fitting of the model. In wet soil (WC = 24.7%), the relationship between transpiration rate and xylem tension was linear. As the soil dried (WC = 12.5%, 9% and 6.4%), this relationship became non-linear at increasing transpiration rates.
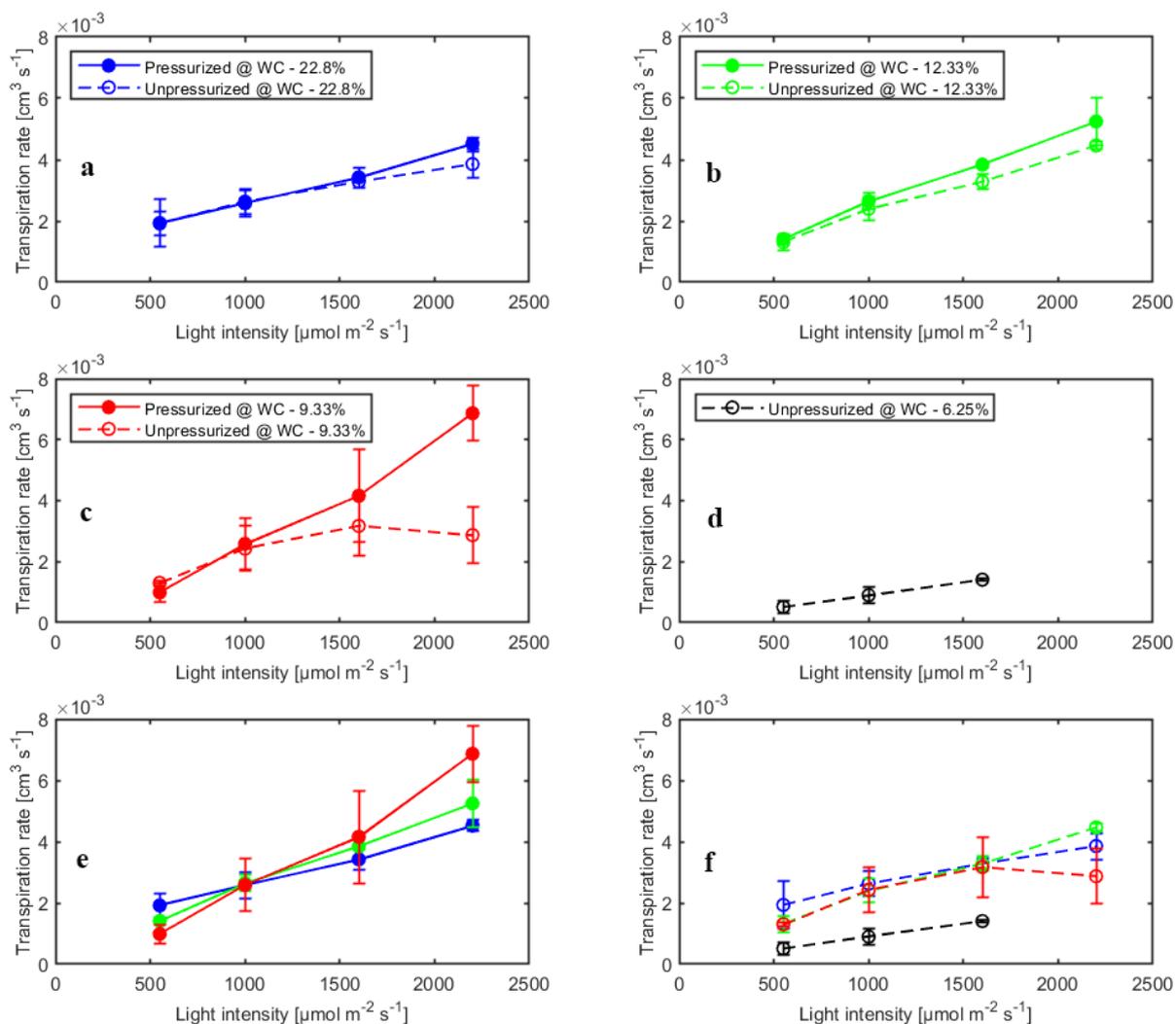
Figure 2. Effect of light intensity and pressurization on transpiration rates for varying soil water contents. (a - d) Effect of pressurization on transpiration. (e) Effect of light intensity and soil moisture on transpiration in pressurized and (f) unpressurized plants.

Table: 1. The conductance of soil-root system, active root length optimized for the model and R2 in each replication.

Replication	K_{plant}	L	R^2
	[cm^3 hPa^{-1} s^{-1}]	[cm]	
1	1.25×10^{-6}	700	0.9808
2	1.05×10^{-6}	200	0.3518
3	5.63×10^{-5}	350	0.8991
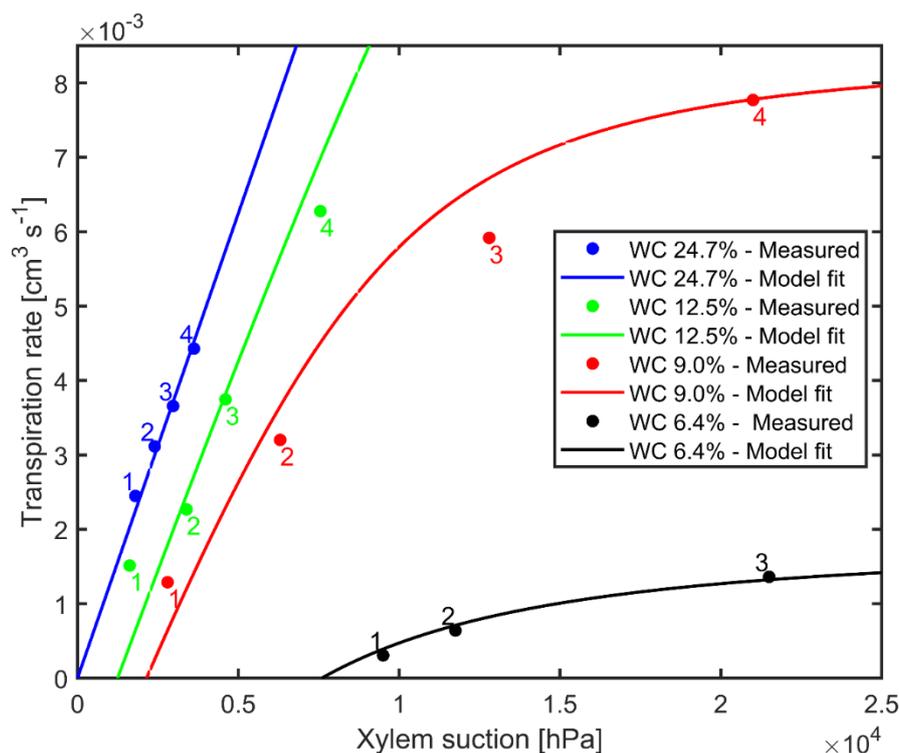
Figure 3. Measured xylem suction and transpiration rate for decreasing water contents (WC) and increasing light intensity (1-4) for replicate 1 (2 and 3 are shown as supplementary material). The solid lines are the model fits.

The slope of linear part of the curve at high water content (at WC = 24.7%) is interpreted as the plant conductance, K_{plant} (i.e. soil resistance is assumed to be negligible). This conductance was used in the simulations. For high water content, the conductance K_{plant} (at WC = 24.7%) was 1.25×10^{-6} [cm^3 hPa^{-1} s^{-1}]. The total soil-plant conductance reduced dramatically in dry soils at high transpiration rates due to the drop of soil hydraulic conductivity around the roots, which is well reproduced by the soil hydraulic model. The relation between transpiration rates, measured xylem tension and the model fitting for different water contents for replication 2 & 3 are shown in supplementary material (Fig. S5). Conductance of the root system, active root length used in the model and coefficient of correlation for each replication are shown in Table. 1.

The effect of light intensity and water content on normalized soil-plant conductance $k*$ is shown in Fig. 4. The $k*$ value is the ratio of soil-plant conductance to the maximum conductance measured in wet soil and low light intensity. In general, soil water content and light intensity and their interaction affected $k*$ extremely significantly ($p < 0.01$, Table S2). $k*$ is approximately constant in wet soil at each imposed light intensity. In drier soil (WC = 12.33% and 9.33%), $k*$ reduced with increasing light intensity. The reduction was extremely

significant ($p < 0.01$, Tukey-Kramer test) at WC = 9.33% where it occurred at light intensity of ca. 1500-2000 µmol m^{-2} s^{-1}. At WC = 12.33% the drop was only significant ($p < 0.05$, Tukey-Kramer test) at light intensity above 2000 µmol m^{-2} s^{-1}. Note that these were the conditions when transpiration was reduced in the unpressurized plants (Fig. 2b and c).
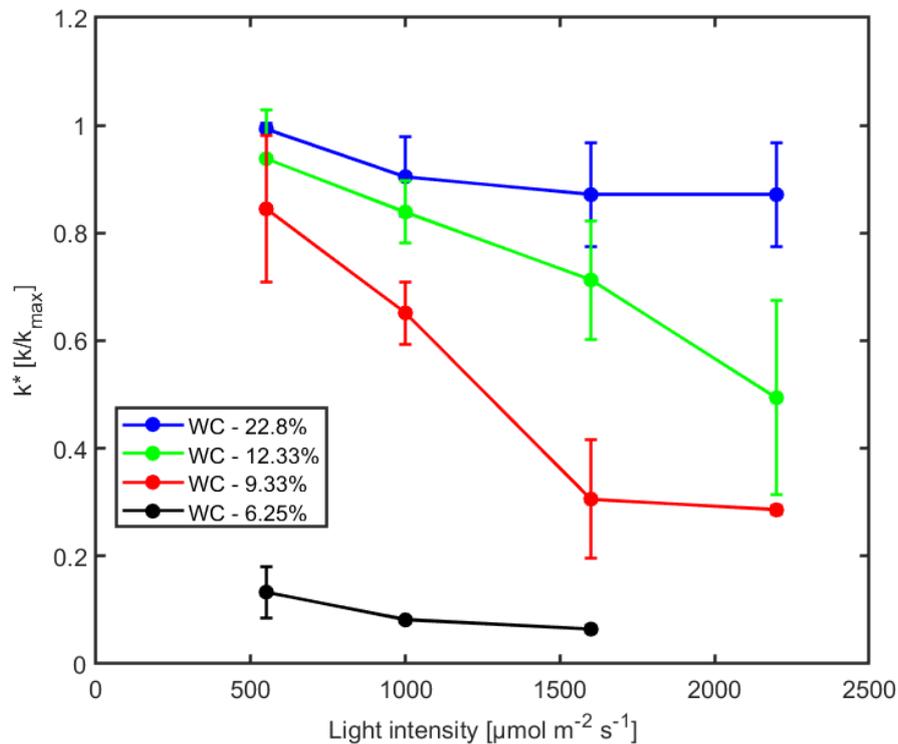
Figure 4. Effect of light intensity on normalized soil-plant conductance k*=k/k$_{max}$ (where k$_{max}$ is the soil-plant conductance in the wettest soil and lowest light intensity) at varying soil water contents (WC). Relative soil-plant conductance k* decreased with increasing light intensity due to higher transpiration rates and with decreasing soil water contents due to the decreasing soil hydraulic conductivity.

The relationship between P_0 [hPa] (intercept of xylem pressure and transpiration rate) and minus the soil matric potential [hPa] is plotted in Fig. 5. In principle, these values should fit unless there was a large osmotic gradient between the xylem and the soil. In dry soil, the values fitted rather well (consider that the estimation of the soil matric potential based on water retention curve are prone to errors in the dry range). In wet soil, (i.e. WC between 21.4% and 24.7%), the soil matric potential was slightly more negative than the fitted P_0, which indicates a more positive pressure in the xylem than in the soil, possibly caused by a more negative osmotic potential in the xylem than in the soil. The difference of ca. 50 -100 hPa is not detectable at more negative soil water potential (as explained in the note above).
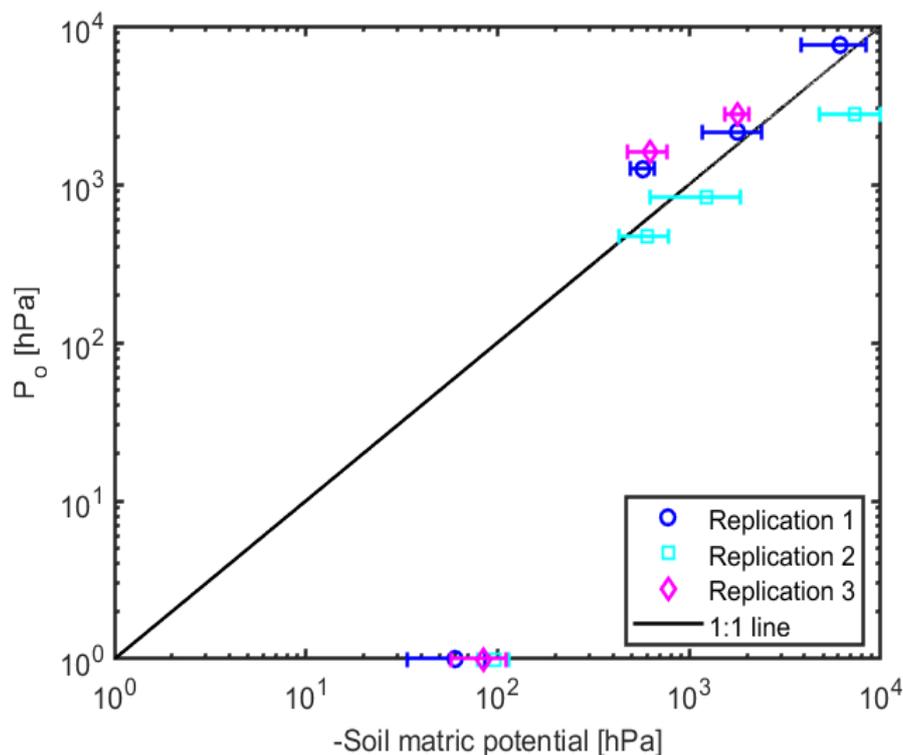
Figure 5. The relation between intercept (Po) and the soil matric potential. The points below (above) the 1:1 line indicate a more negative (positive) osmotic potential in the leaf xylem than in the soil.

3.5   Discussion and conclusions

We measured the relationship between leaf water potential and transpiration rates in maize at various soil water contents and light intensity. From this relationship, we estimated the soil-plant hydraulic conductance and its decrease with increasing transpiration rates and decreasing soil moistures. In parallel, we have measured the transpiration rates (for unpressurized plants). We have found that reductions in transpiration occurred in correspondence to reductions in soil-plant hydraulic conductance, which were caused by the loss of soil hydraulic conductivity around roots.

Pressurization increased the transpiration rates almost at all soil water contents and each imposed light intensity (see Fig. 2). However, this effect was particularly visible only in dry soil conditions and high light intensity. At WC = 9.33% and high light intensity (2200 µmol m^{-2} s^{-1}) pressurization increased transpiration by a factor of 3 (Fig. 2c) compared to unpressurized plants. At this condition, the leaf potential would have been around -2.1 MPa if the plant had not been pressurized (Fig. 3) and the relationship between leaf water potential and transpiration rate would have been extremely nonlinear (Fig. 3, red line, point 4). At low

soil water content and high light intensity the soil-plant hydraulic conductance was significantly reduced. Interestingly, the soil-plant hydraulic conductance was already reduced in wetter soil (WC = 12.33%) and at lower light intensity (WC = 9.33%, LI ≈ 1600 µmol m^{-2} s^{-1}). This suggests that the drop in hydraulic conductance anticipated (and possibly triggered) the reduction in transpiration. It also shows that stomatal regulation (prevented in the pressurized plants) occurred when the soil-plant hydraulic conductance decreased.

The relationship between leaf xylem tension and transpiration rate (under pressure) was linear in wet soils and became non-linear at drier soil conditions and increasing transpiration rates (Fig. 3). The non-linearity in this relationship corresponds to a decrease in soil-plant conductance shown in Fig. 4. This finding is consistent with previous measurements with barley (*Hordeum vulgare*) (Carminati et al., 2017) and wheat (*Triticum*) (Passioura., 1980), and fits well with early model of root water uptake (Gardner and Ehlig, 1963).

The soil-root hydraulics model was capable to reproduce the measured relationship between xylem tension and transpiration rate. The only unknown parameters of the model were: 1) the plant conductance K_{plant}, equal to the inverse of the slope of the xylem suction versus transpiration rate at high WC; and 2) the active root length *L*, which is the effective length of the roots actually taking up water, and which determines the onset of nonlinearity in the curves. The best fits were obtained with *L* = 200, 350 and 700 cm. Note that the measured total root length was much higher in the order of ca. 30000 cm. The active root length thus only represented 0.7-2.5% of the total root length. In reality, all roots might take up water, but at variable rates. For instance, Ahmed et al, (2018) showed that in mature maize most of the water uptake are taken up by crown roots were seminal roots and their lateral had a minor contribution to root water uptake. In addition, L might compensate experimental errors in measuring the soil conductivity or in assuming that soil and rhizosphere hydraulic properties are similar. Therefore, these values are fitting parameters and they should be cautiously interpreted.

Note also that active root length and root conductance are physically linked to each other, i.e. the longer the root, the larger its interface to soil and the bigger its conductance. These two variables were treated as independent in this study but this could be further investigated using allometric relations (F Meunier et al., 2017; Meunier et al., 2018).

The relation of estimated plant hydraulic conductivity and imposed matric potential for each replication showed that the soil-plant hydraulic conductance was constant in the wet soil and that the drop in soil-plant hydraulic conductance observed at increasing transpiration rate and

decreasing soil water content were well explained by the loss of soil hydraulic conductivity around the roots taking up water. Due to pressurization, xylem cavitation was likely to be prevented during the measurements and thus the decrease in conductivity was caused by soil drying.

In conclusion, we have shown that stomatal regulation reduces transpiration when soil-plat hydraulic conductance drops, preventing marked non-linearities in the relationship between leaf water potential and transpiration rate, as hypothesized in Sperry and Love, (2015). Soil-plant hydraulic conductance decreased at high transpiration rates and low soil water contents, as predicted by hydraulic models (Sperry et al., 1998). This result provides novel experimental evidence supporting the use of soil-plant hydraulic models to predict stomatal response to soil drying. Compared to studies focusing on xylem vulnerability (e.g. Anderegg et al., 2017), here we focused on soil drying as the cause of hydraulic limitation. Contrary to Anderegg et al. (2017), who found that stomata close much before the xylem cavitates, we found that stomata close when the soil hydraulic conductivity dropped. It means that for the tested maize in the silt-sand mixture, loss of soil hydraulic conductivity is the primary constraint to transpiration.

Acknowledgment

3.6   References

Ahmed, M.A., Passioura, J., Carminati, A., 2018. Hydraulic processes in roots and the rhizosphere pertinent to increasing yield of water-limited grain crops : a critical review. J. Exp. Bot. 69, 3255–3265. https://doi.org/10.1093/jxb/ery183

Anderegg, W.R.L., Wolf, A., Arango-Velez, A., Choat, B., Chmura, D.J., Jansen, S., Kolb, T., Li, S., Meinzer, F., Pita, P., Resco de Dios, V., Sperry, J.S., Wolfe, B.T., Pacala, S., 2017. Plant water potential improves prediction of empirical stomatal models. PLoS One 12, 1–17. https://doi.org/10.1371/journal.pone.0185481

Bates, L.M., Hall, A.E., Sciences, P., 1981. Stomatal Closure with Soil Water Depletion Not Associated with Changes in Bulk Leaf Water Status. Oecologia 50, 62–65.

Brodribb, T.J., McAdam, S.A.M., 2017. Evolution of the stomatal regulation of plant water content. Plant Physiol. 174, 639–649. https://doi.org/10.1104/pp.17.00078

Brooks, R.H., Corey, A.T., 1964. Hydraulic properties of porous media. Color. State Univ. Hydrol. Pap. Collins, USA. https://doi.org/citeulike-article-id:711012

Buckley, T.N., 2017. Modeling stomatal conductance. Plant Physiol. 174, 572–582. https://doi.org/10.1104/pp.16.01772

Carminati, A., Moradi, A.B., Vetterlein, D., Vontobel, P., Lehmann, E., Weller, U., Vogel, H.J., Oswald, S.E., 2010. Dynamics of soil water content in the rhizosphere. Plant Soil 332, 163–176. https://doi.org/10.1007/s11104-010-0283-8

Carminati, A., Passioura, J.B., Zarebanadkouki, M., Ahmed, M.A., Ryan, P.R., Watt, M., Delhaize, E., 2017. Root hairs enable high transpiration rates in drying soils. New Phytol. 216, 771–781. https://doi.org/10.1111/nph.14715

Carminati, A., Vetterlein, D., Koebernick, N., Blaser, S., Weller, U., Vogel, H.J., 2013. Do roots mind the gap? Plant Soil 367, 651–661. https://doi.org/10.1007/s11104-012-1496-9

Carter, J.N., Jensen, M.E., Traveller, D.J., 1980. Effect of mid- and late-season water stress on sugarbeet growth and yield. Agron. J. 72, 806–815. https://doi.org/10.2134/agronj1980.00021962007200050028x

Chaumont, F., Tyerman, S.D., 2014. Aquaporins: Highly Regulated Channels Controlling Plant Water Relations. Plant Physiol. 164, 1600–1618.

https://doi.org/10.1104/pp.113.233791

Comstock, J.P., 2002. Hydraulic and chemical signalling in the control of stomatal conductance and transpiration. J. Exp. Bot. 53, 195–200. https://doi.org/10.1093/jexbot/53.367.195

Cowan, I.R., 1965. Transport of Water in the Soil-Plant-Atmosphere System. J. Appl. Ecol. 2, 221–239. https://doi.org/10.2307/2401706

Draye, X., Kim, Y., Lobet, G., Javaux, M., 2010. Model-assisted integration of physiological and environmental constraints affecting the dynamic and spatial patterns of root water uptake from soils. J. Exp. Bot. 61, 2145–2155. https://doi.org/10.1093/jxb/erq077

Ehlert, C., Maurel, C., Tardieu, F., Simonneau, T., 2009. Aquaporin-Mediated Reduction in Maize Root Hydraulic Conductivity Impacts Cell Turgor and Leaf Elongation Even without Changing Transpiration. Plant Physiol. 150, 1093–1104. https://doi.org/10.1104/pp.108.131458

Gardner, W.R., 1960. Dynamic aspects of water availability to plants. Soil Sci. https://doi.org/10.1097/00010694-196002000-00001

Gardner, W.R., Ehlig, C.F., 1963. The influence of soil water on transpiration by plants. J. Geophys. Res. 68, 5719–5724. https://doi.org/10.1029/JZ068i020p05719

Hayat, F., Ahmed, M.A., Zarebanadkouki, M., Cai, G., Carminati, A., 2018. Measurements and simulation of leaf xylem water potential and root water uptake in heterogeneous soil water contents. Adv. Water Resour. 124, 96–105. https://doi.org/10.1016/J.ADVWATRES.2018.12.009

Knipfer, T., Besse, M., Verdeil, J.L., Fricke, W., 2011. Aquaporin-facilitated water uptake in barley (Hordeum vulgare L.) roots. J. Exp. Bot. 62, 4115–4126. https://doi.org/10.1093/jxb/err075

Mencuccini, M., Manzoni, S., Christoffersen, B., 2019. Modelling water fluxes in plants: from tissues to biosphere. New Phytol. 222, 1207–1222. https://doi.org/10.1111/nph.15681

Meunier, F., Couvreur, V., Draye, X., Vanderborght, J., Javaux, M., 2017. Towards quantitative root hydraulic phenotyping : novel mathematical functions to calculate plant-scale hydraulic parameters from root system functional and structural traits. J. Math. Biol. 75, 1133–1170. https://doi.org/10.1007/s00285-017-1111-z

Meunier, F., Zarebanadkouki, M., Ahmed, M.A., Carminati, A., Couvreur, V., Javaux, M., 2018. Hydraulic conductivity of soil-grown lupine and maize unbranched roots and maize root-shoot junctions. J. Plant Physiol. 227, 31–44. https://doi.org/10.1016/j.jplph.2017.12.019

Meyer, W.S., Green, G.C., 1980. Water Use by Wheat and Plant Indicators of Available Soil Water1. Agron. J. 72, 253–257. https://doi.org/10.2134/agronj1980.00021962007200020002x

Passioura, J.B., 1980. The Transport of Water from Soil to Shoot in Wheat Seedlings. J Exp Bot. 31, 333–345.

Peters, A., Durner, W., 2008. Simplified evaporation method for determining soil hydraulic properties. J. Hydrol. 356, 147–162. https://doi.org/10.1016/j.jhydrol.2008.04.016

Pickard, W.F., 1981. The ascent of sap in plants. Prog. Biophys. Mol. Biol. 37, 181–229. https://doi.org/10.1016/0079-6107(82)90023-2

Redondo, E., Hachez, C., Parent, B., Tardieu, F., Chaumont, F., Simonneau, T., 2009. Drought and Abscisic Acid Effects on Aquaporin Content Translate into Changes in Hydraulic Conductivity and Leaf Growth Rate: A Trans-Scale Approach. Plant Physiol. 149, 2000–2012. https://doi.org/10.1104/pp.108.130682

Schindler, U., Durner, W., Unold, G. Von, Mueller, L., Wieland, R., 2010. The evaporation method : Extending the measurement range of soil hydraulic properties using the air-entry pressure of the ceramic cup. J. Plant Nutr. Soil Sci. 173, 563–572. https://doi.org/10.1002/jpln.200900201

Schröder, T., Javaux, M., Vanderborght, J., Vereecken, H., 2007. Comment on ''Root Water Extraction and Limiting Soil Hydraulic Conditions Estimated by Numerical Simulation''. Vadose Zo. J. 6, 524–526. https://doi.org/10.2136/vzj2007.0042l

Simonneau, T., Ehlert, C., Maurel, C., Tardieu, F., 2009. Integrated control of leaf growth by cell turgor in response to combinations of evaporative demands and aquaporin-mediated reductions in root hydraulic conductivity. Comp. Biochem. Physiol. Part A Mol. Integr. Physiol. 153A, S228. https://doi.org/10.1016/j.cbpa.2009.04.572

Sinclair, T.R., Holbrook, N.M., Zwieniecki, M.A., 2005. Daily transpiration rates of woody species on drying soil. Tree Physiol. 25, 1469–1472.

https://doi.org/10.1093/treephys/25.11.1469

Sperry, John S, Adler, F.R., Campbell, G.S., Comstock, J.P., 1998. Limitation of plant water use by rhizosphere and xylem conductance: Results from a model. Plant, Cell Environ. 21, 347–359. https://doi.org/10.1046/j.1365-3040.1998.00287.x

Sperry, J.S., Love, D.M., 2015. What plant hydraulics can tell us about responses to climate-change droughts. New Phytol. 207, 14–27. https://doi.org/10.1111/j.1469-8137.2010.03195.x

Sperry, J.S., Wang, Y., Wolfe, B.T., Mackay, D.S., Anderegg, W.R.L., Mcdowell, N.G., Pockman, W.T., 2016. Pragmatic hydraulic theory predicts stomatal responses to climatic water deficits. New Phytol. 212, 577–589.

Tardieu, F., Davies, W.J., 1993. Integration of hydraulic and chemical signalling in the control of stomatal conductance and water status of droughted plants. Plant. Cell Environ. 16, 341–349. https://doi.org/10.1111/j.1365-3040.1993.tb00880.x

van Lier, Q. de J., Metselaar, K., van Dam, J.C., 2006. Root Water Extraction and Limiting Soil Hydraulic Conditions Estimated by Numerical Simulation. Vadose Zo. J. 5, 1264–1277. https://doi.org/10.2136/vzj2006.0056

Van Lier, Q.D.J., Van Dam, J.C., Metselaar, K., De Jong, R., Duijnisveld, W.H.M., 2008. Macroscopic root water uptake distribution using a matric flux potential approach. Vadose Zo. J. 7, 1065–1078. https://doi.org/10.2136/vzj2007.0083

3.7   Supplementary material
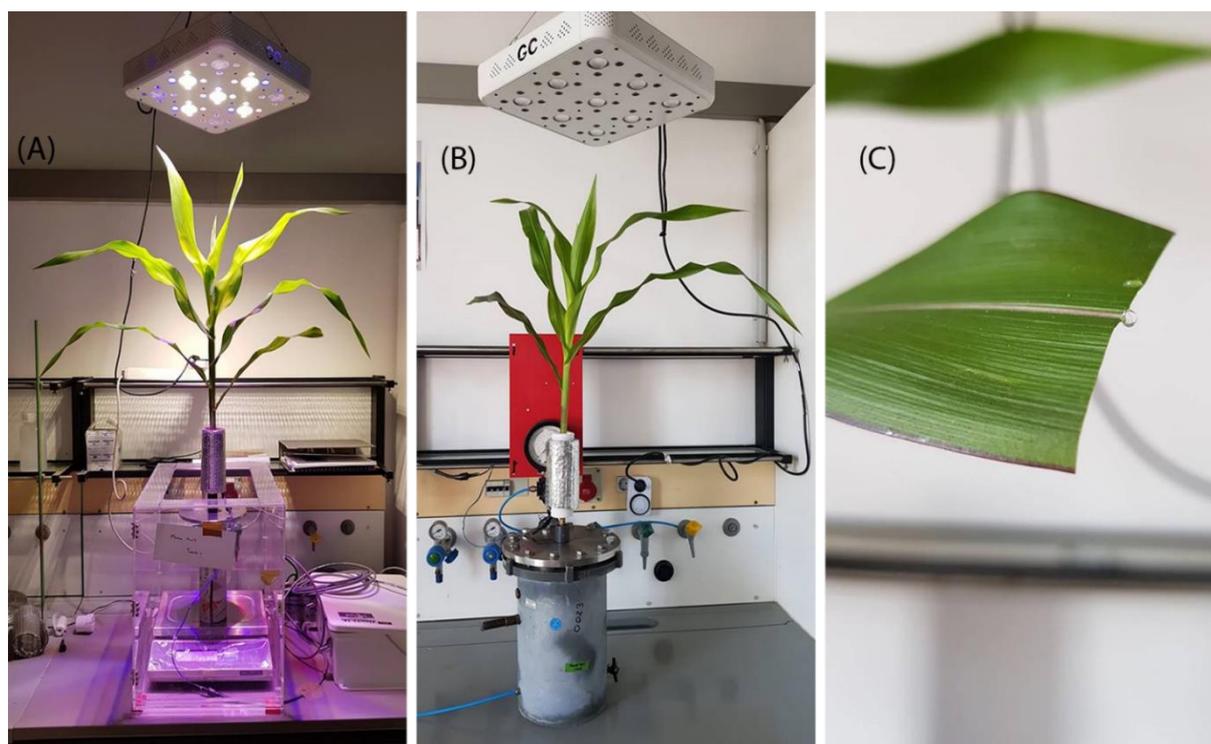
Figure S1. (a) Transpiration measurements using the sap flow sensor and balance; (b) plant in the pressure chamber with sap flow sensor connected; (c) water bleeding from the cut leaf.
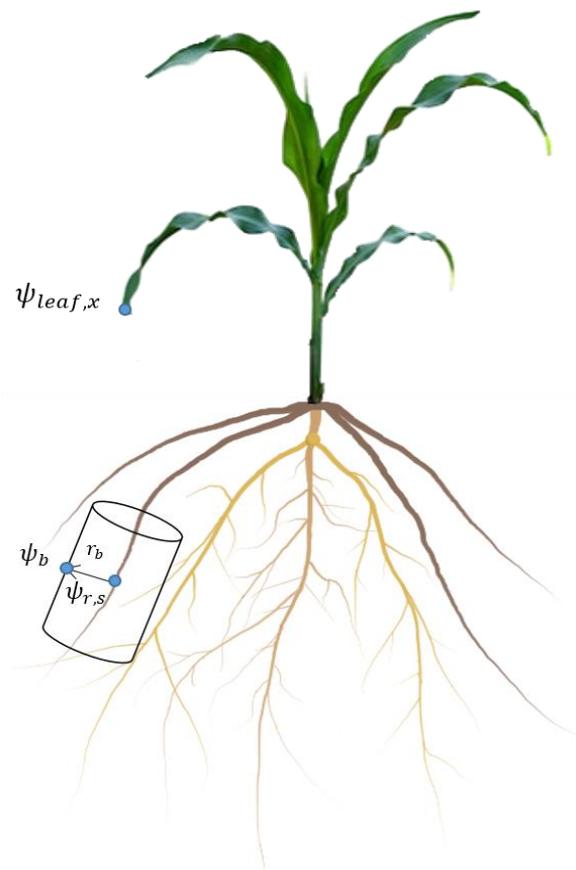
Figure S2. Schematic of the model used for simulation of leaf water potential. Here, ψ_b, $\psi_{r,s}$ and $\psi_{leaf,x}$ are the matric flux potential in the bulk soil, soil-root interface and in leaf xylem, respectively.
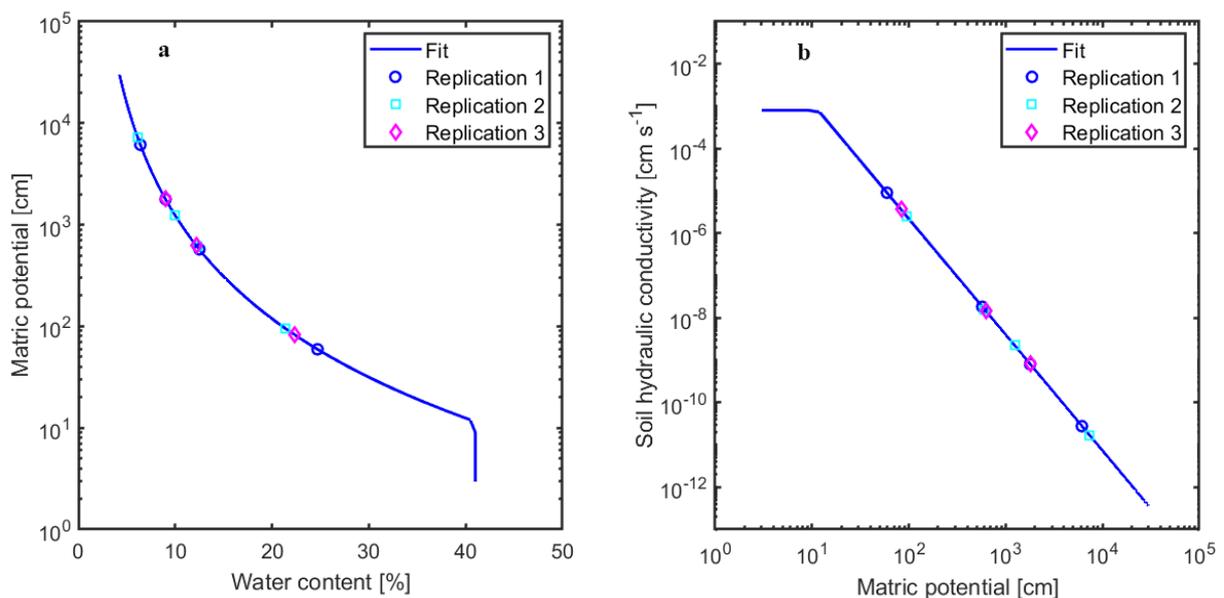
Figure S3. Brooks and Corey parameterization of hydraulic properties of soil: a) fitted soil water retention curve, b) fitted hydraulic conductivity curve. The dots show water the potential and the hydraulic conductivity of soil at different measured water contents for each replication.
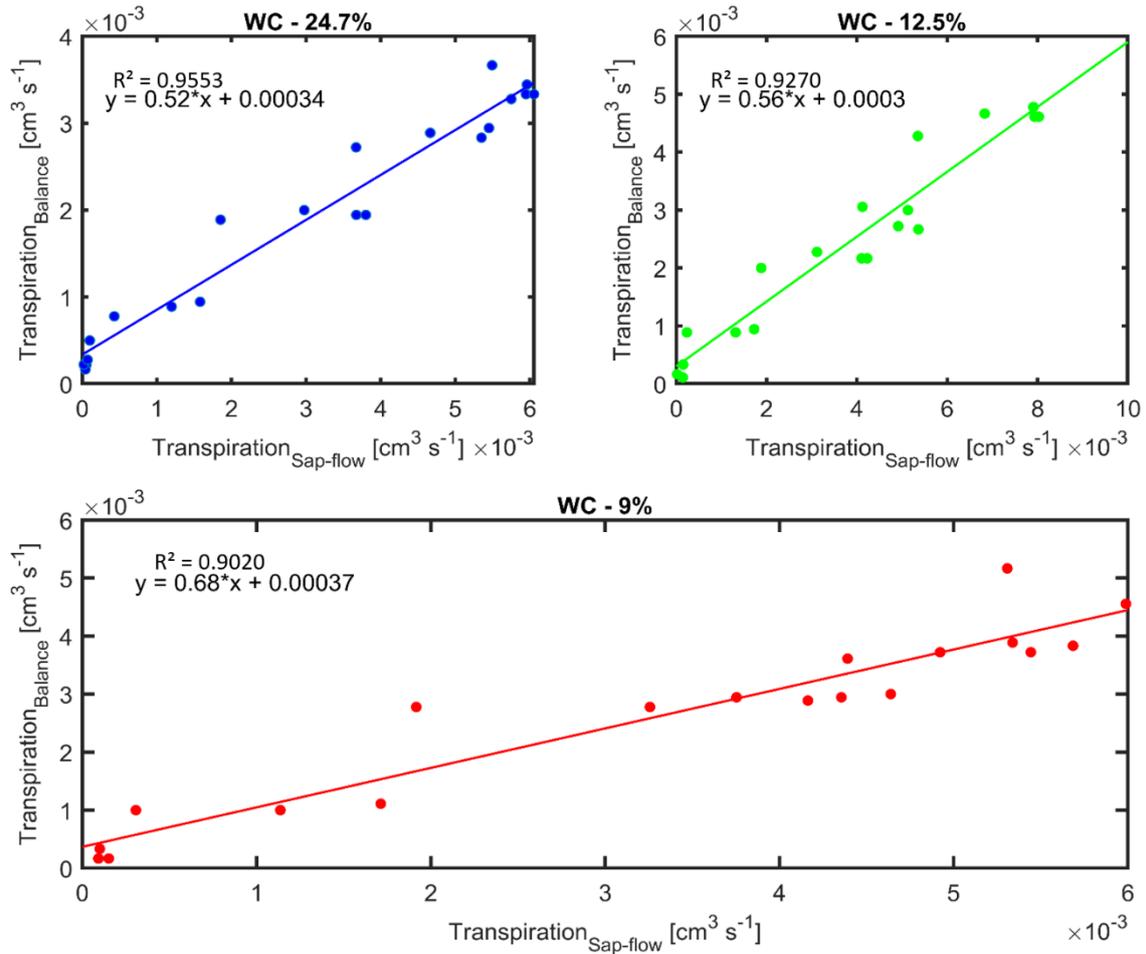
Figure S4. Calibration of transpiration rates measured by sap flow with gravimetric measurements.
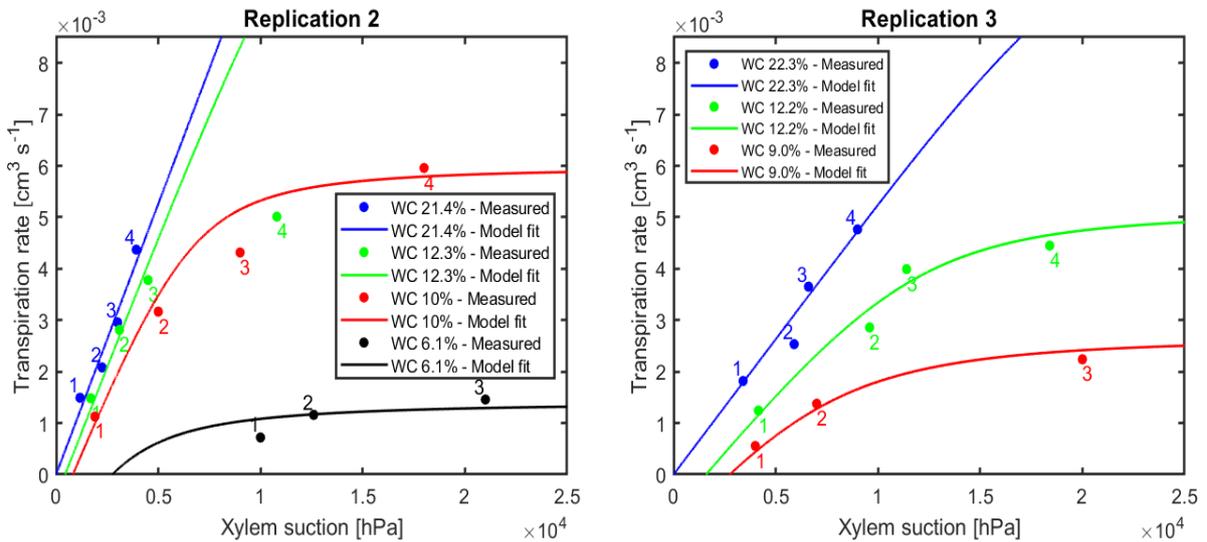
Figure S5. Measured xylem suction and transpiration rate for replication 2 & 3.

Table: S1. The analysis of variance (N-way ANOVA) for the influence of different factors on transpiration rate (P<0.001***, P<0.01**, P<0.05*).

Source[†]	SS[¶]	DF	MS	F	Prob > F
Pressurization	0.00001	1	5.29×10^{-6}	8.86	**0.0044****
Soil moisture	0	2	1.93×10^{-8}	0.03	0.9683
Light intensity	9.00×10^{-5}	3	3.06×10^{-5}	51.13	**<0.001*****
Pressurization * Soil	0	2	1.13×10^{-6}	1.88	0.1621
Pressurization * light	1.00×10^{-5}	3	2.34×10^{-6}	3.91	**0.0135***
Soil moisture * light	0	6	6.54×10^{-7}	1.09	0.3788
Error	3.00×10^{-5}	52	5.98×10^{-7}	-	-
Total	1.40×10^{-4}	69	-	-	-

[†]The measurements with the soil water content of 0.06 were not included since the transpiration was missing from the sap flow measurement. SS[¶]: sum of squares, DF: degree of freedom, MS: mean sum of squares, F: F-statistic value.

Table: S2. The analysis of variance (N-way ANOVA) for the influence of different factors on k* (P<0.001***, P<0.01**, P<0.05*).

Source[†]	SS[¶]	DF	MS	F	Prob > F
Soil moisture	0.85326	2	0.42663	48.12	**<0.001*****
Light intensity	0.30498	2	0.15249	17.20	**<0.001*****
Soil moisture * light intensity	0.30416	8	0.03802	4.29	**0.0022****
Error	0.2305	26	0.00887	-	-
Total	4.11164	40	-	-	-

[†]The measurements with the soil water content of 0.06 were not included since the transpiration was missing from the sap flow measurement. SS[¶]: sum of squares, DF: degree of freedom, MS: mean sum of squares, F: F-statistic value.

84

4   Chapter Four

Quantification of hydraulic redistribution in maize roots using neutron radiography

Faisal Hayat[1*], Mohsen Zarebanadkouki[1], Mutez Ali Ahmed[1], Thomas Buecherl[2], Andrea Carminati[1]

[1]   Chair of Soil Physics, University of Bayreuth, Bayreuth D-95447, Germany

[2]   Radiochemie München, Technische Universität München, 85748 Garching, Germany

[*]   Corresponding author: Faisal.Hayat@uni-bayreuth.de

4.1 Abstract

Plants redistribute water from wet to dry soil layers through their roots, in the process called hydraulic redistribution. Although the relevance and occurrence of this process are well accepted, resolving the spatial distribution of hydraulic redistribution remains challenging. Here we show how to use neutron radiography to quantify the rate of water efflux from the roots to the soil.

Maize (*Zea mays* L.) plants were grown in a sandy substrate 40 cm deep. Deuterated water (D_2O) was injected in the bottom wet compartment and its transport through the roots to the top dry soil was imaged using neutron radiography. A diffusion-convection model was used to simulate the transport of D_2O in soil and root and inversely estimate the convective fluxes.

Overnight, D_2O appeared in nodal and lateral roots in the top compartment. By inverse modelling, we estimated an efflux from lateral roots into the dry soil equal to j_r=2.35×10^{-7} cm s^{-1}. A significant fraction of the redistributed water flew toward the tips of nodal roots (3.85×10^{-8} cm^3 s^{-1} per root) to sustain their growth. The efflux from nodal roots depended on the roots' length and growth rate.

In summary, neutron imaging was successfully used to quantify hydraulic redistribution. A numerical model was needed to differentiate the effects of diffusion and convection. The highly resolved images showed the spatial heterogeneity of hydraulic redistribution.

Abbreviations

D_2O, deuterated water; HR, hydraulic redistribution; LED, light-emitting diode, SWC, soil water content.

Core Ideas

- Measuring the spatial distribution of HR along the root system remains challenging.
- Neutron radiography was used to trace the transport of D_2O from wet to dry soil layers.
- Radial fluxes were estimated using diffusion–convection model of D_2O transport in soil and root.
- Water was redistributed from wet to dry soil layers through fine lateral roots.
- A fraction of HR water was used to sustain the growth of young nodal roots.

Key words

Zea maize. L*,* nodal roots, neutron radiography, hydraulic redistribution, root growth

4.2   Introduction

Water is heterogeneously distributed in soils, and understanding how root water uptake and root growth respond to such heterogeneity is crucial to predict plant response to drought. Root water uptake from deep wet soil layers helps plants to tolerate drought periods (Sharp & Davies, 1985; Zegada-Lizarazu & Iijima, 2004). Besides sustaining the transpiration demand of plants, a fraction of the water extracted from the subsoil is redistributed within the root system to dry soil layers due to gradients in water potential in the process called hydraulic redistribution (HR; Burgess, Adams, Turner, & Ong, 1998; Caldwell & Richards, 1989; Richards & Caldwell, 1987). Hydraulic redistribution is also referred to as hydraulic lift when water moves from deep wet soil to top dry soil layers (Brooks, Meinzer, Coulombe, & Gregg, 2002; Smart, Carlisle, Goebel, & Núñez, 2005). Redistributed water can replenish up to 35% of the total daily used water from the upper 2 m of soil layers under drought conditions (Brooks et al., 2002). The redistributed water sustains root growth or life span of fine roots (Bauerle, Richards, Smart, & Eissenstat, 2008) and increases nutrient availability in drier soil (Caldwell, Dawson, & Richards, 1998; Snyder, James, Richards, & Donovan, 2008; Wang, Tang, Guppy, & Sale, 2009).

Although the occurrence, relevance, and amount of HR are well accepted and documented, resolving the spatial distribution of HR along the root system and into the soil remains challenging. Neutron radiography, thanks to its high sensitivity to water and thus to roots, is an imaging method with great potential to quantitatively estimate root distribution and water flow in soil and roots (Moradi et al., 2011; Oswald et al., 2008). Warren, Bilheux, Kang, et al., (2013) used neutron radiography and deuterated water (D_2O) to trace HR in seedlings of *Zea mays* L. and *Panicum virgatum* L. The authors showed a high sensitivity of neutron radiography to small changes in D_2O concentrations, which enables them to visualize the translocation of D_2O through the roots of young plants.

Interpretation of time-series radiographs of D_2O is challenging (Carminati & Zarebanadkouki, 2013; Warren, Bilheux, Cheng, and Perfect 2013), and several possible artifacts should be considered. The neutron attenuation coefficient of D_2O is much lower than that of H_2O. When

D_2O replaces H_2O in a given root or soil region, the attenuation coefficient of that region largely drops, making the redistribution of D_2O visible over time. However, neutron attenuation does not depend only on the fraction of D_2O and H_2O, but also on the total content of liquid (the sum of D_2O and H_2O). This value changes in soils due to water uptake and HR and small increases (or decreases) in liquid content can cause significant underestimation (or overestimation) of the concentration of D_2O (Carminati & Zarebanadkouki, 2013). This problem is more critical for soils (whose moisture content easily varies from 0 to 0.4) than for roots. However, root shrinkage might similarly affect the interpretation of the neutron signal. An additional complexity is that the transport of D_2O in soils and plants depends on both diffusion and convection. It means that an increase (or decrease) of D_2O in roots and soil does not necessarily indicate a net flow into (or from) roots, but it might be caused by diffusion driven by gradients in D_2O concentration. Zarebanadkouki, Kroener, Kaestner, and Carminati (2014) conducted a series of D_2O tracing experiments during the day and nighttime and developed a numerical model simulating diffusion and convection of D_2O in soil and roots. The authors proved that the diffusion of D_2O from the root surface to its xylem is as significant as the convective fluxes, also during the daytime, and it should be properly modeled to quantify the local fluxes of water. The method was used for quantifying root water uptake in homogeneous soil moisture conditions (Ahmed, Zarebanadkouki, Kaestner, & Carminati, 2016; Ahmed et al., 2018), but it has not yet been tested to quantify the efflux of water from the roots during nighttime.

The objective of this technical note was to test whether the combination of neutron radiography, D_2O injection, and a diffusion–convection model allows quantification of HR and hydraulic lift. To test the feasibility of the method, we grew maize (*Z. mays*) plants in a sandy substrate that was partitioned into two horizontal compartments hydraulically separated by a 1-cm layer of coarse sand acting as a capillary barrier. When plants were well established, we let the upper compartment dry while we kept the lower compartment wet. Then D_2O was injected at the lower wet compartment, and its transport within the root system was monitored for a period of ~15 h (a daytime cycle followed by a nighttime cycle) using a time series neutron radiography. We also made two additional tests: (a) we injected H_2O instead of D_2O to monitor possible root shrinkage and swelling; and (b) we injected D_2O in a sample whose top and bottom compartments were both kept wet, to test the effect of diffusion on D_2O dynamics in the top compartment.

4.3   Materials and methods

4.3.1   Soil and plant preparation

Three maize plants were grown in aluminum containers (40 cm high, 40 cm wide and 1 cm thick). The containers were filled with a mixture of silt and sand (1:1 ratio) with particle size < 1 mm and a bulk density of 1.4 g cm^{-3}. A 1 cm layer of fine gravels (particle size of 2-2.5 mm) was placed at a depth of 20 cm to hydraulically disconnect the top and bottom soil compartments without hindering the root growth (similar to Ahmed et al., 2016; Zarebanadkouki et al., 2012).

Maize seeds were germinated for 48 hours and then planted in the containers (one seed per container). The soil surface was covered with fine gravels (particle size of 2 to 2.5 mm) to minimize evaporation. Plants were grown in a climate room with a photoperiod of 14 hours (from 7 am to 9 pm), day/night temperature of 24 °C/19°C, relative humidity of 60% and light intensity of 750 µmol m^2 s^{-1}. Plants were irrigated every third day during the first 3 wk allowing roots to grow uniformly in both compartments. Afterwards, the soil water contents (SWC) were adjusted in the top and bottom compartments to the following scenarios. First, in two plants, the top soil compartment was kept dry (SWC ≤ 0.06, corresponding to a matric potential < −1000 hPa, as estimated according to the water retention measured in Hayat et al., 2020) and the bottom compartment was kept wet (SWC ≈ 0.22, corresponding to a water matric potential of ca. -80 hPa); we refer to this scenario as dry-wet. Second, in one plant both compartments were kept wet (SWC ≈ 0.22); we refer to this scenario as wet-wet. Prior to neutron radiography experiments, a light-emitting diode (LED) lamp (GC 9, Greenception, with specifications: photon flux intensity at height of 30 cm above plant ≈ 1800 µmol m^2 s^{-1} and maximum spectrum wavelength of 700 nm) was installed above the plants. The average transpiration at day time of dry-wet and wet-wet samples was 4.66 ± 0.26 and 4.87 g h^{-1}, respectively. The neutron radiography measurements started when plants were 40 days old.

4.3.2   Neutron radiography

Neutron radiography is a noninvasive imaging technique that allows for imaging water and root distribution in the soil (Carminati et al., 2010; Tumlinson, Liu, Silk, & Hopmans, 2008; Zarebanadkouki, Kim, & Carminati, 2013). The transmitted neutrons beam carries the

information of the sample composition and thickness. The Beer-Lambert law describes the attenuation of the neutron beam (Kasperl & Vontobel, 2005) through the sample by:

$$\frac{I}{I_0} = exp\left[-\sum_{i=1}^{i=n}(\mu_i d_i)\right] \qquad \text{(Eq. 1)}$$

where, I is the detected neutron intensity [cm^{-2} s^{-1}], I_0 is the incident neutron intensity [cm^{-2} s^{-1}], μ_i is the neutron attenuation coefficient [cm^{-1}] and d_i is the thickness [cm] of the material i. The material composing our samples were aluminum, dry soil, root (here intended as dry mass), H_2O and D_2O. The attenuation of dry soil and aluminum were derived from the radiograph of a container filled with dry soil. The attenuation coefficients of H_2O and D_2O were experimentally estimated from the radiograph of control samples with a known thickness of normal and deuterated water.

The neutron radiography experiments were carried out at the NECTAR (neutron computed tomography and radiography) facility (Bücherl & Söllradl, 2015) at the Heinz Maier-Leibnitz center, Technical University Munich (TUM) using its new option of thermal neutron radiography (Mühlbauer et al., 2018).

The thermal neutron spectrum is provided at the measurement position through a flight tube of 4 m in length with an entrance aperture of 25 mm in diameter. This resulted in a calculated length/diameter ratio of 240 and a measured integral neutron intensity of 7.9×10^6 cm^{-2} s^{-1} at the sample position. The detector system consists of a ^{6}LiF/ZnS scintillator screen of 100 μm thickness, which converts the neutrons into light, which is mirrored on a Andor iKon-L-BV charge-coupled device (CCD) camera (model DZ936N BV) with 2048 x 2048 pixels and a pixel size of 13.5μm x 13.5μm. The CCD-camera was operated at a temperature of -97°C, thus having a dark current of less than 0.0001 electrons/pixel/s.

The samples were placed as close as possible to the scintillator screen of the detector system (i.e. in a distance of about 3 cm). This setup corresponds to a quasiparallel neutron beam geometry.

A complete set of data for one radiograph consisted of dark current images (i.e. images with the camera shutter and the neutron beam closed), flat field images (i.e. images without sample) and images with sample. All images were recorded for 20s, each. From series of dark images and flat field images the mean dark image $I_{DC}(x,y)$ and the flat field image $I_{FF}(x,y)$ were calculated, respectively. As the sample sizes were larger than the beam area, succeeding

measurements at two vertical and two horizontal positions, each, could be performed to scan the complete sample on a two-by-two grid with overlapping margins.

An identical LED lamp, used prior to neutron radiography, was installed above the plants during the day measurements.

4.3.3 D₂O experiment

Deuterated water (D_2O) was used to trace the flow of water in soil and roots. Due to its lower neutron attenuation coefficient compared with H_2O, D_2O is easily distinguishable in neutron radiographs. We injected 30 ml of D_2O (purity of 99.97%) at two selected locations in the bottom wet compartment (15 ml at each location) using fine syringes (Figure 1). The spatiotemporal distribution of D_2O in each compartment and its transport along the roots were monitored by time-series neutron radiography with a temporal resolution of one frame every 20 s. The D_2O tracing measurements started during the daytime (between 4:30 and 6:00 p.m.) and continued till the next morning (around 8:00 a.m.). The light was turned off at 7:00 p.m. and turned on again at 7:00 a.m. The samples were not moved throughout the time series to avoid artifacts due to imprecise referencing. The reconstructed image of one entire sample before injection of D_2O is shown in Figure 1. The image was obtained by overlapping four radiographs. The gray values show the water content in the sample (i.e., the darker the image, the higher the soil water content). As roots have high water content, they appear dark. The roots in which D_2O transport is quantified are shown in colors. Here, three different root types are selected: seminal roots reaching the bottom compartment and immersed in D_2O after D_2O injection, lateral roots, and nodal roots with their tips in the top compartment.

4.3.4 Control experiments

To ensure that the D_2O measurements were correctly interpreted (see discussion later), in one of the samples of the dry-wet scenario, we first injected 30 ml of H_2O in the bottom wet compartment and monitor water redistribution within the root system overnight. D_2O was injected 24 hours later.
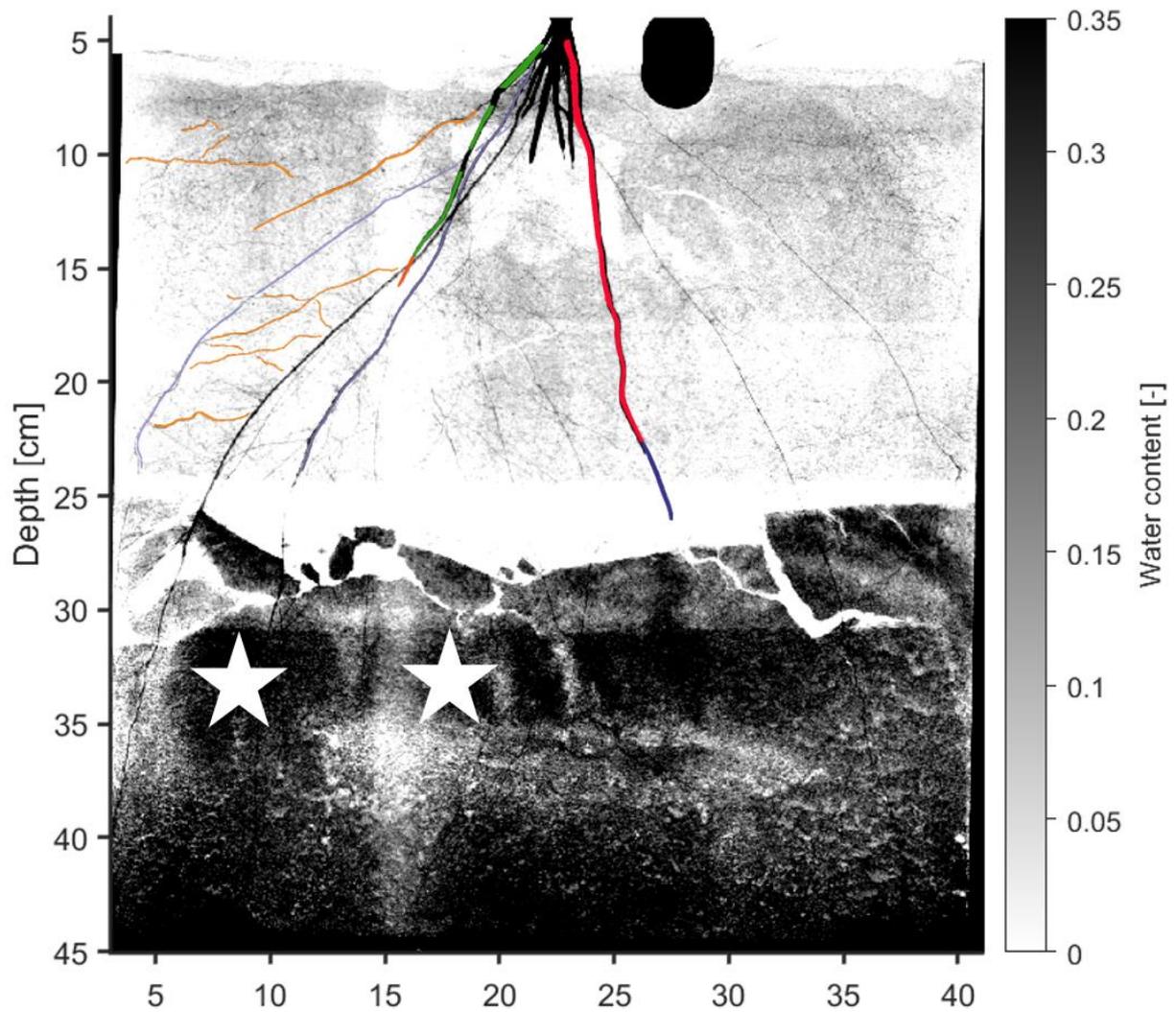
Fig 1. Reconstructed image of entire sample (dry-wet) before the injection of deuterated water (D₂O). The stars indicate the locations where D₂O was injected (in the bottom compartment). The image was obtained by overlapping 4 radiographs. The gray values represent water content (the darker the image, the higher the soil water content). The segmented roots in which we quantified the D₂O concentration are shown in light purple orange and red + green colors and are categorized as seminal roots, laterals and nodal (long + short), respectively.

4.3.5   Image analysis

The obtained neutron radiographs were normalized for the flat field (radiograph without sample) and dark current (signals recorded by the camera in the absence of a beam) as:

$$I_{norm}(x,y,t) = \frac{I(x,y,t) - I_{DC}(x,y)}{I_{FF}(x,y) - I_{DC}(x,y)} \times \frac{D_0}{D(t)} \qquad \text{(Eq. 2)}$$

where x and y refer to the spatial coordinates of pixels in x and y direction, t refers to the time after D₂O injection, $I_{norm}(x,y,t)$ is the normalized image, $I(x,y,t)$ is the recorded image at

time t, $I_{DC}(x, y)$ is the dark current image, $I_{FF}(x, y)$ is the flat field image and D_0 and $D(t)$ are scalar values proportional to the neutron attenuation at time zero and any given time t in a blank area of radiographs, respectively. By combining the Beer-Lambert law for these samples:

$$-log\left(\frac{I_{norm}(x,y,t)}{I_{dry}(x,y)}\right) = \mu_{H2O}d_{H2O}(x,y,t) + \mu_{D2O}d_{D2O}(x,y,t) \qquad \text{(Eq. 3)}$$

where $I_{dry}(x, y)$ is the radiography of the dry sample, μ_{H2O} [cm^{-1}] and d_{H2O} [cm] are the attenuation coefficient and thickness of normal water (H$_2$O), and μ_{D2O} [cm^{-1}] and d_{D2O} [cm] are the attenuation coefficient and thickness of heavy water (D$_2$O). The measured attenuation coefficients for normal water (μ_{H_2O}) and deuterated water (μ_{D_2O}) were 1.04 cm^{-1} and 0.335 cm^{-1}, respectively. The sharp difference in water contents between roots and the surrounding soil allowed us to segment roots. We segmented roots using Matlab (2018b, MathWorks). Length and diameter of segmented roots were calculated using the Euclidean distance mapping functions in Matlab (2018b).

The concentration of D$_2$O within the roots were calculated according to the protocol presented in Zarebanadkouki et al., (2012). We define $\mu_{root}(t)$ [cm cm^{-1}] as the neutron attenuation in the pixel containing roots as

$$\mu_{root}(t) = -log\left(\frac{I_{norm}(x,y,t)}{I_{dry}(x,y)}\right)\frac{1}{d_{root}} \qquad \text{(Eq. 4)}$$

where d_{root} is the root thickness [cm]. We assumed that the volumetric liquid content of the root tissue did not change after immersion in D$_2$O. It follows that

$$d_{root}^{H2O}(t = 0) = d_{root}^{D2O}(t) + d_{root}^{H2O}(t) \qquad \text{(Eq. 5)}$$

Then the pixel-wise concentration of D$_2$O in the pixel containing root can be calculated as

$$C_{D2O,root} = \frac{d_{root}^{D2O}}{d_{root}^{liq}} \qquad \text{(Eq. 6)}$$

where

$$d_{root}^{D2O} = \frac{\left(\mu_{root}(t) - \mu_{root}(t=0)\right) d_{root}}{\mu_{D2O} - \mu_{H2O}} \qquad \text{(Eq. 7)}$$

The total liquid thickness in the root (d_{root}^{liq}) was calculated as H$_2$O thickness in the first radiograph before D$_2$O was injected – i.e. $d_{root}^{liq} = d_{root}^{H2O}(t = 0)$. Here we assumed that the

change in pixel-wise water content of the soil in the upper compartment is negligible. The concentration of D₂O in the root was averaged along the root segment.

We calculated the growth rate of roots assuming that the water constitutes the major fraction of the root tissue:

$$\Delta V_{root}^{H2O} = \Sigma \left(\frac{(\mu_{root}(t) - \mu_{root}(t=0))\, d_{root}}{\mu_{H2O}} \right) \times Res^2 \qquad \text{(Eq. 8)}$$

where the right hand side of equation (8) refers to the summation of neutron attenuation in both x and y coordinates of pixels containing root tissue, $\mu_{root}(t)$ refers to the average neutron attenuation across the thickness of root tissue in the radiographs, and Res is the pixel size.

We calculated the concentration of D₂O in three different root types in the top soil compartment as illustrated in Figure 1. The first were seminal and primary root segments that reached the bottom compartment where D₂O was injected. These roots took up D₂O from the soil and transported it axially upwards towards the shoot via transpiration stream; we refer to these roots as seminal roots. The second were lateral roots that were located in the top compartment and were not immersed in D₂O but received D₂O from the seminal roots; we refer to these roots as lateral roots. The third were nodal and crown roots located in the top compartment and that had not yet crossed the capillary barriers and reached the D₂O injected compartment; we refer to these roots as nodal roots. The second and third types of roots could only receive D₂O from the root–shoot conjunction.

4.3.6   Model of D₂O transport into roots

To derive the fluxes of water from the temporal dynamics of D₂O concentration, we employed a diffusion-convection model (Ahmed et al., 2016, 2018; Zarebanadkouki, Kroener, Kaestner, & Carminati, 2014). The transport of D₂O in roots and soil depends on (a) diffusion due to gradients in the concentration of D₂O in soil and root and (b) convection due to water fluxes driven by transpiration and hydraulic redistribution.

We simulated the D₂O transport in a single root, in which water flow axially along the xylem and radially across the cortex (Figure 2). The change in D₂O concentration in the root is described by:

$$\theta \frac{\partial c}{\partial t} = \frac{\partial}{r \partial r}\left(rD\left(\frac{\partial c}{\partial r} \right) \right) - \frac{\partial}{r \partial r}(r j_r C) - \frac{\partial}{\partial x}(j_x C) \qquad \text{(Eq. 9)}$$

where, $\theta(r,x)$ is the water content [cm^3 cm^{-3}], $C(r,x,t)$ is the D$_2$O concentration in the root [cm^{3}cm^{-3}], t is the time [s], r is the radial coordinate [cm], x is the longitudinal coordinate [cm], $j_r(r)$ is the radial flux of water [cm s^{-1}], $j_x(r,x)$ is the axial flux of water [cm s^{-1}] and D is an effective diffusion coefficient of D$_2$O [cm^2 s^{-1}]. The axial flux of water within the root xylem is estimated by mass conservation equation, assuming that the axial transport of D$_2$O occurs only in the root xylem, as

$$\pi r^2 \frac{\partial j_x(x)}{\partial x} = -2\pi r j_r \quad \text{(Eq. 10)}$$

where the axial flux j_x changes along x while j_r is assumed to be uniform along x. The water flux into the roots at the basal part is referred to as $j_{x,basal}$ and at the root tip is called $j_{x,tip}$ (Figure 2). The axial fluxes can be positive or negative and indicate HR and water uptake, respectively (x increases toward the root tip). A positive j_r indicates the efflux of water from the root to the soil and negative j_r indicates root water uptake.
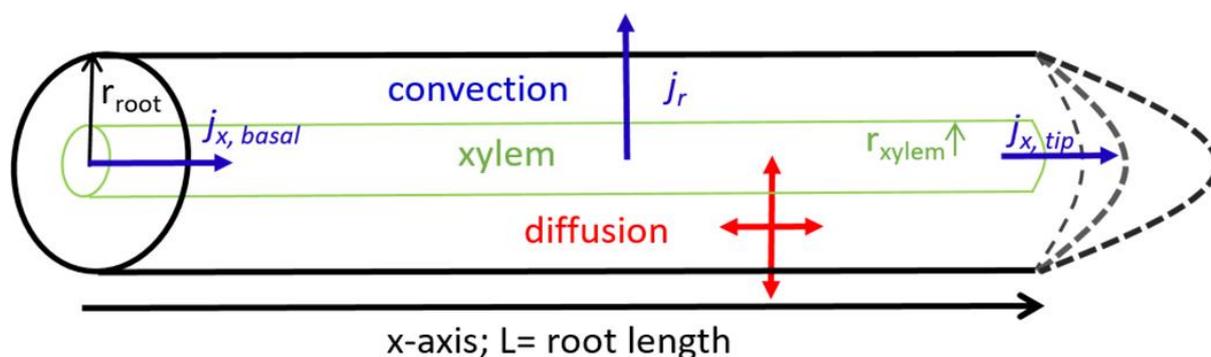

Fig 2. Illustration of deuterated water (D$_2$O) transport model into the root. Here, red and blue arrows show diffusive and convective fluxes, respectively. Radial water fluxes j_r can be directed toward the root surface (water uptake) or toward the soil (hydraulic lift). Axial fluxes could be toward the root tip (to sustain growth and hydraulic lift) or toward the basal part (to sustain transpiration).

4.3.7   Model implementation

We modeled the transport of D$_2$O into roots in the top soil that had no direct access to D$_2$O from the soil (lateral and nodal roots, Figure 1). D$_2$O transport was simulated in single roots (no branching) from their basal parts to the root tips. As roots grew during the measurements (16 h), root growth was included as convective flux toward the root tip (see below).

The diffusion-convection equation (Eq. 9) was numerically solved in radially symmetric coordinates using a finite difference method. The flow domain from soil towards the root xylem

and from the tip roots towards the basal parts was represented in a 2D computational grid with 40 equally spaced grid elements along the root radius and 110 grid elements along the root length. The diffusion-convection equation was solved assuming the following initial and boundary conditions:

$$C(r, x, t = 0) = 0$$

$$\frac{\partial C(r = 0, x, t)}{\partial r} = 0$$

$$C(r \leq r_{xylem}, x = x_{basal}, t) = C_0(t)$$

$$j_r(r = r_{out}) = \frac{r_{root}}{r_{out}} j_{root}$$

$$j_x(r \leq r_{xylem}, x = x_{tip}, t) = j_{x,tip}(t)$$

$$j_x(r \leq r_{xylem}, x = x_{basal}, t) = j_{x,basal}(t)$$

where $r = 0$ is the root center, r_{out} is the outer radius of soil (radius of the root, $r_{root,}$ plus the thickness of soil used in our simulation), C_0 is the quantified D_2O concentration at the root surface in the soil during the measurements, j_{root} is the radial flux of water at the root surface, $x = x_{tip}$ refers to the position of the root tip, $j_{x,tip}$ is the axial flux of water at the root tip, x_{basal} refers to the position of the root at its basal parts at which the root segment was connected to the seminal roots (for the case of lateral roots) and the root-shoot conjunction (for the case of crown roots), and $j_{x,basal}$ is the axial flux that the basal parts of each root segment. The diffusion coefficient of D_2O in the soil was taken from the value of diffusion coefficient D_2O in free water and scaled for the porosity and soil water content, according to Millington and Quirk (1959). The values of diffusion coefficient across the root tissues were taken from Ahmed et al, (2016). The inverse problem was solved in Matlab (2019b) using the patternsearch solver from its optimization toolbox.

4.4   Results

Some selected neutron radiographs at different times after D_2O injection in one of the two dry–wet samples are presented in Figure 3 (same plant as shown in Figure 1). The radiographs show the difference between the actual radiograph and that before D_2O injection. The brighter is the color the higher is the D_2O concentration. Shortly after being injected, D_2O was taken up by

seminal roots and was axially transported upwards towards the shoot following the transpiration stream (Figure 3a). During nighttime (from 7:00 p.m. to 7:00 a.m.), the lateral roots that were not in direct contact with D_2O in the injected compartment gradually turned bright. Similarly, the nodal roots that were not in direct contact with D_2O in the injected compartment also turned gradually bright. With time, the tip of nodal roots grew and appeared dark in the radiographs (Figure 3e). These observations (lateral roots turning bright over time) were consistent in the second sample (Supplemental Figure S1).

In the sample in which both top and bottom compartments were kept wet (Supplemental Figure S2), no increase of D_2O in lateral and nodal roots was detectable overnight. When only H_2O was injected, lateral roots did not change their attenuation coefficient, indicating that neither shrinking nor swelling were detectable. The latter experiment was done to exclude that the increasing root transparency (observed in the case of the dry–wet scenario) was caused by root shrinkage.

The average D_2O concentrations in roots located in the top compartment are shown in Figure 4. In seminal roots, the concentration of D_2O increased shortly after D_2O injection during daytime, and then it decreased and reached rather constant values during nighttime. The concentration increased again as transpiration restarted in the next morning. In the dry–wet scenario, D_2O concentration in lateral roots progressively increased during the nighttime. On the contrary, lateral roots in the wet–wet scenario showed a slight increase in the concentration of D_2O only in the first hour when the plant was still transpiring, whereas there was no increase overnight. Finally, we also plot the D_2O concentration in the nodal roots, which was similar to those of the laterals.

We used the diffusion–convection model (Equation 9) to simulate the measured D_2O concentration in laterals and nodal roots in the dry–wet scenarios. By inversely fitting the measured concentrations, we quantified the radial fluxes (j_r) of water during the night. The best fits are shown as solid lines in Figures 4b and 4c. The radial flux of water into or out of the root (j_r) was the only unknown parameter which was inversely adjusted. The best fits for the laterals in the two dry-wet samples were $j_r = 2.4 \times 10^{-7}$ and $j_r = 2.3 \times 10^{-7}$ cm s^{-1}, respectively. For the nodal roots, which grew over night, the axial flux at the root tips was set to be equal to the root growth. The radial fluxes varied between the two nodal roots. In the longer nodal root it was negligible ($j_r = 1 \times 10^{-11}$ cm s^{-1}) as compared to the laterals, indicating that water was mainly redistributed to the dry soil through the laterals. Note that such a low flux is probably

below the detection limit. However, this nodal root tip received a significant flux of water to sustain its growth ($j_x=1.94\times10^{-4}$ cm s^{-1}). For the shorter nodal (denoted by the dark yellow color in Figure 4c), the estimated radial flux was $j_r = 5\times10^{-7}$ cm s^{-1}, which is close to the value measured for laterals.
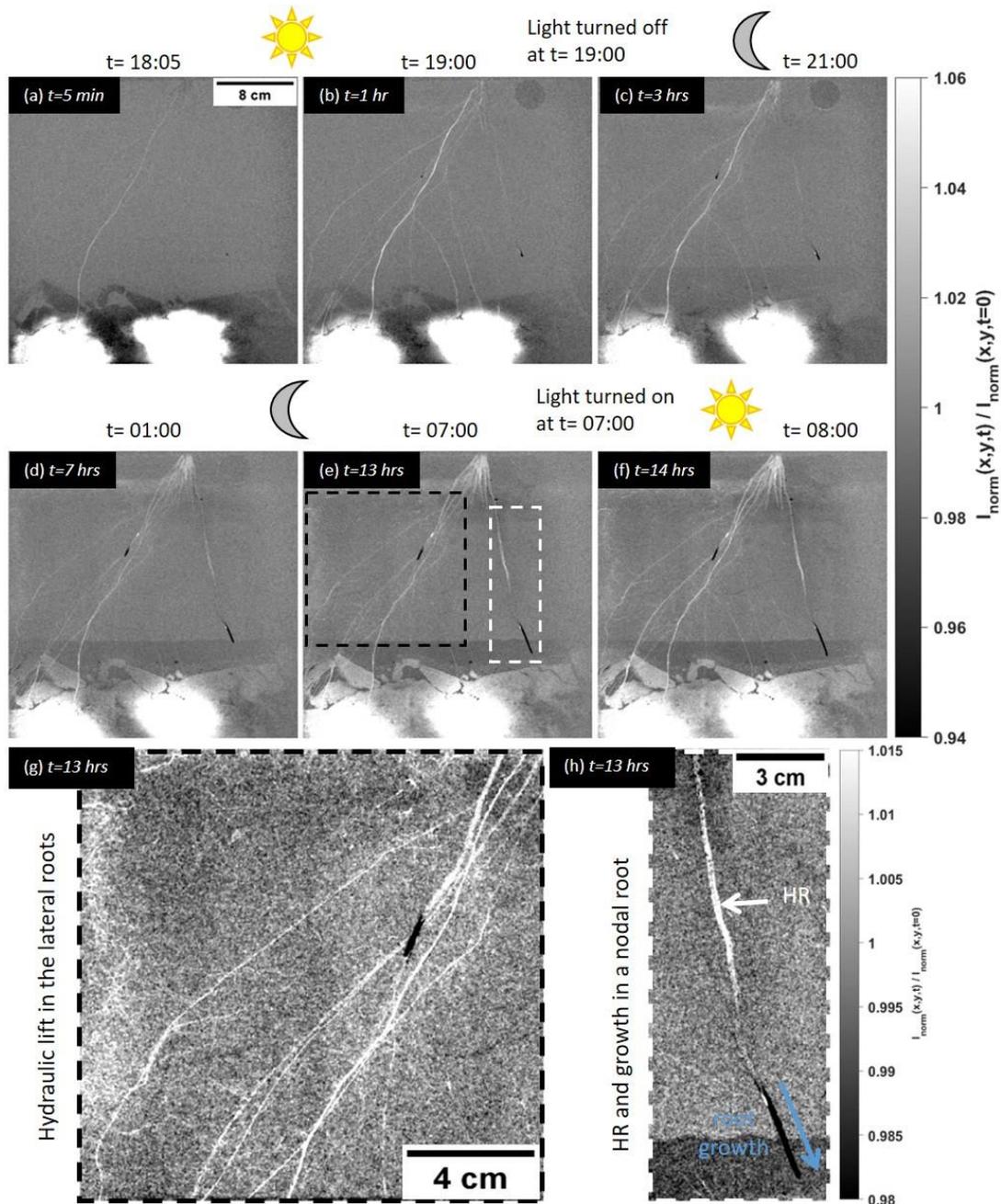

*Fig 3. Neutron radiographs of deuterated water (D₂O) injection in a sample with dry top compartment and wet bottom compartment. The radiographs show the difference between the actual radiograph at time t and that before D₂O injection. Panels **a-f** show the D₂O transport during day and its redistribution overnight. Panels **g & h** are zoom-in of the radiograph (**e**). Brighter colors indicate higher D₂O concentration and dark colors indicate root growth. $I_{norm}(x,y,t)$ and $I_{norm}(x,y,t = 0)$ are the normalized radiographs at spatial coordinates in x and y direction at time t and at t=0, respectively. HR denotes hydraulic redistribution.*
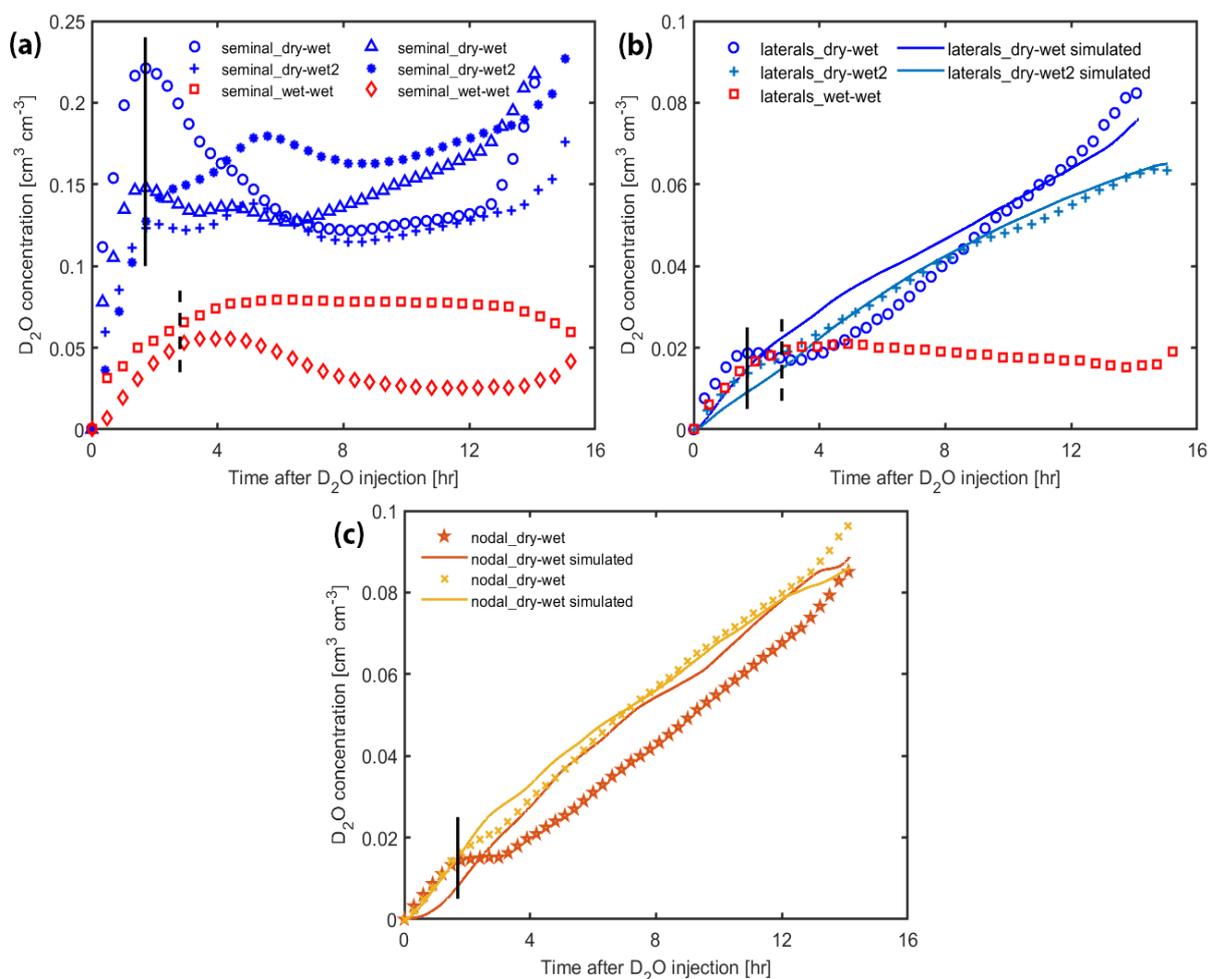
Fig 4. Average concentration of deuterated water (D₂O) in (a) seminal (b) lateral and (c) nodal roots in both dry-wet and wet-wet scenarios. The best fits of the model are shown for the dry-wet scenario in (b and c). The vertical solid and dashed black lines show when the light turned off in the two dry-wet and wet-wet samples, respectively. The R^2 values for the laterals of the two dry-wet samples are .89 and .98, respectively. The R^2 values for the nodal roots are .86 and .96.

4.5   Discussion and conclusions

We successfully showed that neutron radiography allows visualization of HR. Using a diffusion–convection model, the water fluxes in different root types were estimated. We performed two measurements with heterogeneous soil water contents (top soil compartment dry and bottom soil compartment wet; i.e., dry–wet) and one with homogeneous soil water content (both soil compartments wet; i.e., wet–wet). Additionally, in one of the two dry–wet samples, we injected H_2O the day before injecting D_2O. The experiments with H_2O and the wet–wet scenario were needed to test whether the decreasing neutron attenuation in the roots in the top compartment overnight was caused by root shrinkage or diffusion of D_2O along the

xylem (note that diffusion does not require a mass flow). The two tests showed no detectable decrease in neutron attenuation in the upper roots, which confirms our interpretation that HR (a convective flux of water from the bottom to the top soil layer through the roots) was responsible for the detected signal in the dry–wet scenarios.

In the dry–wet scenario, lateral roots slowly turned more transparent during nighttime. This observation can be explained by two processes: (a) the roots located in the upper dry compartment shrunk and therefore appeared brighter in the radiographs; and (b) these roots received D_2O from the main root axes (root transporting D_2O upwards during the day), either via diffusion or HR (convection). The root shrinkage was not the case as we did not detect any change of root shrinking–swelling overnight (Supplemental Figure S3). Therefore, we conclude that increasing transparency of the laterals of the sample shown in Figure 1 was caused by an increase of D_2O concentration. As laterals showed no growth and no detectable swelling, as observed in control experiments, a convective flow of water toward the lateral root tips means that water predominantly moved into the soil. On the contrary, nodal roots did grow. The convective fluxes toward the tip of nodal roots delivered water to the growing root tip. The efflux of water from the two nodal roots varied between the two roots. For the shorter one, the flux of water into the soil was similar to that from the lateral roots. For the longer roots, the flux of water into the soil was negligible. The differences in j_r between the two nodal roots might be explained by their different length and growth rate. The faster growth rate of the longer nodal root (3.4 cm per 15.5 h, compared with 1.2 cm per 15.5 h for the shorter nodal) is likely to have caused a stronger suction at the root tip (to drive water toward the tip) and consequently along all the root, decreasing the gradient in water potential between the root and the soil needed to drive the water efflux into the soil. Additionally, the root radial hydraulic conductivity typically decreases with increasing distance from the root tip (Meunier et al., 2018), which might have further reduced the water efflux from the long nodal root. These results show that HR varies between root types, and that the fraction of water that sustains root growth (dominant for nodal roots) and the one that flows into the soil (dominant for laterals) vary even more. The estimated fluxes are summarized in Figure 5.

The convective fluxes were estimated using inverse modeling. The model was needed to separate the effect of diffusion from that of convection. Therefore, the estimations are affected by the model assumptions. Relevant assumptions are constant diffusion coefficient during day and night, and uniform diffusion coefficient within the root tissue. These assumptions were instrumental to keep our model as simple as possible and to reduce the number of unknowns

in the inverse problem. The assumption of uniform diffusion coefficient within the root tissue was tested by Zarebanadkouki et al. (2014), who showed that the model results were not sensitive to the different pathways across the root. An additional assumption was that roots did not swell and shrink during the experiments. Root swelling (shrinking) would cause an underestimation (overestimation) of D_2O concentration and, thus, of the HR. However, the test with H_2O showed no detectable changes in root volume and water content in our experiment.

It has to be noted that the reported measurements are specific of the tested setup, in which the small container size (40-cm depth), the use of sandy substrate, and the low number of replicates might limit the generalization of the estimated fluxes.

Despite these limits, we have shown how to quantify HR by combining neutron radiography, injection of D_2O, and a diffusion–convection model. For young maize, HR was highly variable along the root system and was root type specific. In conclusion, this method can be used for quantitative estimation of the spatial distribution of hydraulic lift in detailed laboratory experiments.
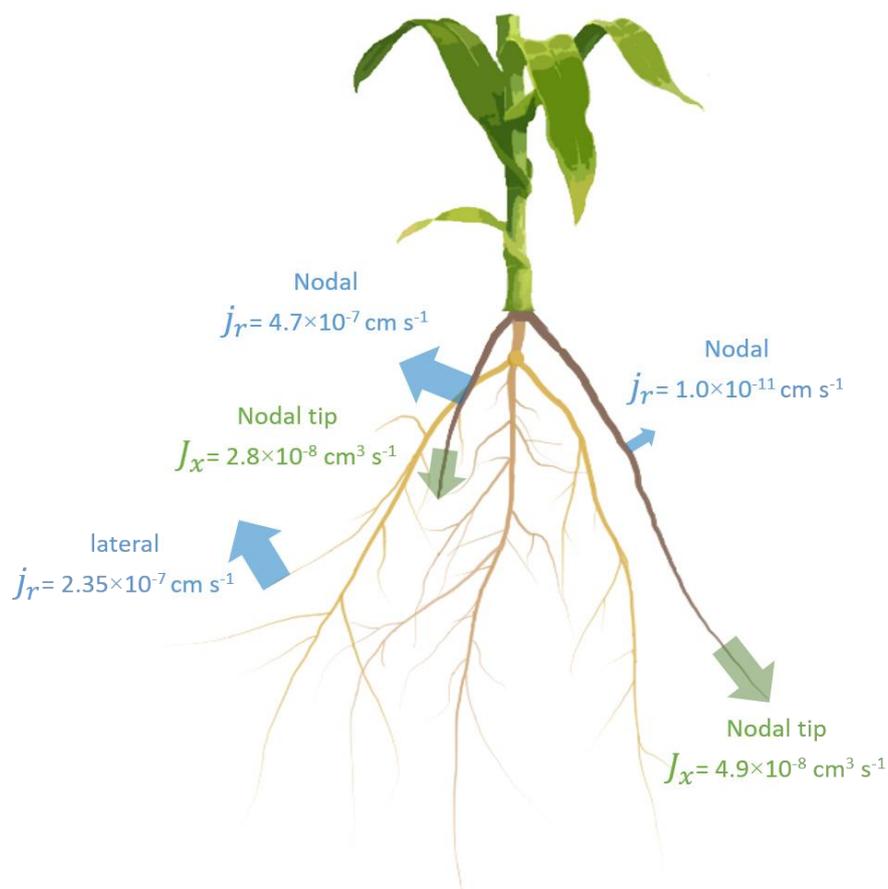
Fig 5. The summary of estimated fluxes along the measured root maize system. The fluxes of water from the root to the soil are shown in blue. The fluxes of water toward the root tip to sustain root growth are shown in green. j_r is the radial flux of water and J_x is the axial flow of water.

4.6   References

Ahmed, M.A., Zarebanadkouki, M., Kaestner, A., Carminati, A., 2016. Measurements of water uptake of maize roots: the key function of lateral roots. Plant Soil 398, 59–77. https://doi.org/10.1007/s11104-015-2639-6

Ahmed, M.A., Zarebanadkouki, M., Meunier, F., Javaux, M., Kaestner, A., Carminati, A., 2018. Root type matters: Measurement of water uptake by seminal, crown, and lateral roots in maize. J. Exp. Bot. 69, 1199–1206. https://doi.org/10.1093/jxb/erx439

Bauerle, T.L., Richards, J.H., Smart, D.R., Eissenstat, D.M., 2008. Importance of internal hydraulic redistribution for prolonging the lifespan of roots in dry soil. Plant, Cell Environ. 31, 177–186. https://doi.org/10.1111/j.1365-3040.2007.01749.x

Brooks, J.R., Meinzer, F.C., Coulombe, R., Gregg, J., 2002. Hydraulic redistribution of soil water during summer drought in two contrasting Pacific Northwest coniferous forests. Tree Physiol. 22, 1107–1117. https://doi.org/10.1093/treephys/22.15-16.1107

Bücherl, T., Söllradl, S., 2015. NECTAR: Radiography and tomography station using fission neutrons. J. large-scale Res. Facil. JLSRF 1, 8–10. https://doi.org/10.17815/jlsrf-1-45

Burgess, S.S.O., Adams, M.A., Turner, N.C., Ong, C.K., 1998. The redistribution of soil water by tree root systems. Oecologia 115, 306–311. https://doi.org/10.1007/s004420050521

Caldwell, M.M., Dawson, T.E., Richards, J.H., 1998. Hydraulic lift: Consequences of water efflux from the roots of plants. Oecologia 113, 151–161. https://doi.org/10.1007/s004420050363

Caldwell, M.M., Richards, J.H., 1989. Hydraulic lift: water efflux from upper roots improves effectiveness of water uptake by deep roots. Oecologia 79, 1–5. https://doi.org/10.1007/BF00378231

Carminati, A., Moradi, A.B., Vetterlein, D., Vontobel, P., Lehmann, E., Weller, U., Vogel, H.J., Oswald, S.E., 2010. Dynamics of soil water content in the rhizosphere. Plant Soil 332, 163–176. https://doi.org/10.1007/s11104-010-0283-8

Carminati, A., Zarebanadkouki, M., 2013. Comment on: "neutron imaging reveals internal plant water dynamics." Plant Soil 369, 25–27. https://doi.org/10.1007/s11104-013-1780-3

Hayat, F., Ahmed, M.A., Zarebanadkouki, M., Javaux, M., Cai, G., Carminati, A., 2020. Transpiration Reduction in Maize (Zea mays L) in Response to Soil Drying. Front. Plant Sci. 10. https://doi.org/10.3389/fpls.2019.01695

Kasperl, S., Vontobel, P., 2005. Application of an iterative artefact reduction method to neutron tomography. Nucl. Instruments Methods Phys. Res. Sect. A Accel. Spectrometers, Detect. Assoc. Equip. 542, 392–398. https://doi.org/10.1016/J.NIMA.2005.01.167

Meunier, F., Zarebanadkouki, M., Ahmed, M.A., Carminati, A., Couvreur, V., Javaux, M., 2018. Hydraulic conductivity of soil-grown lupine and maize unbranched roots and maize root-shoot junctions. J. Plant Physiol. 227, 31–44. https://doi.org/10.1016/j.jplph.2017.12.019

Millington, R.J., Quirk, J.P., 1959. Permeability of porous media. Nature 183, 387–388. https://doi.org/https://doi.org/10.1038/183387a0

Moradi, A.B., Carminati, A., Vetterlein, D., Vontobel, P., Lehmann, E., Weller, U., Hopmans, J.W., Vogel, H.-J., Oswald, S.E., 2011. Three-dimensional visualization and quantification of water content in the rhizosphere. New Phytol. 192, 653–663. https://doi.org/10.1111/j.1469-8137.2011.03826.x

Mühlbauer, M.J., Bücherl, T., Kellermeier, M., Knapp, M., Makowska, M., Schulz, M., Zimnik, S., Ehrenberg, H., 2018. Neutron imaging with fission and thermal neutrons at NECTAR at MLZ. Phys. B Condens. Matter 551, 359–363. https://doi.org/10.1016/j.physb.2017.11.088

Oswald, S.E., Menon, M., Carminati, A., Vontobel, P., Lehmann, E., Schulin, R., 2008. Quantitative Imaging of Infiltration, Root Growth, and Root Water Uptake via Neutron Radiography. Vadose Zo. J. 7, 1035–1047. https://doi.org/10.2136/vzj2007.0156

Richards, J.H., Caldwell, M.M., 1987. Hydraulic lift: Substantial nocturnal water transport between soil layers by Artemisia tridentata roots. Oecologia 73, 486–489. https://doi.org/10.1007/BF00379405

Sharp, R.E., Davies, W.J., 1985. Root growth and water uptake by maize plants in drying soil. J. Exp. Bot. 36, 1441–1456. https://doi.org/10.1093/jxb/36.9.1441

Smart, D.R., Carlisle, E., Goebel, M., Núñez, B.A., 2005. Transverse hydraulic redistribution by a grapevine. Plant, Cell Environ. 28, 157–166. https://doi.org/10.1111/j.1365-

3040.2004.01254.x

Snyder, K.A., James, J.J., Richards, J.H., Donovan, L.A., 2008. Does hydraulic lift or nighttime transpiration facilitate nitrogen acquisition? Plant Soil 306, 159–166. https://doi.org/10.1007/s11104-008-9567-7

Tumlinson, L.G., Liu, H., Silk, W.K., Hopmans, J.., 2008. Thermal Neutron Computed Tomography of Soil Water and Plant Roots. Soil Sci. Soc. Am. J. 72, 1234–1242. https://doi.org/10.2136/sssaj2007.0302

Wang, X., Tang, C., Guppy, C.N., Sale, P.W.G., 2009. The role of hydraulic lift and subsoil P placement in P uptake of cotton (Gossypium hirsutum L.). Plant Soil 325, 263–275. https://doi.org/10.1007/s11104-009-9977-1

Warren, Jeffrey M., Bilheux, H., Cheng, C.L., Perfect, E., 2013. Reply to: Comment on "neutron imaging reveals internal plant water dynamics." Plant Soil 371, 15–17. https://doi.org/10.1007/s11104-013-1858-y

Warren, J. M, Bilheux, H., Kang, M., Voisin, S., Cheng, C., Horita, J., Perfect, E., 2013. Neutron imaging reveals internal plant water dynamics. Plant Soil 366, 683–693. https://doi.org/10.2307/42952412

Zarebanadkouki, M., Kim, Y.X., Carminati, A., 2013. Where do roots take up water? Neutron radiography of water flow into the roots of transpiring plants growing in soil. New Phytol. 199, 1034–1044. https://doi.org/10.1111/nph.12330

Zarebanadkouki, M., Kim, Y.X., Moradi, A.B., Vogel, H.J., Kaestner, A., Carminati, A., 2012. Quantification and Modeling of Local Root Water Uptake Using Neutron Radiography and Deuterated Water. Vadose Zo. J. 11. https://doi.org/10.2136/vzj2011.0196

Zarebanadkouki, M., Kroener, E., Kaestner, A., Carminati, A., 2014. Visualization of root water uptake: quantification of deuterated water transport in roots using neutron radiography and numerical modeling. Plant Physiol 166, 487–499. https://doi.org/10.1104/pp.114.243212

Zegada-Lizarazu, W., Iijima, M., 2004. Hydrogen stable isotope analysis of water acquisition ability of deep roots and hydraulic lift in sixteen food crop species. Plant Prod. Sci. 7, 427–434. https://doi.org/10.1626/pps.7.427

4.7   Supplementary material
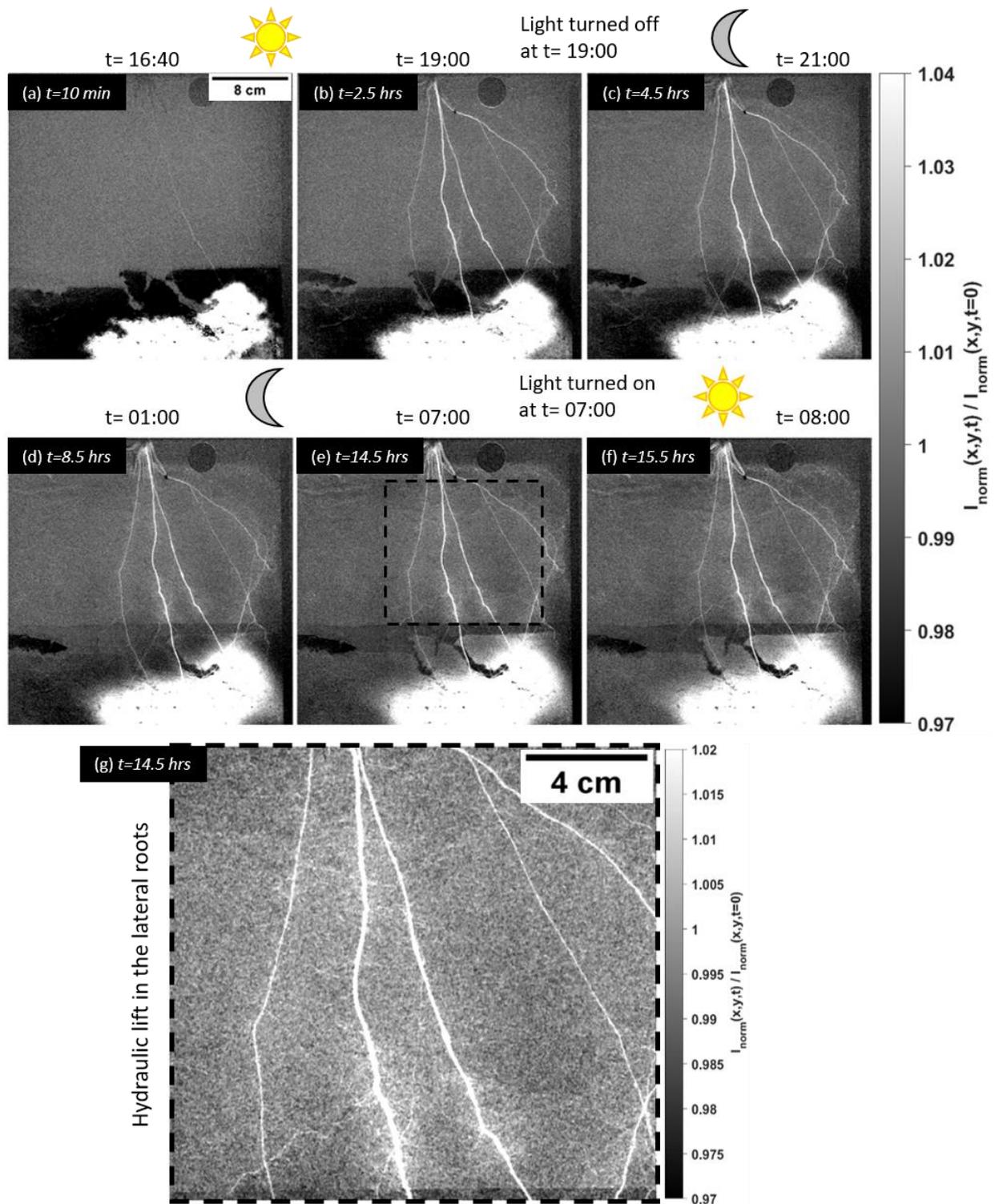
Supplemental Fig S1. Neutron radiographs of D₂O injection in the dry–wet2 sample with dry top compartment and wet bottom compartment. The radiographs show the difference between the actual radiograph at time t and the one before D₂O injection.
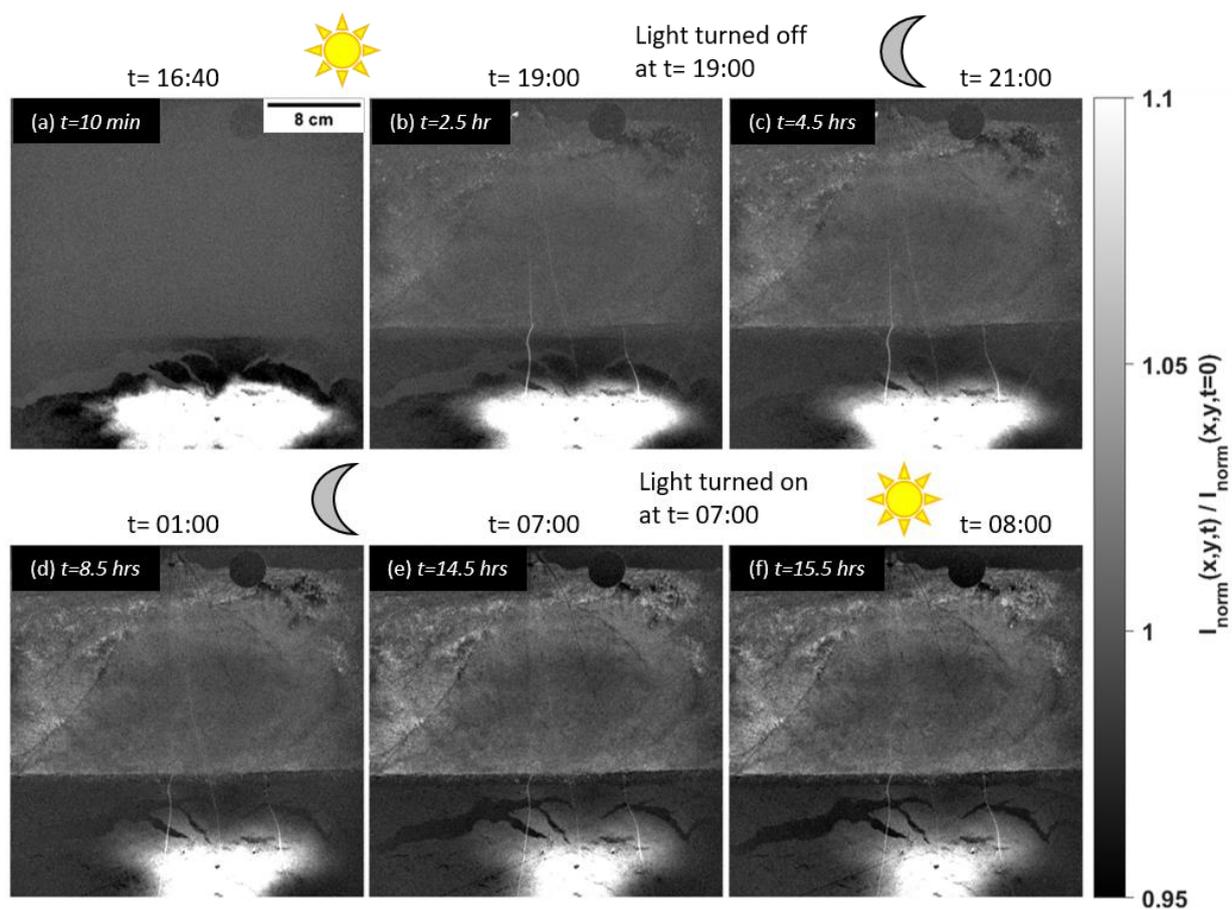
Supplemental Fig S2. Neutron radiographs of D₂O injection in the wet–wet sample with both top and bottom wet compartments. The radiographs show the difference between the actual radiograph at time t and the one before D₂O injection.
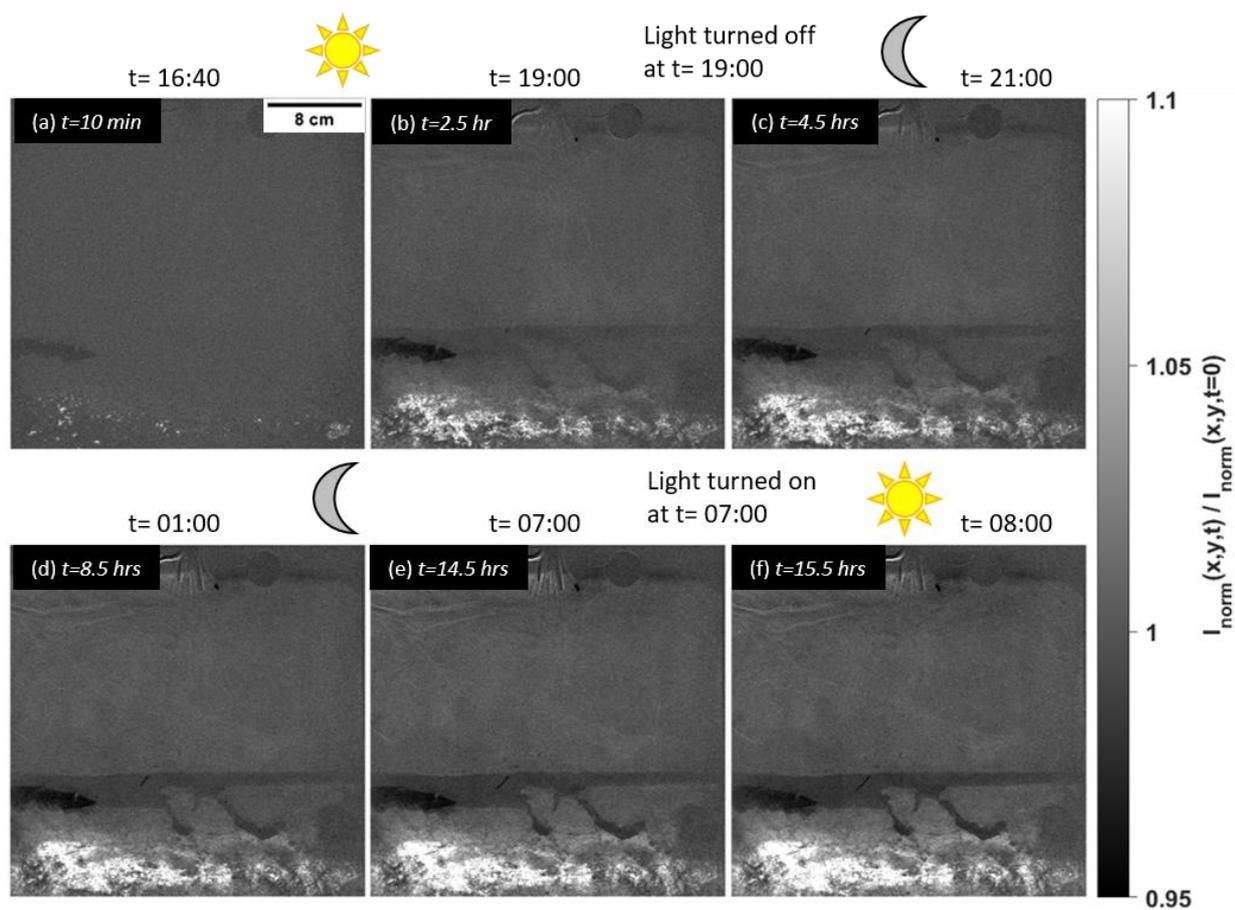
Supplemental Fig S3. Neutron radiographs of H_2O injection in the dry–wet sample during day and night time period to observe root swelling.

(Eidesstattliche) Versicherungen und Erklärungen

(§ 8 Satz 2 Nr. 3 PromO Fakultät)

Hiermit versichere ich eidesstattlich, dass ich die Arbeit selbstständig verfasst und keine anderen als die von mir angegebenen Quellen und Hilfsmittel benutzt habe (vgl. Art. 64 Abs. 1 Satz 6 BayHSchG).

(§ 8 Satz 2 Nr. 3 PromO Fakultät)

Hiermit erkläre ich, dass ich die Dissertation nicht bereits zur Erlangung eines akademischen Grades eingereicht habe und dass ich nicht bereits diese oder eine gleichartige Doktorprüfung endgültig nicht bestanden habe.

(§ 8 Satz 2 Nr. 4 PromO Fakultät)

Hiermit erkläre ich, dass ich Hilfe von gewerblichen Promotionsberatern bzw. – vermittlern oder ähnlichen Dienstleistern weder bisher in Anspruch genommen habe noch künftig in Anspruch nehmen werde.

(§ 8 Satz 2 Nr. 7 PromO Fakultät)

Hiermit erkläre ich mein Einverständnis, dass die elektronische Fassung der Dissertation unter Wahrung meiner Urheberrechte und des Datenschutzes einer gesonderten Überprüfung unterzogen werden kann.

(§ 8 Satz 2 Nr. 8 PromO Fakultät)

Hiermit erkläre ich mein Einverständnis, dass bei Verdacht wissenschaftlichen Fehlverhaltens Ermittlungen durch universitätsinterne Organe der wissenschaftlichen Selbstkontrolle stattfinden können.

………………………………………………………………………………

Ort, Datum, Unterschrift